Attention-dependent processing of motion in middle temporal area and striate cortex and its relation to behavioral detection speed

---

Dissertation

submitted in fulfilment of the requirements

for the academic degree of doctor of natural sciences

(Dr. rer. nat.)

by

Bastian Schledde

to the Faculty 2 (Biology/Chemistry) at the University of Bremen

July 31, 2019

Supervisor: Dr. Detlef Wegener

Referee: Dr. Detlef Wegener

Prof. Dr. Michael Koch

Table of content

Publication List

Publications in peer-review journals

The articles that contribute to this cumulative thesis are marked with a star (*)

Schledde B, **Galashan FO**, **Przybyla M**, **Kreiter AK**, **Wegener D**. Task-specific, dimension-based attentional shaping of motion processing in monkey area MT. *J Neurophysiol* 118: 1542–1555, 2017.*

Drebitz E, Schledde B, Wegener D, Kreiter A. K. Optimizing the Yield of Multi-Unit Activity by Including the Entire Spiking Activity. *Frontiers in Neuroscience*, 13:83, 2019.*

Schledde B, **Wegener D**. Phase shifts of cross frequency coupling predicts reaction time. *In prep.* 2019. *

Conference contributions

Schledde B., Galashan F.O., Kreiter A.K., und Wegener D. Task- specific and feature dimension-based attentional modulation of neural responses in visual area MT. *Perception*, 42 (Suppl.): 150, 2013.

Drebitz E., Schledde B., Kreiter AK., Wegener D. Mapping RFs from chronically recorded low-SNR signals in monkey visual cortex. Program No. 60.28/Z35. *2014 Neuroscience Meeting Planner*. Washington, DC: Society for Neuroscience, 2014.

Wegener D., Galashan F.O., Kreiter A.K., Schledde B. Area MT Neurons Are Modulated By Task And Stimulus Dimension. FENS Abstracts 7: 3562, 2014.

Schledde B, Galashan FO, Kreiter AK, Wegener D. Area MT neurons are modulated by feature dimension-based attention. *8th Annual Meeting of Primate Neurobiology, Göttingen,* 2015.

Schledde B., Wegener D. Latency of stimulus onset and change transients in visual areas V1 and MT relate to reaction time. Program No. 531.08/XX20. *2016 Neuroscience Meeting Planner*. San Diego, CA: Society for Neuroscience, 2016.

Wegener D, Galashan FO, Przybyla M, Kreiter AK, Schledde B. Task-specific, dimension-based modulation of neuronal responses in monkey area MT. *39th Annual Meeting of the Japan Neuroscience Society, Yokohama*. 2016

Schledde B, Galashan FO, Kreiter AK, Wegener D. V1-MT synchrony predicts reaction time and relates to latency shifts of transient responses. *10th Annual Meeting of Primate Neurobiology, Göttingen.* 2017

Schledde B., Wegener D. Phase shifts of monkey V1-MT cross-frequency coupling predict reaction time. Program No. 145.24. *2018 Neuroscience Meeting Planner*. San Diego, CA: Society for Neuroscience, 2018.

Summary

This thesis consists of two peer-reviewed published articles, one in the Journal of Neurophysiology (Chapter II) and one in Frontiers of Neuroscience (Chapter IV), one manuscript (Chapter III) in preparation and another section that includes complementary results to that manuscript (Chapter V). The first section (Chapter I) serves as a general Introduction to scientific background.

In the scope of this thesis I have investigated mechanisms that underlie the attention-dependent facilitation of neural responses in area MT and V1. In order to do so I have trained two animals on a feature-change detection task that is described in detail in Schledde et al. (2017), the first published article in this thesis. The two monkeys were presented with two visual intrinsically moving stimuli and were spatially cued to attend to one of the two. Monkeys were trained on two variants of the task, for which visual stimulation was identical but target events could either be a color change or a speed change. In this way, animals either attended color information or motion information of the stimulus. The recorded data was used for two independent investigations.

The first investigation (Chapter II) led to the publication in the Journal of Neurophysiology and revealed that neurons in area MT are targeted by a feature-dimension specific attentional modulation. Neurons in area MT are highly selective to motion-direction and their responses were shown to be shaped by feature-based attention. Because neurons that are non-optimally tuned to the features of the currently attended stimulus are fundamental for the expression of evoked transient responses towards changes in the visual environment (Traschütz et al. 2012), we hypothesized that attentional facilitation does not only target neurons that prefer the currently attended feature as predicted by the Feature-similarity-gain-hypothesis (FSGH, Treue and Martínez Trujillo 1999), but also all other neurons that process the feature dimension that is of behavioral relevance. We directly test this hypothesis by comparing firing rate modulations of MT neurons between the two variants of the task. In the crucial condition the following scenario occurs: Attention is shifted outside of the RF such that rate increases cannot be related to spatially oriented attention. The stimulus that is attended is moving into the anti-preferred direction while the motion direction inside the RF is preferred. In that case FSGH predicts a suppression of firing rate as the

dissimilarity between the attended and preferred direction is maximal. However, we found that MT neurons exhibit higher firing rate in this condition in the task requiring the animals to attend the motion information as compared to the task where the color information is crucial. Additionally, we have shown that the Fano-Factor and noise correlation decrease, effectively increasing the signal-to-noise ratio and that rate modulations between tasks can be observed even without visual stimulation. Because these effects were independent of the specific feature-tuning (indexed by the combination of speed and direction tuning) we concluded that all neurons in area MT, a central hub in the processing stream that analyzes motion information, receive attentional facilitation if motion information is crucial for the behavioral goal and in consequence that the cortical representation of the motion signal is enhanced.

In the second investigation (Chapter III) I turned to the behavioral consequences of attention-dependent processing. I made use of the condition during which animals had to detect a speed change inside the RF of the recorded neurons and analyzed successfully completed trials. Monkeys were required to respond to the speed change in a certain time frame afterwards. The reaction time of the monkeys could vary between trials up to a few hundred milliseconds. As on these timescales structural connectivity and brain anatomy do not change, the variability of RT must arise from variations in the processing along the cortical trajectory that is involved. In a previous study using the same experimental paradigm it was found that mean firing rates of MT neurons preceding the target event were not correlating with the fluctuations in RT, although the transient response evoked by the speed change was (Galashan et al. 2013). In order to investigate where and how processing variations that lead to variations in RT occur, I pooled trials into three RT fractions and investigated the coupling of oscillations at different frequencies, a phenomenon that is suggested to play a crucial role for the communication and signal transmission between cortical areas. Area MT, as mentioned above, analyzes visual content for the perception of motion. However, most of its inputs originate from area V1 that itself extracts direction and orientation information. Since area MT neurons are highly dependent on V1 output, I hypothesized that fluctuations in RT are caused by fluctuations in the communication between these areas. Communication between neurons in remote areas is suggested to depend on the precise alignment of high frequent repetitive neural discharges (Fries 2005). A prerequisite of

this alignment is that this high frequent oscillations occur simultaneously in both areas and thus need coordination via a common global reference. Recent findings indicate that low-frequent oscillations that impact large extents of the cortical tissue may be instrumental for the coordination of local high-frequent activity. I have indeed found that local gamma-band activity in area MT and V1 are coupled to the phases of an alpha-band oscillation of the respective remote area. I quantified this relation via phase-amplitude coupling. Most interestingly, my analysis showed that between RT fractions, and even on a single trial level, the specific phase of the alpha oscillation to which local gamma activity is locked was predictive of the ensuing RT of that trial. I conclude that fluctuations in RT are, to some extent, inherited from fluctuations in the signal transmission between areas MT and V1, and that the quality of signal transmission is dependent on the temporal coordination of local gamma-band activity relative to a predominant alpha band oscillation.

Chapter IV of this thesis is a published article in the the Journal “Frontiers in Neuroscience”. This article relates to the other studies in more general context as it quantifies an innovative method that serves the investigation of neural activity. In this article we quantify the performance of an alternative measure for spiking activity in intracranial recordings. In state-of-the-art neuroscience and neurotechnology the need for chronic multi-channel intracranial recordings increases. However, these recordings often suffer from signal deterioration across the life-time of these permanently implanted devices. Furthermore, modern application in the neurotechnology field (e.g. brain-computer interfaces, neuro-prostheses) require automated, fast and reliable signal detection in a variety of recording conditions. In order to meet these requirements we tested and quantified an alternative measure of multi-unit spiking activity that was formerly introduced (Eckhorn 1991, 1992; Eckhorn and Obermueller 1993; Brosch et al. 1997). It constitutes the rectified and low-pass filtered version of the high-pass content of the raw data. It entails all information of the high-pass filtered data and does not, as for example is done by thresholding, reject large amounts of data. It was thus termed “entire spiking activity” (ESA). Conventional thresholding and subsequent spike train analysis is often a good and precise measure of single- and multi-unit activity but when the recorded action potentials are small with respect to neural or electrical noise in the recording they are often not captured by conventional thresholds

or their detection requires intensive computational power or manual intervention. Therefore, we quantified the performance of the ESA signal and compared it to the performance of the spike trains as obtained from conventional thresholding and to the performance of the power of the local field potential in detecting and characterizing RFs of V1 neurons in five macaque monkeys. The ESA signal achieves a detection rate that is 2.5 times higher than conventional MUA estimation for low signal-to-noise (SNR) data and even for medium and high SNR recordings detection rates were 30% higher. Receptive fields computed with this measure were consistently larger but revealed tuning characteristics comparable to the spike trains. The easy usage and computationally cheap application of the ESA signal in combination with its outstanding performance even for low SNR data makes it an ideal candidate for e.g. brain computer interfaces.

Finally, I present complementary results that have been produced in parallel to the investigation presented in Chapter III of this thesis and that make use of the previously introduced ESA signal. These are not included in the main article for reason of readability, but consist of findings that are relevant and new to the scientific body with regard to the effect of attention-dependent processing on behavioral RT.

Zusammenfassung

Diese Arbeit umfasst zwei Artikel, die in den Fachzeitschriften „Journal of Neurophysiology“ (Chapter II) und „Frontiers of Neuroscience“ (Chapter IV) veröffentlicht wurden, ein Manuskript (Chapter III), das sich zum Zeitpunkt der Abgabe noch in der Vorbereitung einer Veröffentlichung befindet, und ein Kapitel (Chapter V), das sich mit erweiternden Ergebnissen der vorhergehenden Untersuchungen befasst. Das erste Kapitel (Chapter I) dient der generellen Einführung in die wissenschaftliche Thematik.

Im Rahmen dieser Arbeit habe ich die Mechanismen aufmerksamkeitsabhängiger neuronaler Informationsverarbeitung im visuellen Kortex erforscht. Insbesondere habe ich die Hirnareale MT und V1 zweier Makaken Affen untersucht, während diese eine Farb- oder Geschwindigkeitsveränderung an zwei unterschiedlichen visuellen Stimuli detektieren mussten. Die Details des Experimentes sind in der ersten Publikation dieser Arbeit (Schledde et al. 2017) genauer beschrieben. Beiden Affen wurden zwei visuelle Stimuli gezeigt die sich intrinsisch bewegen und von denen einer zwischenzeitlich mit einem räumlichen Hinweis versehen wurde. Die Affen waren darauf trainiert, den räumlich vorgemerkten Stimulus zu beachten und an diesem entweder eine Farb- oder eine Geschwindigkeitsänderung zu detektieren. Gleichzeitig mussten die Tiere Distraktoren, also die nicht angezeigte Eigenschaftsänderung und Änderungen an der falschen Position, ignorieren. Mittels dieser Stimulation mussten die Affen in der einen Aufgabe die Farbinformationen des Stimulus beachten und in der anderen Aufgabe die Bewegungsinformation. Die Daten, die währenddessen aufgenommen wurden, konnten für zwei unabhängige Studien verwendet werden.

Die erste Studie (Chapter II) führte zu der Publikation in der Fachzeitschrift „Journal of Neurophysiology“ und widmet sich dem Einfluss eines Aufmerksamkeitsaspektes, der auf der Eigenschaftsdimension basiert. Die untersuchten Neuronen stammen aus dem Hirnareal MT und sind hochsensibel für die Bewegungsrichtung der Stimuli. Außerdem werden ihre neuronalen Antworten durch den Einfluss eigenschaftsbasierter Aufmerksamkeit geformt. Neurone, die nicht optimal auf die gerade beachtete

Bewegungsrichtung reagieren sind laut einer einschlägigen Hypothese nicht Ziel einer Aufmerksamkeitsabhängigen Erhöhung ihrer Aktivität. In unserem Labor konnten wir allerdings zeigen das es besonders diese Neurone sind, die besonders wichtig für die Detektion einer Änderung der Bewegungsrichtung sind, da sie darauf mit besonders ausgeprägten Transienten reagieren (Traschütz et al. 2012). Daher haben wir die Hypothese aufgestellt, dass es einen Aufmerksamkeitsprozess gibt, der für die verbesserte Wahrnehmung der kompletten Eigenschaftsdimension sorgt, der also alle Neuronen unterstützt, die Bewegungsinformationen verarbeiten, auch jene, die nicht optimal auf die gerade beachtete Bewegungsrichtung reagieren. Diese Hypothese steht in diesem Punkt im Konflikt mit der „Feature-similarity-gain-hypothese“ (FSGH, Treue and Martínez Trujillo 1999), die besagt dass nur die Neuronen unterstützt werden, die die gerade beachtete Bewegungsrichtung bevorzugen. In dieser Studie haben wir anhand der gemessenen Feuerraten im Hirnareal MT diese Hypothese direkt untersucht. In den beiden Schlüsselkonditionen wurden die Neuronen nicht mit räumlicher Aufmerksamkeit belegt; der Stimulus, auf den die Neuronen antworten, bewegte sich in die präferierte Richtung und der beachtete Stimulus außerhalb des Rezeptiven Feldes in anti-präferierte Richtung. In dieser Situation ist die beachtete und präferierte Bewegungsrichtung maximal ungleich und die FSGH sagt eine Unterdrückung der Feuerraten voraus. Wir konnten entgegen dieser Vorhersage zeigen, dass Feuerraten höher waren, wenn die Bewegungsinformation, also die präferierte Eigenschaftsdimension, beachtet worden ist als wenn Farbinformation, also die nicht-präferierte Eigenschaftsdimension, beachtet worden ist. Da wir für diese Bedingungen den Einfluss räumlicher Aufmerksamkeit und den des FSG ausschließen können, schreiben wir diesem Feuerrateneffekt einen dimensionsbasierten Aufmerksamkeitsprozess - wie oben beschrieben - zu. Wir konnten außerdem zeigen, dass in dieser Situation nicht nur Feuerraten erhöht, sondern auch der „Fano-Faktor“ und die „Noise-Correlation“ reduziert wurden. Beides weist darauf hin, dass auch das Signal-Rausch-Verhältnis verbessert wird. Außerdem blieb der Feuerrateneffekt bestehen, wenn wir die Neuronen in Gruppen verschiedener Stimulus-Selektivitäten aufteilten. Dies untermauert zusätzlich, dass das ganze Hirnareal MT einem Aufmerksamkeitseinfluss unterliegt, der auf der Eigenschaftsdimension basiert.

In der zweiten Studie (Chapter III), die diese Arbeit umfasst, habe ich mich mit den Auswirkungen der Aufmerksamkeitsleistung auf das Verhalten der Tiere beschäftigt. In einer Bedingung der Geschwindigkeitsdetektionsaufgabe mussten die Tiere innerhalb eines bestimmten Zeitintervalls reagieren, nachdem die Geschwindigkeit verändert wurde. Ihre Reaktionszeit (RZ) konnte sich um mehrere hundert Millisekunden von Durchlauf zu Durchlauf unterscheiden. Innerhalb solch kurzer Zeitskalen werden die neuronalen Verbindungen, die der Signalweiterleitung unterliegen, in der Regel nicht moduliert. Dies lässt den Schluss zu, dass die Variabilität in der Signalverarbeitung selbst Grund der Reaktionszeitvariabilität ist. In einer vorhergehenden Studie, die eine identische visuelle Stimulation benutze, wurde gezeigt, dass transiente Feuerraten im Areal MT, die durch eine Beschleunigung des bewegten Stimulus hervorgerufen wurde, mit der Reaktionszeit korrelierten. Gleichzeitig wurde aber auch gezeigt, dass vorhergehende gleichmäßige Feuerraten nicht korrelierten. Auf Grund dieser Vorarbeiten habe ich untersucht, wie sich die Variabilität der Signalverarbeitung auf die Reaktionszeit auswirkt. Dafür habe ich insbesondere die Interaktion verschieden schneller Oszillationen in zwei Hirnarealen untersucht. Die Kupplung oder Korrelation neuronaler Aktivitätsoszillationen zwischen Arealen wird oft als grundlegend für eine funktionale Verbindung und somit potentieller Signalweiterleitung angesehen. Variationen in diesem Mechanismus könnten sich demnach auch auf die resultieren RZ auswirken. Diese Interaktion basiert oft auf der präzisen Angleichung der Phasenlagen hochfrequenter Oszillationen. Damit diese überhaupt möglich ist, müssen die hochfrequenten Oszillationen zeitlich so koordiniert werden, dass sie zwischen den Arealen auch gleichzeitig auftreten. Diese Koordination könnte wiederum durch eine niederfrequente Oszillation realisiert werden. Kürzlich veröffentlichte Studien legen in der Tat nahe, dass die Stärke der hochfrequenten Oszillationen zeitlich (phasengebunden) durch niederfrequente Oszillationen, die sich über einen größeren Teil des Kortex erstrecken, koordiniert wird. In meiner Untersuchung konnte ich zeigen, dass die lokale hochfrequente (gamma-band) Aktivität durch die Phasenlage einer niederfrequenten (alpha-band) Aktivität in einem anderen Areal koordiniert wird. Außerdem konnte ich darlegen, dass das Verhältnis der alpha-band Phasenlage zu der Stärke der gamma-band Aktivität mit der RZ korreliert, also die Variation der zeitlichen

Koordination der gamma-band Aktivität zwischen Arealen eine wichtige Rolle in der Wahrnehmung und ultimativ der Latenz der Reaktion der Tiere spielt.

In dem vierten Kapitel dieser Arbeit (Chapter IV) ist ein Artikel, der in der Zeitschrift „Frontiers in Neuroscience“ veröffentlicht wurde. Dieser steht in einem allgemeineren Zusammenhang zu den anderen Studien, da er eine innovative Methodik, die der Untersuchung neuronaler Aktivität dient, evaluiert. In diesem Artikel quantifizierten wir die Leistung eines alternativen Maßes für Aktionspotentiale bei intrakranialen Ableitungen. In der modernen Neurowissenschaft und in der Neurotechnologie nimmt der Bedarf an chronischen intrakranialen Mehrkanalaufzeichnungen zu. Diese Aufnahmen leiden jedoch häufig unter einer Signalverschlechterung, die über die Lebensdauer dieser permanent implantierten Geräte zunimmt. Darüber hinaus erfordern moderne Anwendungen auf dem Gebiet der Neurotechnologie (z.B. Gehirn-Computer-Schnittstellen, Neuroprothesen) eine automatisierte, schnelle und zuverlässige Signalerkennung in einer Vielzahl von Ableitbedingungen. Um diesen Anforderungen zu entsprechen, haben wir ein alternatives Maß für „Multi-Unit-Spiking“-Aktivität (MUA) (Eckhorn 1991, 1992; Eckhorn and Obermueller 1993; Brosch et al. 1997) getestet und quantifiziert. Im Kern entspricht das Maß einer rektifizierten und tiefpassgefilterten Version des Hochpassinhalts der Rohdaten. Sie enthält alle Informationen der hochpassgefilterten Daten und verwirft keine großen Datenmengen, wie dies beispielsweise durch das Anlegen einer Schwelle geschieht. Es wird daher von uns als "entire spiking activity" (ESA) bezeichnet. Konventionelles „Thresholding“ und eine nachfolgende „spike-train“- Analyse ist häufig ein gutes und genaues Maß für die Aktivität von Einzel- und Mehrfacheinheiten. Wenn jedoch die aufgezeichneten Aktionspotentiale in Bezug auf das neuronale oder elektrische Rauschen in der Aufzeichnung klein sind, werden sie oft nicht durch herkömmliche Schwellenwerte erfasst. Die Erkennung erfordert intensive Rechenleistung oder das manuelle Anpassen der Schwellenwerte. Daher haben wir die Leistung des ESA-Signals mit der Leistung der „spike-trians“, wie sie durch konventionelles „Thresholding“ erhalten wird, und mit der Leistung des lokalen Feldpotenzials beim Erfassen und Charakterisieren von Rezeptiven Feldern von V1-Neuronen in fünf Makakenaffen verglichen. Das ESA-Signal erreichte

eine Erkennungsrate, die 2,5-fach höher ist als die herkömmliche MUA für Daten mit niedrigem Signal-Rausch-Verhältnis (SNR), und selbst für mittlere und hohe SNR-Aufzeichnungen waren die Erkennungsraten um 30% höher. Die mit dieser Maßnahme berechneten Rezeptiven Felder waren konstant größer, zeigten jedoch ähnliche Abstimmungsmerkmale wie die der spike-trains. Die einfache Verwendung und rechnerisch günstigere Anwendung des ESA-Signals in Kombination mit seiner hervorragenden Leistung - selbst für Daten mit niedrigem SNR - macht es unter anderem zu einem idealen Kandidaten für Gehirn-Computer-Schnittstellen.

Im letzten Teil der Arbeit (Chapter V) stelle ich ergänzende Ergebnisse vor, die parallel zu den in Kapitel III dieser Arbeit vorgestellten Untersuchungen erstellt wurden und unter anderem auf das vorgenannte ESA Signal zurückgreifen. Diese Ergebnisse sind aus Gründen der Lesbarkeit nicht im Hauptartikel enthalten, bestehen aber aus Erkenntnissen, die dem Verständnis der Auswirkungen aufmerksamkeitsabhängiger Informationsverarbeitung im Zusammenhang mit dem Verhalten wichtig und neu sind.

Chapter I: Introduction

Throughout many years scientists have investigated a particular neural process that is a core element of human and non-human perception. It is central to the functioning and malfunctioning of the brain because it serves to overcome the fact that the computational power of the brain is severely capacity limited. Despite the massive parallel processing power made by the 10^{11} neurons making 10^{15} connections in the neocortex alone (Braitenberg and Schüz 1991; Murre and Sturdy 1995), humans are surprisingly poor at performing more than one task at a time.

While the notion that human perception is capacity limited dates back to Aristotle (Neumann 1996) it was since the late 1950's that models of selective operations which are performed on perceptual inputs have evolved. The "Y-shaped tube" whose stem only takes one of many small balls at a time entering the two branches, while a central flap routes either of the two streams (Broadbent 1957), resembles the core idea of the perceptual bottleneck problem and the selection process solving it. Today, the central idea that sensory input is pruned and only a fraction is selected for conscious perception prevails, though the theoretical underpinnings have shifted from a pure filter mechanism that prevents limit resources to overload, to a richer functionality of a selection and integration mechanism that has been collectively labelled as "attention" (Neumann 1996).

Various functional models of selective attention exists which try to explain the neuronal implementation of this routing or gating of perceptual input. In the visual domain, different perceptual forms of selective attention have been identified for which spatial attention, the ability to focus on a particular location in the visual field; feature- based attention, the ability to enhance perception of a given feature in the visual field (e.g. the color red), and object- based attention, the ability to perceive all parts of an attended object in particular, are amongst the most influential concepts of visual attention.

This thesis aims to contribute to the work on attention in the visual domain by describing the neural correlates of yet a novel form of it in Chapter II and by illuminating the relationship between the selective facilitation of neural computation and its impact on behavior in Chapter III. Chapter IV contributes to the methodological toolset of neurophysiological research by quantifying the performance of an alternative method for the estimation of neuronal activity from intra-cranial recordings. In Chapter V accompanying results are presented that were produced in the general context of the investigation in Chapter III. First off, I will introduce the basics of visual processing in the human and non-human primate brain with a special focus on motion processing and deepen the insight into models and concepts of attention-dependent information processing.

Image Processing in the visual Cortex

Vision in the primate brain is organized through hierarchically ordered, yet parallel and convergent information processing steps. It starts by sensing photon influx in the retina, forwarding compressed and preprocessed signals via the optic nerve to the first subcortical structures. The majority of projections enter the lateral geniculate nucleus (LGN) in the dorsal thalamus and continue to highly sophisticated image processing stages in the primary visual cortex (or striate cortex or area V1). Some retinal projections enter the hypothalamus and about 10 % innervate the superior colliculus (SC) in the midbrain tectum. From primary visual cortex information is funneled through a variety of areas in parallel which are specialized to process different properties of the images that will be ultimately perceived. In this thesis the *macaque mulatta* was as a model organism and the following description is based mostly on studies relying on the macaque's brain. Vision processing in the cortex of these animals is generally viewed as a good estimate of the human equivalent (Tootell et al. 1996; Bear et al. 2007; Horwitz 2015).

The projections of retinal ganglion cells, cells of the first layer following photosensitive cells in the retina, diverge in three parallel pathways (magnocellular, parvocellular and koniocellular) giving rise to two cortical streams forming large networks of visual processing. One extending dorsally across a variety of visual areas in the occipital and

parietal lobe and one that extends ventrally across the temporal lobe. The dorsal pathway processes, amongst a variety of other functions, visual content that serves the percept of motion and the properties of its neurons resemble properties of neurons in the magnocellular pathway. The ventral pathway is mainly concerned with the recognition of objects and the processing of color and shape and inherits properties that are also processed in the parvo- and koniocellular pathway.

General properties of the visual cortex

Three of the most defining properties of the visual cortex are *retinotopy*, *magnification* and *lamination*.

Neighboring cells in the retina respond to sensory input in neighboring places in the visual field (receptive fields, RF) and neighboring cells in the retina project to neighboring cells in their target projection zone. This organizational concept, propagated throughout the visual processing hierarchy, is called retinotopy and maintains a 2D representation of the retinal input on the 2D surface of the cortex (Bear et al. 2007).

The retinotopic organization of the cortex is accompanied by a highly convergent connectivity structure between subsequent visual areas. A downstream neuron (neurons in areas at higher stages of the processing hierarchy) may receive input from many upstream neurons (neurons in areas that are at the beginning of the processing hierarchy), leading to an effective magnification of the RF size and enabling downstream areas to integrate information from many neurons representing various types of information about the visual field. A V1-RF, for example, may be of a magnitude smaller than a RF of neurons in the downstream middle temporal area (MT) (Desimone and Ungerleider 1986; Mikami et al. 1986; Raiguel et al. 1995; Born and Bradley 2005; Richert et al. 2013).

Lamination denotes the fact that the neocortex is divided into six layers (I-VI) that are anatomically and functionally distinct (Brodmann 1909). Striate cortex layer IV can be divided into A,B,Cα,Cβ amounting to a total of nine to ten distinct layers depending on the level of sublayers counted (Hubel and Wiesel 1968; Bear et al. 2007). Unlike layers

defined in the LGN, not all layers in visual cortex contain cells that both receive and send information from other areas. LGN projections mainly target layer IVC in area V1, maintaining anatomical segregation of cellular type-specific pathways (magnocellular pathway in IVCα and parvocellular pathway in IVCβ). Area V1 layer II,III,IVA project to other cortical layers and layer V and VI to subcortical structures (superior colliculus (SC) and back to LGN) (Hubel 1995). With the exception of the subdivision of layer IV in area V1, the layer-specific targets are identical throughout the visual cortex. Expressed in a simplified way, the cortical circuit is organized such that upstream input arrives in layer IV, subcortical projections originate from layer V and VI and downstream projections to other cortical areas come from layer II and III. Within an area, horizontal and reciprocal connections are made between layer IV to II and III, within layer III and II and layer III projects back to layer V and layer V to VI (Hubel and Wiesel 1962; Gilbert and Wiesel 1983).

Motion processing in the visual cortex

The magnocellular pathway originates from M-type retinal ganglion cells and projects via the LGN onto layer IVCα in area V1 and terminates in layer IVB of the striate cortex (Felleman and Van Essen 1991; Born and Bradley 2005; Bear et al. 2007). The primary visual cortex is the first site at which visual motion of an object is decoded from the retinal input. V1 neurons respond to the changes in the orientation of a stimulus (orientation-selective) (Hubel and Wiesel 1968), are sensitive to speed changes (speed selective) (Orban et al. 1986) and may have a motion direction preference (direction-selective) (Movshon and Newsome 1996). A V1 cortical module, a three-dimensional volume of cortical tissue representing a single point in visual space, is organized in neighboring orientation columns with a linear succession of orientation preferences, interleaved with patches of color-sensitive neurons (Blobs) and segregated in columns of ocular dominance (Hubel and Wiesel 1977).

Although velocity of an object is already decoded in V1, the small size of RFs constitutes the “aperture problem” in area V1 which refers to the problem to detect the true motion direction of an object. Motion direction always appears orthogonal to the length of the object if the boundaries of the object are occluded by an aperture (Fennema and

Thompson 1979; Adelson and Movshon 1982). Neurons in V1 sample retinal motion through small RFs, resulting in a high resolution of the visual field but larger objects exceed most RFs such that for individual neurons, boundaries of the object are hidden (Pack and Born 2001). Thus, neurons in V1 only decode normal (orthogonal) velocities (Hubel and Wiesel 1968; Heeger 1987) and are unable to code for global motion (e.g. pattern motion). The computation of pattern motion is evidence for the integration of multiple normal velocities and provides a solution to the aperture problem. Many models have been proposed for the detection of pattern motion, most assuming a two stage process. The first stage incorporates the detection of local velocities presumably via V1 cells that act as spatiotemporal filters with small RFs followed by an integration and nonlinear computation step that calculates global motion (Movshon et al. 1985; Heeger 1987; Yuille and Grzywacz 1988; Koch et al. 1989; Grzywacz and Yuille 1990; Nowlan and Sejnowski 1993; Simoncelli and Heeger 1998).

Neurons which are selective for pattern motion were found in area MT (or V5, located in the middle temporal lobe), the first extra striate area of the dorsal stream and a direct projection zone of layer IVB V1 neurons. The fact that about 25% of the neurons are pattern-selective (Movshon et al. 1985) identifies area MT as a direct recipient and integrator of V1 information. Further evidence supporting this view is that about 90% of the input to MT is directly projected from V1 (Maunsell and van Essen 1983; Shipp and Zeki 1989); MT receptive field sizes are about a magnitude larger at the same eccentricities (Desimone and Ungerleider 1986; Mikami et al. 1986; Raiguel et al. 1995; Born and Bradley 2005; Richert et al. 2013), directional and speed tuning is broader in MT than in V1 (Albright 1984; Mikami et al. 1986), and MT cells are suppressed if transparent motion induces two local opposite motion directions (motion opponency), whereas V1 neurons respond to their preferred motion vector (Snowden et al. 1991). Area MT receives indirect input from thick stripes in V2 via V3 (Shipp and Zeki 1989; Yabuta et al. 2001) and to some extent from subcortical structures (Rodman et al. 1990; Girard et al. 1992; Stepniewska et al. 1999), leaving parts of MT neural activity intact after the removal of the striate cortex (Rodman et al. 1989). Neurons in area MT prefer a specific motion direction and are suggested to be anatomically organized in a columnar structure with continuously changing direction preferences, similar to orientation columns in V1, and are aligned with another set of columns with locally opposite

direction preferences (Dubner and Zeki 1971; Albright et al. 1984; Geesaman et al. 1997). MT neurons are also tuned and organized according to binocular disparity (DeAngelis and Newsome 1999) and most neurons encode three-dimensional motion information (Czuba et al. 2014). Preferences of speed selective cells in MT are within a broad range 2 – 256 degrees/s (Maunsell and Van Essen 1983), have either low-pass, high-pass, or broadband speed tuning (Lagae et al. 1993) and are distributed in clusters of speed preferences (Liu and Newsome 2003).

Area MT is suggested to play a crucial role in noise reduction in the motion processing stream. Neurons are silenced if two local opposite motion directions are introduced (Snowden et al. 1991), a property that might limit the propagation of broadband energy emitted from noisy V1 input and it has been shown that lesion to the human homologue, area MT/V5, impairs motion processing only if noise is introduced to the motion stimuli (Zihl et al. 1983; Marcar et al. 1997).

There are many more studies that show that MT neurons are involved in the processing of different aspects of motion perception, strengthening the role of MT as a processing unit fundamental for the detection of moving object in the visual field (Born and Bradley 2005) .

Area MT has further connections into the temporal lobe to area FST, into the parietal lobe connecting to MST, PIP, VIP, LIP and into the frontal lobe to FEF (Felleman and Van Essen 1991), feeding target structures of the dorsal processing stream associated with the optic flow (MST, VIP and area 7a) and with the control of eye-movements (LIP, FEF) (Mishkin et al. 1983; Maunsell et al. 1987). Thus, area MT is central to dorsal processing stream and because of its key role an ideal candidate area for the investigation of the neurophysiological basis of motion perception.

The complementary second visual processing pathway extends ventrally from V1 and originates from layer II & III of the blob and interblob regions. It encompasses V2, V4, PIT and areas of the inferior temporal cortex. It is generally concerned with the analysis and perception of objects, where area V4 is a central hub in the processing hierarchy, an analogue to area MT in the dorsal stream that consists of color and shape selective neurons (Ungerleider and Mishkin 1982; Maunsell et al. 1987; Felleman and Van Essen 1991; Kravitz et al. 2013).

Attention

As described earlier, the processing of sensory information was thought to be subject to a selection mechanism that counter the central problem of capacity limitation of the brain's computational resources. Nowadays, the role of attention is generally viewed not merely as a solution to restricted processing capacities, but rather to an optimization process that shapes and restricts perception towards the sensory content that is behaviorally relevant (Neumann 1996). For successful behavior, most of the information from e.g. the retina is not relevant. For example, information from peripheral vision is in most cases not relevant for the current task, though in some situations lifesaving. These processes that I describe in the following will be collectively termed as "attentional processes" and in the context of this thesis can be generally defined as the selective facilitation of cortical information processing that is of behavioral importance.

A number of properties of the processes that constitute attentional selection are characteristic for the type of attention being deployed. On the one hand, the process can be fast, automatic and involuntarily executed. This process is exogenous or bottom-up as they are triggered by external very salient events that "pop-out" of an otherwise homogenous visual environment. In the example above the speeding car or racing lion entering peripheral vison is salient and a very important event to detect for survival. On the other hand, attention can be intentionally allocated to relevant image features or objects that require a detailed and accurate neural representation and a highly sensitive observation that allows fast perception of any perturbations to the current state of the object. This process is endogenous or top-down, as it is inherently internal and based on the voluntary decision of the subject to deploy attention, for example in order to read this thesis. In contrast to the bottom-up attention this process can be slow due to the computational complexity of the task at hand.

The focus of visual attention can be shifted away from the center of gaze, outside the foveal representation of the visual scene and is then termed as "covert attention". A seminal study that made the case for the existence of visual attention illustrate the benefit of deploying covert visual attention for the behavioral performance. Posner et al. (1980) developed a paradigm (Posner paradigm) that required subjects to fixate on a

central fixation spot while they were told to respond to the occurrence of a brief light flash on either side of the fixation spot outside the focus of gaze. Prior to the flash, participants were spatially cued, i.e. received a hint that the occurrence of the flash will be at a specific side. This cue was valid in 80% of the trials. Participants learned that incorporating the cue in their decision where to shift attention yielded a benefit for the detection of the flash. In the remaining trials, however the cue was wrong and the flash occurred at the opposite site of the fixation spot. Posner et al. (1980) found that in trials with valid cues the reaction time (RT) to the light flash was shorter as compared to trials with invalid cue. It was thus assumed that the deployment of covert visual attention yielded a behavioral benefit for the detection of a perturbation of the visual scene. The fact that the RT to the light flash is shorter with correctly oriented covert attention is perceived as evidence that visual attention enhances the perceptibility of objects occurring within the focus of attention. This seminal study was one of the first that led to the proposition of the famous metaphor of "the spotlight of attention". Throughout the rest of the thesis the term "attention" or "selective attention" will be used synonymously with "covert attention".

Before turning to the models and neural correlates of selective attention that have been established in the scientific community, a general concept is introduced that most models incorporate or implicitly assume. Attentional modulation of neurons or populations of neurons, which will be described in the following, was always an enhancement of neural activity or increase of signal transmission quality between neurons and areas in comparison to the non-attended case. The resulting pattern of enhanced neural representation of neurons coding for the attended stimulus (position or feature) versus all other neurons can be projected onto a two-dimensional representation of the visual field.

Furthermore, Koch and Ullman (1985) originally constructed the idea of a central and two-dimensional saliency map that is used to guide saccades on the basis of bottom-up saliency cues. The two-dimensional input image is decomposed into several layers that, at a pre-attentive stage, analyzes different image properties with regard to saliency and recombines the resulting feature maps to a unified bottom-up saliency map (Itti et al. 2001). Both two-dimensional topographic representations of the visual scene are

suggested to be integrated into a saliency map that represents the combination of bottom-up saliency and top-down attentional modulation, a unified neural representation of the stimulus (Treue 2003).

The investigation of selective attention has evolved in two parallel lines of research. On the one hand, attention was described based on evidence from psychophysical studies and, on the other hand, models of attention were established based on attentional modulations of neuronal activity. Models of the first line of research established more abstract conceptualizations that aim to explain how endogenous and exogenous attention shapes perception. These models consists of weighted saliency maps of the visual environment through which perception is biased. In the subsection "Attention and visual search" I will review the most influential concept in this line of research. In the second line of research, models evolved that explain how the neuronal representation of the visual environment is biased, such that the attended content is prioritized for further processing. For these models, the convergent structure of the visual processing hierarchy plays an important role since anatomy dictates that neurons downstream the processing pathway often receive visual content of multiple objects or locations in the visual field that may have multiple behavioral relevancies. I will turn to these models in the subsection "Neurophysiological models of attentional selection". Both lines of research cannot be viewed strictly separate, as both are influenced by each other and share mutual concepts and ideas.

Attention and visual search

The feature integration theory (FIT; Treisman and Sato 1990) describes an attention architecture that incorporates a first, parallel, and fast process based on the evaluation of features maps. This model was designed to fit the reaction time (RT) functions obtained during visual search task with feature pop-out stimuli. In such a task, subjects have to detect a salient stimulus amongst a number of distractor stimuli. The difficulty of the task can be varied by the number of distractors and the complexity of the target stimulus. For simple stimuli, RTs are fast and independent of the number of distractors suggesting a fast and parallel mechanism. If stimuli are constructed with conjunction of features (e.g. color and direction), RTs increase linearly with the number of distractors, indicating a serial process that integrates feature information. This integration step is

suggested to be restricted to the attentional focus, e.g. through a spotlight in the master map of locations (Treisman and Gormican 1988; Treisman and Sato 1990; Müller et al. 1995). The FIT model was revised (Treisman and Sato 1990) and made more explicit to incorporate the idea that feature maps exists not only for single features but for whole dimensions. Wolfe (1994) adds in the guided search model (GS) a computational layer as feature maps for specific types (orientation, color etc.) that contain largely independent representations of e.g. the different colors. The interesting part of the GS model is that the "spotlight" of attention originates from feature-dimension specific saliency maps that highlight differences between all feature units. The dimension-specific saliency maps predict the location of feature differences and these may compete for processing at the master (saliency) map level. Wolfe (1994) incorporates the possibility that the stimuli do not have to be known in advance and establishes a bottom-up, feedforward mechanism that explains pop-out target detection in a visual search task. The existence of such domain-specific saliency maps was supported by the finding that the prior knowledge of the feature-dimension of the target item is beneficial for detection (Treisman and Gormican 1988; Müller et al. 1995). The idea that dimension-specific maps compute feature saliency in parallel at a pre- attentive state led to the proposal of a dimension weighting account (DWA). In this account, the dimension-specific maps are weighted through an attentional process, according to the dimension of subsequent targets, such that feature units of this dimension will be amplified and thus receive a benefit at the master map level. It further predicts that weights need to be shifted from one to another dimension if the target dimension is not known. Found and Müller (1996) showed in two tasks, either involving the detection of a feature or the enumeration of items, that the prior knowledge of the target dimension resulted in faster reaction times as compared to the case when this knowledge is lacking. These findings were thought to confirm the assumption that dimension shifting, a time-consuming process, is involved if the target dimension is not known and thus were considered an approval of the predictions of the DWA.

Neurophysiological models of attentional selection

As described above, one of the defining properties of the primate brain is its highly convergent anatomical architecture that results in progressively growing RF sizes. The RF of an MT neuron, for example, integrates information from multiple V1 RFs and is large enough to contain multiple objects in the visual environment that may or may not be of behavioral importance. Thus, at the level of e.g. MT neurons, afferent input delivers a mixture of signals that need biasing in order for the neural code to disambiguate between multiple objects that carry multiple behavioral relevancies.

The normalization model of attention (NMoA; Reynolds and Heeger 2009) proposes an attentional framework that achieves this bias by pooling and weighting the afferent input. The models consists of 3 modules, each organized according to feature preference and RF position. First, a stimulus in the visual vicinity activates a subset of neurons that respond to the location of the stimulus (RF position) and their responses are scaled depending on their feature preference and the properties of the stimulus (feature tuning). This activation map is called the stimulus drive emphasizing the bottom-up nature of the map and may, for example, represent the total afferent input to a downstream neuron. Second, an attentional field that spans the entire stimulus drive map is multiplied point-wise with the stimulus drive, emphasizing attended regions by using higher factors for neurons with RFs in that region. The product of the bottom-up stimulus drive and the top-down attention results in a suppressive drive that is used for normalization. The population response is the division of the stimulus drive by a single factor that represents the pooled activity of the suppressive field. The processes in this model result in a multiplicative enhancement of the response to the attended and preferred stimulus and suppression of all other neurons. Such modulation disambiguates the neural code to the extent that only those neurons increase their response that represent the attended visual object and therefore realizes selection bias. It further provides an explanation for the observation that attention in some cases causes a change in the neural sensitivity and in other cases not.

Neurons in areas V4 and MT were found to increase firing rate without changing their tuning curve, i.e. attention multiplicatively scales the response of single neurons (McAdams and Maunsell 1999; Treue and Martínez Trujillo 1999; Treue and Maunsell

1999). This means that neurons responding to a preferred stimulus or alternatively to a stimulus of high contrast receive larger attentional enhancement than other neurons. If, on the one hand, attention was independent of the stimulus contrast (or stimulus preference for that matter) and only resembles a multiplicative factor, the typical sigmoid contrast response function (CRF) would simply be multiplied by that factor (response gain model). On the other hand, if attention does depend on the bottom-up stimulus properties attention might shift the CRF to lower contrasts effectively increasing sensitivity of the population to intermediate contrasts, while saturating at high contrasts (contrast gain model). These different hypothetical effects of attention would become apparent at intermediate contrasts. Contrast gain predicts large response increases at intermediate contrast, while at low and high contrast no modulation would be expected. Response gain predicts a different pattern where high contrast receives the largest attentional enhancements and the absolute response increases as a function of contrast. While there is evidence for both types of attentional modulation in area V4 and MT (Reynolds et al. 2000; Martinez-Trujillo and Treue 2002) and even evidence for both types in a single study (Williford and Maunsell 2006) a theoretical explanation of its co-existence was lacking. The NMoA solves this discrepancy by arguing that the stimuli and task requirements might determine whether attention scales activation according to response or contrast gain. Neurons might exhibit a tendency towards a contrast gain if attention is oriented towards a larger spatial extent than the stimulus size or alternatively might receive predominantly response gain if the attentional field is much smaller than the stimulus size (Reynolds and Heeger 2009). Herrmann et al. (2010) later showed evidence on the basis of behavioral performance that explicitly supported the view that the stimulus configuration in relation to the size of the attentional field dominated the tendency towards one or the other gain effect while simultaneously monitoring and validating the cortical extend of the attentional field via a complementary neuroimaging experiment.

The concept of communication through coherence (CTC; Fries 2005) incorporates the idea that the effective signal transmission is modulated as a function of selective attention rather than a modulation of the afferent output as described above. Signal transmission between areas can increase its effectiveness if the timing of spikes arriving at the post-synapse is synchronized. If spikes accumulated within short millisecond time

scales at the post-synapse, the probability that the postsynaptic neuron will fire is substantially increased (Niebur and Koch 1994; Singer 1999; Steinmetz et al. 2000; Fries et al. 2001; Kreiter 2001; Taylor et al. 2005). This idea is supported by the findings that gamma-band synchrony (30 – 100 Hz, oscillations that fluctuate at millisecond timescales) increases between pairs of neurons that share the attended RF (Gray et al. 1992; Fries et al. 1997; Friedman-Hill et al. 2000; Maldonado et al. 2000; Taylor et al. 2005; Womelsdorf et al. 2006b; Tochitsky et al. 2014). Furthermore, if attention-dependent effectiveness of signal transmission occurs in an oscillatory (e.g. gamma-band frequency) pattern, the phase difference between the two oscillations is crucial for signal transmission, i.e. spikes should accumulate at sensitive phases of the post-synapse to maximize its impact (Fries 2005; Kreiter 2006; Battaglia et al. 2012). Selection is then mediated by coupling and decoupling afferent inputs to and from the post-synapse by modulating the phase difference between subsequent neural processing areas (Grothe et al. 2012).

A similarly influential concept of a neural mechanism implementing attentional selection is formulated in the Gating-by-inhibition (GBI) theory. At the core of the concept is the idea that signal transmission of a non-relevant subset of neural input is actively inhibited. It is motivated by the observation that neurons representing the non-attended stimulus often synchronize in the alpha band, and alpha band activity has been suggested to reflect local inhibition (Jensen and Mazaheri 2010; Jensen et al. 2012). In this framework, inhibition is maximal at the peak of the alpha oscillation and decreases at the falling flank. At a certain phase (beginning of the “duty-cycle”) inhibition has decreased enough that intrinsic fast local gamma oscillation or spikes for that matter may occur. If alpha power is high, as observed in the non-attended case, higher levels of inhibition will be reached earlier and the length of the duty-cycle is reduced. In such a scenario gamma band activity may only occur during short time intervals, effectively reducing the probability of firing or gamma band synchronization between areas.

Neural correlates of selective attention

The largest body of research in visual neuroscience that associates selective attention with neurophysiological phenomena was conducted in the general context of spatial attention. The effects of spatial attention are manifold, but always result in an effective

saliency increase of the cortical representation of attended sensory content. For example, neurons exhibit higher firing rates (Treue and Maunsell 1996), increase their sensitivity (Martinez-Trujillo and Treue 2002; Williford and Maunsell 2006) and adhere more consistently to the representation of the stimulus in the RF (Wegener et al. 2004) if attention is oriented towards its position. Furthermore, neurons were reported to decrease their susceptibility to neural noise, effectively increasing their signal-to-noise ratio (SNR). Cortical neurons are under the constant influence of afferent input that is independent of the external activation from the RF. This neural noise can originate from distant cortical areas or neighboring columns and feed substantial variability into the activation signal of single neurons. As a consequence, single neurons respond to multiple presentations of a single stimulus with large variations and decrease the reliability of the response to that stimulus. Variability can be averaged out across a large population of neurons if it is independent between neurons, however if neural responses underlie a common variation pooling does not lead to a diminishing of common neural noise. Both, individual and common neural noise can decrease the SNR of the population signals substantially (Shadlen and Newsome 1998; Mitchell et al. 2009; Cohen and Kohn 2011) and were shown to decrease if attention is focused on the receptive field of the involved neurons (Cohen and Newsome 2008; Mitchell et al. 2009; Galashan et al. 2013; Schledde et al. 2017). Furthermore, attention has been shown to modulate the synchrony of neural activity on a millisecond scale (γ- frequency band, ~30 – 100 Hz) within a population of neurons potentially increasing the effectiveness of signal transmission between areas, as predicted by the CTC (Fries 2005). Neurons with overlapping RFs increase coherent oscillatory activity if they represent the attended stimulus (Gray et al. 1992; Fries et al. 1997; Friedman-Hill et al. 2000; Maldonado et al. 2000; Taylor et al. 2005; Womelsdorf et al. 2006b; Tochitsky et al. 2014). Repetitive synchronous spiking activity in a population of neurons was suggested to strengthen the impact on the downstream area as coincident spikes lead to accumulations of spikes at the post synapse (Niebur and Koch 1994; Singer 1999; Steinmetz et al. 2000; Fries et al. 2001; Kreiter 2001; Taylor et al. 2005).

In light of these studies, attention always seems to enhance the activation and functional connectivity of neurons or neural populations whose RF overlap with the

spotlight of attention. However, attention has also been shown to suppress the activity of cortical neurons in order to facilitate processing behavioral relevant information.

Neurons of visual processing pathways have increasingly larger RFs downstream the pathway, a concept that was previously introduce as cortical magnification. If attentional enhancement of neurons would only occur when attention is directed into vs. out of the RF, spatial attention would have only a very poor spatial resolution. In a seminal study by Moran and Desimone (1985), two stimuli were positioned inside the RF of the V4 neurons. One of the stimuli was preferentially processed by the neuron, the other was not. Paying attention to the preferred stimulus always enhanced the firing rate of V4 neurons, while firing rate decreased when attention was directed at the un-preferred stimulus. This decrease went even below the rates exhibited in a neutral condition where attention was directed outside the RF. These findings led to the proposal of the "biased competition" framework that states that attention biases the neuron's activity towards the representation of the preferred stimulus by both suppressing responses to a non-preferred stimulus inside the receptive field and enhancing responses to a preferred stimulus (Desimone and Duncan 1995). Within this framework, attention differentially modulates the responses of neurons even though it is always directed inside the RF and thus achieves a finer resolution than the RF size. Such dynamic changes of the RF were also found in area MT where the RF's location and the spatial extend were biased towards and closer around the attended stimulus (Womelsdorf et al. 2006a, 2008).

Another example of a differential modulation of firing pattern is that the tuning curve of visual neurons is multiplicatively scaled by spatial attention. The tuning curve is commonly referred to as the function that describes the level of activation in relation to the stimulus properties. For example, a direction-selective neuron in area MT will respond to a specific motion direction maximally (preferred direction) and to the opposite direction minimally. Extending the function across other motion directions results in a bell shaped tuning function centered on the preferred direction of the MT neuron (Albright 1984). McAdams and Maunsell (2000) and Treue and Martínez Trujillo (1999) measured tuning curves of neurons in area V4 and MT, respectively, and found that attention modulates the tuning curve in a multiplicative manner. That means that

responses to the non-preferred stimulus were less enhanced than responses to the preferred stimulus or even led to a suppression of responses to non-preferred stimuli (Martinez-Trujillo and Treue 2004).

Both the neural correlates and neural mechanisms that are related to selective attention are highly versatile and draw a complex yet convergent picture of how attention impacts on neural processing of visual content. Within the scope of this thesis I have mentioned some of the physiological findings but do not claim to provide a comprehensive review of all remaining findings that relate spatial attention to physiology.

Neurophysiological models and evidence of non-spatial attention

While the previous neurophysiological models of selective attention evolved mainly from studies that investigate attentional selection from visual space (spatial attention), there are other properties in the visual environment that may require improved neuronal representation. For example, for an object whose most distinct characteristic is its color, it is desirable to increase perceptibility to that specific color when searching for the object in an otherwise heterogeneously colored scene. The ability to direct attention towards a property or feature throughout the entire visual scene is called feature-based attention (FBA). The previously described psychophysical models GS and FIT are both based on a feature-selection mechanism but restrict their impact to the spatial focus of attention.

On a neurophysiological level, FBA has been shown to modulate neural activity also outside of the spotlight of attention. Early evidence for a global effect of FBA on a cellular level was provided by McAdams and Maunsell (2000). They recorded neurons in area V4 and investigated the effect of spatial and spatial + feature based attention. Monkeys were trained on a delayed-match-to-sample task in which two stimuli were presented. One occurred in the RF of the recorded neurons and the other one outside. Monkeys were trained to attend the orientation of the grating and to report whether it changed from sample to match presentations. In one task gratings were identical between presentations inside RF and outside and the measured firing rate differences were only related to whether attention was directed inside or outside the RF. In the other task, the

stimulus inside the RF was the same, but outside the RF was a colored 2D Gaussian. In the attend-inside condition monkeys had to report the same orientation change, while in the attend-outside condition they had to report whether a color change occurred. In this case spatial *and* feature based attention could be applied because attention could be shifted between features (color outside vs orientation inside the RF) and location. Firing rates were quantified as modulations between the attend-into and attend-out of the RF conditions and the authors found that in the second stimulus configuration

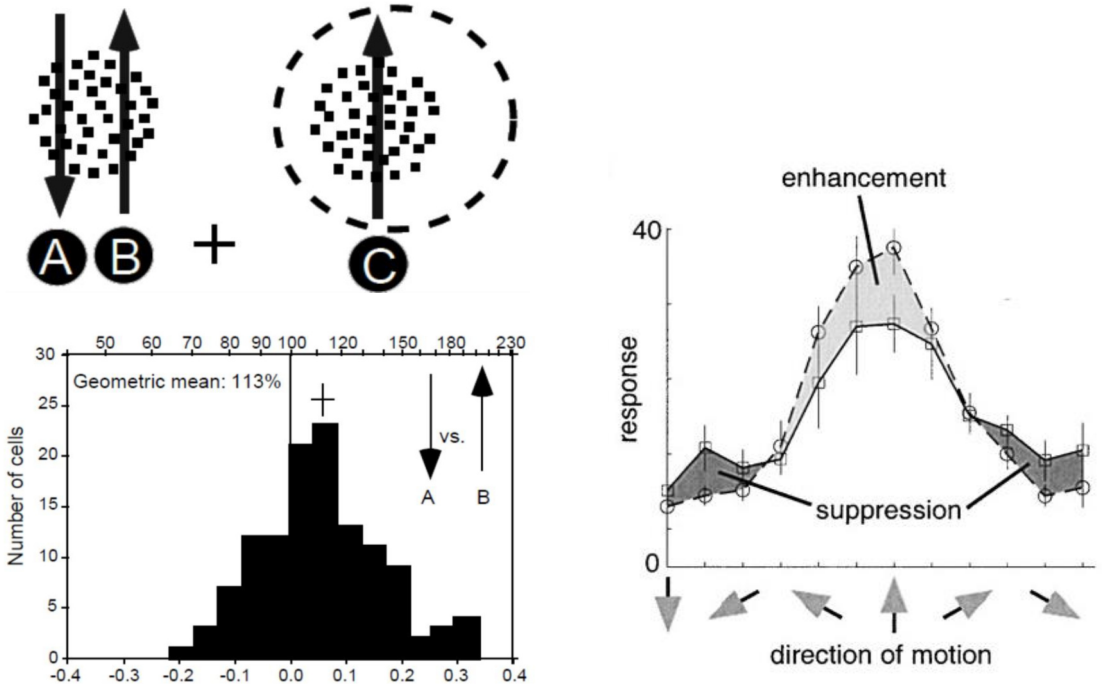

Figure 1 Neural correlates of feature-based attention of cortical neurons of the resus monkey. ***I*** *&* ***II*** *are obtained with permission from* ***Treue S, Martínez Trujillo JC****. (1999) and* ***III*** *from* ***Martinez-Trujillo JC, Treue S****. (2004).* ***I*** *two random dot pattern (RDP) were presented inside (right) and outside (left) the RF of neurons in area MT. Motion of the RDP inside the RF was always into the preferred direction of the recorded neuron(C) while the RDP outside the RF could either move into the preferred (B) or opposite direction (A). The animals attended the stimuli outside the RF and were required to detect a brief change in motion speed. In* ***II*** *the firing rate modulation of 131 MT neurons are displayed. The histogram of modulation indices (A. vs. B.) is shifted to the right and therefore indicates higher firing rates for attending the preferred motion direction (113% increase).* ***III*** *incorporates the finding that neurons that are stimulated with the anti-preferred direction are suppressed if attention outside the RF is directed at the anti-preferred direction (open circles on the left and right side). Together with the enhancement of firing rates if the preferred motion direction is attended and is used for stimulation this led to the definition of the FSGH that constitutes a multiplicative shaping of the tuning curve by FBA.*

modulations were significantly higher. They dissociated this modulation from the

differing stimulus properties and concluded that in the second variant of the tasks two types of attentional modulation, namely spatial and feature-directed attention occurred. Since in the crucial condition attention was paid outside the RF, the data suggest a global, location unspecific effect.

In other studies utilizing neuroimaging and electroencephalography (EEG) techniques it was shown that if attending towards a specific color attribute (e.g. the color: red) neurons that respond to objects at arbitrary positions in the visual field increase their activity if that object matches the attended color (Saenz et al. 2002; Stormer et al. 2014). Similar findings have been reported for shape, orientation and motion direction (Corbetta et al. 1991; Saenz et al. 2002; Liu et al. 2007).

The studies above show that allocating attention to specific features of the visual scene and not only to spatial location mediates attentional enhancement of neural activity that accompanies the impact of spatial attention. Further investigation of this feature directed attention revealed that neural activity of single neurons increase for neurons that prefer to process the currently attended feature attribute (e.g. the color red) (Motter 1994; Treue and Martínez Trujillo 1999; Bichot et al. 2005; Bisley 2011). In particular the work of Treue and Martínez Trujillo (1999) contributed to a, nowadays well established, model that describes the modulation of single neurons if attention is directed to features of a stimulus (Figure 1). They recorded neurons in area MT that were driven by a random dot pattern (RDP) inside the RF and moved into the preferred direction of the neurons. Another RDP outside the RF was presented and moved either in preferred or anti-preferred direction. The animals were required to detect motion changes in the RDP outside the RF. If they attended an RDP that moved into the preferred direction of the recorded neuron firing rates were higher than in the case when they attended a RDP that moved into the anti-preferred direction. In a later study they found that neurons that prefer the opposite, unattended stimulus feature attribute were even suppressed (Martinez-Trujillo and Treue 2004). The resulting attentional gain can be described as a multiplicative factor of the tuning curve of single neurons and is termed through rest of the thesis as feature-similarity gain (FSG) (but see Figure 1).

The FSG hypothesis describes the suppression of neurons that preferentially process stimulus attributes that are not attended. For example, an MT neuron that is driven by

its preferred motion direction will be suppressed if the opposite motion direction is attended. In particular this property of the FSG counteracts the ability of the visual system to detect changes in the visual environment. This is because neurons that do not preferentially process the momentary feature of the visual stimulus are substantial for the expression of transient responses towards changes of the stimulus. Traschütz et al. (2015) investigated MT transient responses towards accelerations and deceleration of a motion stimulus and found that the transient response exceed the response that would be expected from the firing rate that was observed during a sustained response to the new speed. While the sign of the speed change was preserved, the magnitude of the transient response exceeded the rates that were expected from the tuning properties of the neurons. Interestingly, this increase in magnitude was highest for neurons that did not preferentially process the motion speed preceding the change. Therefore, the data suggest that the population transient response carrying information of the speed change are carried mainly by neurons sup-optimally tuned to the speed before the change. If the feature-attribute, in this case speed, is attended, rates of the neurons most informative of a potential subsequent change of the stimulus are suppressed. The detection of perturbations or changes in the visual environment, however, is often vital for successful behavior or survival. Thus, it is unlikely that attentional facilitation occurs only for neurons that are well tuned to the currently attended feature attribute, but will include neurons that have a different feature preference. Such a mechanism would constitute attentional facilitation that targets processing units of entire feature domains.

The notion that attention can be directed to entire feature domains or dimensions was established already in the previously described DWA and has received psychophysical evidence (Found and Müller (1996), but see chapter "Attention and visual search"). Neurophysiological evidence was provided in several human EEG studies (Pollmann et al. 2000; Gramann et al. 2007, 2010; Gledhill et al. 2015) and neuroimaging studies (Chawla et al. 1999; Pollmann et al. 2006). For example, Gledhill et al. (2015) investigated the spatial temporal profile of the selection negativity period of the event related potential (ERP). Using a large body of different stimuli and stimulus combinations, attention was either directed to the feature attribute or towards the feature dimension. The analysis showed that the two types of attentional deployment

were accompanied with two distinct spatio-temporal profiles. Dimension-specific modulation of selection negativity originated from frontal electrodes and temporally preceded the modulation of the selection negativity related to feature-attribute specific attention at occipital electrodes.

However, feature-dimension based attention (FDBA) has so far not received evidence on a cellular level. Chen et al. (2012) directly investigated whether neurons in area MT receive facilitation if attention is directed to the feature dimension motion, as this is the dimension that MT neurons prefer. In their task, monkeys had to detect and report either the motion direction or color of a moving grating presented in their receptive fields. 22% of their recorded neurons were modulated by attending one particular feature combination of the stimulus and were thus termed feature-selective. Of these, an almost identical fraction of neurons received either attentional facilitation if attention was directed to the motion direction of the stimulus or if directed to the color of the stimulus. The data therefore did not reveal conclusive evidence about whether the entire MT column receives attentional facilitation, if the feature dimension that is preferentially processed, is attended. Likewise, Katzner et al. (2009) found no evidence that FBA in area MT is modulated in a dimension-specific manner. In this study, monkeys were trained to attend colored random dot patterns (RDP) that moved in either the preferred or anti-preferred direction of the recorded MT neurons. In the crucial condition, monkeys attended outside the RF onto a grating moving into preferred vs. anti-preferred direction. The task was either to detect the color or the motion direction of the RDP. Using the presentation of the preferred and anti-preferred direction, they could quantify the FSG of the recorded neurons and the difference of FSG between tasks. FSG in this study was not modulated between the two tasks, which led the authors to conclude that neurons in area MT receive attentional facilitation independent of the attended feature dimension.

In Chapter II of this thesis I further investigates the hypothesis that motion selective neurons in area MT receive attentional facilitation that is specific to the attended feature dimension. Contrary to the two mentioned studies we do find that neurons in area MT increase firing rate if motion direction in contrast to color is the behaviorally relevant image feature. We furthermore show that this modulation is independent of

the precise tuning function of the neurons and that this modulation is evident already at the beginning of the trials preceding visual stimulation. In the appended original manuscript in Chapter II, we also discuss differences between our study and others and elaborate on potential causes that lead to different results and conclusions.

Neural correlates of attention-dependent behavioral performance

As humans, we rely mainly on visual perception in our daily live. Most actions are based on decisions that are deduced from context and sensory evidence, often visual evidence. Thus, for any action it is vital that sensory evidence originating in visual cortex is transmitted along cortical processing pathways to reach motor and decision-making cortical areas. Trial-to-trial variations of the communication between the involved neural populations must therefore lead to trial-to-trial variations in the speed of the execution of the resulting actions. In the visual domain, these variations can be quantified in psychophysical experiments were fast reactions to a particular visual stimulus are required, for example in a Posner paradigm (Posner et al. 1980) (see above). The observed differences in RT typically result in a Gaussian distribution and occur on a sub-second timescale. Given that brain anatomy does not change on these timescales, trial-wise fluctuations in RT must therefore arise from fluctuations in neural functions. As described earlier, visual attention governs neuronal functionality and was shown to do so on timescales that concur with behavioral timescales, e.g. attention reduces perceptional thresholds leading to reduced RT (Posner 1980; Pashler and Sutherland 1998; van der Heijden 2003). It is therefore a plausible assumption that fluctuations in the mechanism that underlie visual attention are causally related to fluctuations in RT.

A number of studies have indeed shown that the neuronal mechanism that are also related to visual attention do correlate with the perceptibility of visual stimuli and are thus fundamental for behavioral RT.

For example, MT transient firing is related to the perceptibility of visual stimuli as was shown by Galashan et al. (2013). In this study, monkeys performed a change-detection task that required to detect and respond to an acceleration of a moving grating presented inside the receptive field of MT neurons. The recorded MT neurons

responded with sharp transient increases towards the speed change of the stimuli. Monkeys were instructed to attend and respond to the speed change in the RF of the neurons. By calculating the latency of the transient responses, the authors found that in trials resulting in fast reaction times, the latency of the response was shorter as compared to longer RT trials. This relation was evident although the firing rates preceding the transient was not predictive of reaction time. Furthermore, the trial to trial variability measured as the Fano Factor (FF) decreased for fast RT trials. The FF quantifies the reliability of neurons responding to repetitions of the same stimulus and is also known to decrease with attention (see "Neural correlates of selective attention").

Furthermore, the mere sustained firing rate of visual neurons, a quantity that is typically also related to attention (see "Neural correlates of selective attention"), is related to the perceptual decision. Britten et al. (1996) showed that the behavioral choice of the monkeys was significantly related to the firing activity of MT neurons processing the attended stimulus. Monkeys were presented with a random dot pattern (RDP) in the RF of the recorded neuron while varying the coherent motion, i.e. varying the perceptibility of the motion signal. Motion could be in either the preferred direction of the recorded neuron or in the anti-preferred direction and the monkeys were trained to judge and report motion direction. The authors made use of the fact that, at near threshold coherent motion, the perception of the motion direction underlies strong variations and the perceptual judgements varied accordingly. Choice probabilities, a measure that relates spiking activity on a trial-to-trial basis to the monkey's decision, were calculated and showed a significant relationship between the firing of MT neurons and the monkeys' decision. In other words, if a direction-selective neuron on a given trial increased its firing rate, the decision of the monkey for near threshold motion was biased to the preferred motion direction of the neuron. Choice probabilities of single neurons was modest but highly significant in the entire population of neurons recorded. This suggest that MT population activity is indeed fundamental for the perception of motion signals in the visual field.

Moreover, the temporal synchronization of local neuronal population, a network functionality that is related to attention-dependent facilitation of information routing, has been shown to vary in correspondence to trial-wise RT fluctuations. Womelsdorf et

al. (2006) investigated the relationship between RT and the temporal synchronization of large populations of neurons in area V4. Again, monkeys were presented with a moving grating and were trained to react to a subtle color change at the spatially cued position. In this study, both the gamma-band power of the local field potential (LFP) and the temporal synchronization of spikes to the gamma oscillation in the LFP, quantified as spike field coherence (SFC), were investigated. They found that previous to the color change both gamma band power and SFC were increased in trials resulting in fast RT as compared to trials resulting in slower reaction times. Additionally, they could correlate RT and SFC on a trial-by-trial basis and found significant correlations. Similar to Galashan et al. (2013), firing rates previous to the change event were unchanged. Their data suggest that the phase-synchronization within area V4 between input (LFP) and output (spikes) signals increases in trials that result in short RT. Although this is not a direct proof of increased signal transmission between areas, inter-areal phase-synchrony is predicted by the CTC. Thus, the results support the notion that fast signal processing, i.e. during trials resulting in fast RT, underlies efficient and powerful signal transmission between visual areas as predicted by the CTC if phase-synchrony is high.

Along these lines, Ni et al. (2016) investigated the role of the particular gamma phase in the context of attention-dependent information routing and suggest the it is important for and correlative to behavioral RT. The authors used a similar paradigm as the two former studies and animals were trained to detect a color change of a moving grating. The multi-unit activity (MUA) and local field potentials were analyzed at an estimated time point that designates the arrival time of the stimulus change-induced pre-synaptic inputs. The phase of the visually induced gamma oscillation correlated with the peak MUA response to the stimulus change, suggesting that the precise gamma phase that occurred at the pre-synaptic input time is determinant of the following expression of the transient response. Furthermore, they could show that the resulting RT of the trial likewise correlated with the estimated gamma phase.

In summary, the above mentioned studies indicate first, that neural responses even of single neurons but also of populations of neurons, can be directly related to the perceptibility of the information that they represent. Second, they deliver evidence that the transient response to a behaviorally relevant stimulus change carries stimulus

information up to the degree that the characteristic of the transient response is correlative to the perceptibility of the stimulus information. Third, that during the time interval preceding the relevant event, phase-synchrony and phase information in the gamma band may underlie the ability of neurons to produce fast output signals that impact on conscious perception.

In Chapter III of this thesis I contribute to the investigation of neural mechanism that underlie fast and efficient stimulus processing. I present unpreceded evidence for a crucial role of the temporal modulation of the gamma band activity by a low frequent oscillation present in area MT and V1. I utilized the same experimental paradigm as in the study of Galashan et al. (2013) and found that gamma spindles occur predominantly at specific phases of an alpha-band oscillation in a time interval preceding the relevant speed change. I found that the specific phase to which gamma-band amplitude is coupled is predictive of RT. I furthermore replicate and approve of the finding that firing rates in that time interval was not related to RT, while the shape of MT transient responses did relate to RT. The data suggest that the temporal coordination of gamma spindles relative to an alpha oscillation across visual areas may be substantial for the processing of relevant image information and even be a prerequisite for the emergence of coherent gamma activity. In Chapter III, the, yet unpublished, manuscript of the article is appended.

Chapter II: Task-specific, dimension-based attentional shaping of motion processing in monkey area MT

Authors: Bastian Schledde, F. Orlando Galashan, Magdalena Przybyla, Andreas K. Kreiter, Detlef Wegener

Affiliation: Brain Research Institute, Center for Cognitive Sciences, University of Bremen, P.O. Box 33 04 40, 28334 Bremen, Germany

Author contributions: D.W. and A.K.K. conception and design of research; B.S., F.O.G., and M.P. performed experiments; B.S. and D.W. analyzed data; B.S. and D.W. interpreted results of experiments; B.S. and D.W. prepared figures; B.S. and D.W. drafted manuscript; B.S., F.O.G., M.P., A.K.K., and D.W. approved final version of the manuscript.

Publication: Schledde B, Galashan FO, Przybyla M, Kreiter AK, Wegener D. Task-specific, dimension-based attentional shaping of motion processing in monkey area MT. *J Neurophysiol* 118: 1542–1555, 2017.

Abstract

Non-spatial selective attention is based on the notion that specific features or objects in the visual environment are effectively prioritized in cortical visual processing. Feature-based attention (FBA) in particular, is a well- studied process that dynamically and selectively addresses neurons preferentially processing the attended feature attribute (e.g. leftward motion). In everyday life, however, behavior may require high sensitivity for an entire feature dimension (e.g. motion), but experimental evidence for a feature dimension-specific attentional modulation on a cellular level is lacking. Therefore, we investigated neuronal activity in macaque motion-selective medio-temporal area (MT) in an experimental setting requiring the monkeys to detect either a motion change or a color change. We hypothesized that neural activity in MT is enhanced when the task requires perceptual sensitivity to motion. In line with this, we found that mean firing rates were higher in the motion task, and response variability and latency were lower as compared to the color task, despite identical visual stimulation. This task-specific, dimension-based modulation of motion processing emerged already in the absence of visual input, was independent of the relation between the attended and stimulating motion direction, and was accompanied by a spatially global reduction of neuronal variability. The results provide single cell support for the hypothesis of a feature dimension-specific top-down signal emphasizing the processing of an entire feature class.

New & Noteworthy

Cortical processing serving visual perception prioritizes information according to current task- requirements. We here provide evidence in favor of a dimension-based attentional mechanism addressing all neurons that process visual information in the task-relevant feature domain. Behavioral tasks required monkeys to attend either color or motion, causing modulations of response strength, variability, latency, and baseline activity of motion-selective monkey area MT neurons irrespective of the attended motion direction but specific to the attended feature dimension.

Introduction

Neuronal processing of visual information strongly depends on the observer's perceptual requirements (Huk and Heeger 2000; Jack et al. 2006; Chen et al. 2008). Among the several mechanisms involved in this selective, goal-directed processing, feature-based attention (FBA) plays a key role by facilitating the processing of a specific feature in the visual environment, independent of the spatial focus of attention (Maunsell and Treue 2006; Bisley 2011). Evidence from human neuroimaging and EEG studies shows that attending to, for example, a specific color hue elevates the neuronal response to an object at a remote, unattended location if its color matches the currently attended hue, but not if this object is composed of another, unattended hue (Saenz et al. 2002; Stormer et al. 2014). Corresponding findings have been reported for attention directed to a specific motion direction, shape, or orientation (Corbetta et al. 1991; Saenz et al. 2002; Liu et al. 2007).

Monkey neurophysiological studies investigating the neuronal substrate of this feature-specific response facilitation found that at the level of single cells, FBA is characterized by a firing rate (FR) change of neurons well-tuned to the attended feature attribute. For example, attending towards a specific motion direction globally increases the response of direction-selective MT neurons with a tuning preference for the attended direction (Treue and Martínez Trujillo 1999). The same neurons' responses might be unmodulated (or even weakened) if attention is allocated on a motion direction that is significantly deviating from their preferred direction (Martinez-Trujillo and Treue 2004). This feature-similarity gain (FSG), along with its spatially global effectiveness, has been suggested to underlie our ability to actually focus on the portion of the visual input that is behaviorally relevant, and, at the same time, disregard irrelevant, distracting information (Maunsell and Treue 2006; Bisley 2011; Carrasco 2011).

In a rapidly changing perceptual environment, however, successful behavior critically depends on the ability to quickly perceive abrupt changes of sensory input. In area MT, abrupt changes in motion induce strong, transient firing rate changes (Price and Born 2010, 2013), which in turn correlate with measures of perceptual performance (Masse and Cook 2008; Herrington and Assad 2009; Galashan et al. 2013; Traschütz et al. 2015). On the population level, these transients are carried substantially by neurons that are

sub-optimally tuned to the stimulus feature preceding the feature change (Traschütz et al. 2015) – hence, the population response relies significantly on neurons not addressed, or even suppressed, by FSG. We hypothesized, therefore, that under behavioral conditions requiring detection of changes in visual input, attentional facilitation is unlikely to be limited to the sub-class of neurons well-tuned to the currently attended feature attributes (which provide only minor information about the change), but will address all neurons processing information about the attended feature dimension, including those without a tuning preference for the currently attended feature attributes. Such a feature dimension-specific weighting of neural responses is supported by evidence from psychophysics (Müller et al. 1995; Found and Müller 1996), human EEG (Pollmann et al. 2000; Gramann et al. 2007, 2010; Tollner et al. 2008; Gledhill et al. 2015), and neuroimaging studies (Chawla et al. 1999; Weidner et al. 2002; Pollmann et al. 2006), but has not gained experimental support by single cell studies (Katzner et al. 2009; Chen et al. 2012), such that its underlying neuronal mechanisms remain unknown.

To address this issue, we trained monkeys on two variants of a change detection task and performed extracellular recordings in area MT. In the first task, monkeys were required to detect speed changes - a feature MT neurons are highly sensitive to (Nover et al. 2005; Traschütz et al. 2015). In the second task, monkeys were required to detect color changes – a feature for which MT is only weakly sensitive (Croner and Albright 1999; Thiele et al. 1999). When comparing the neuronal representation to physically identical motion and motion change stimuli as a function of spatial attention, motion direction, and task requirements, we found that MT neurons were responding significantly different in the speed and in the color task, at the level of both evoked and spontaneous activity. Notably, this modulation was not only independent of the spatial focus of attention, but also independent of the relation between the attended and the preferred motion direction of a neuron, affecting neurons also when they were not tuned to the attended motion direction or speed. These results suggest a highly flexible, task-dependent shaping of motion processing.

Material and Methods

Electrophysiological recordings

All surgical and experimental procedures followed the Regulation for the Welfare of Experimental Animals issued by the Federal Government of Germany, and were approved by the local authorities. Extracellular recordings were obtained from two male adult rhesus monkeys (*Macaca mulatta*) using tungsten microelectrodes (0.8 - 5 MOhm, 125 µm shank diameter; Frederic Haer, Bowdoin, ME). Surgery was performed under Propofol/Fentanyl anesthesia and strictly aseptic conditions, as previously reported in detail (Wegener et al. 2004). The recording chamber was placed over the middle temporal sulcus; coordinates for electrode penetrations were estimated from structural magnetic resonance imaging scans. During recordings, area MT was identified by the high proportion of direction selective neurons, the size/eccentricity ratio of RFs and the depth of the recording site (Maunsell and Van Essen 1983; Desimone and Ungerleider 1986; Mikami et al. 1986). The amplified electrode signal was sampled at a frequency of 25 kHz and band-pass filtered between 0.7 and 5 kHz, using either a custom-made hardware filter or an equiripple FIR filter in forward and reverse direction. Online detection of spikes was achieved by thresholding. At the beginning of each recording session, one or two electrodes were lowered through a guide tube penetrating the *dura mater* until the electrode's tip reached the desired depth in area MT. Prior to cell recordings, the tissue was allowed to settle for about 30 min.

Visual Stimulation

Visual stimuli were presented on a 22 inch CRT monitor (1280 × 1024 pixels, 100 Hz refresh rate), placed 80 cm from the animal. Stimuli were shown on a grey background (luminance: 10 cd/m²) and consisted of two high-contrast, drifting Gabors (spatial frequency: 2 cycles/deg), enveloped by a Gaussian with 0.75 deg at half height. Gabors had a mean luminance of 10 cd/m² and drifted with 2.17 deg/sec. Speed and color changes were achieved by abruptly increasing the speed to 4.17 deg/sec or changing the color to an isoluminant pale yellow. Eye-movements were monitored with a custom-

made eye-tracking device with a spatial resolution of 0.2 deg. Prior to cell recordings in the behavioral paradigms, monkeys performed a dimming task at fixation to determine basic response characteristics of each unit. RF size and location were mapped manually using a moving bar. If two electrodes were used simultaneously, we searched for units with largely overlapping RFs. Each units' direction tuning was measured using Gabor gratings moving into one of 24 different directions, and preferred direction was estimated prior to recordings in the main experiment by calculating the mean response vector of the unclustered data.

Behavioral task

Monkeys were trained to perform two variants of a feature-change detection task (Figure 2 *A*). They had to attend either inside or outside the RF or the recorded unit, and were required to detect either a speed or a color change. This 2*2 design allowed gathering data under the four experimental conditions illustrated by the inlet in Figure 2 *A*. The monkey initiated a trial by maintaining fixation on a central fixation point (0.14° side length) and pressing a lever. The color of the fixation point indicated the task type (red: speed-change detection, yellow: color-change detection). 1050 ms after lever press (or 350 ms for some recording sessions), a rectangular spatial cue indicating the location of the behaviorally relevant stimulus was displayed for 500 ms and outside the RF of the recorded neuron(s), followed by a 500 ms delay period. Subsequently, two static Gabor gratings appeared simultaneously. One grating was placed inside the RF and the other one at a mirror-inverted position in the opposite hemifield. 200 ms later, both gratings started to move intrinsically. If we recorded from two electrodes at the same time, the stimulus was placed in the joint RF of the units and motion direction of the RF stimulus was chosen to drive one of the recorded units with its preferred direction. If neurons had very different preferred motion directions, we chose a motion direction capable to drive both units efficiently. Thus, for a number of neurons we obtained data following stimulation with motion directions deviating to some degree from their preferred motion direction. Motion direction of the stimulus outside the RF was in opposite direction. Thus, when the monkey attended to the Gabor outside the RF, the recorded neuron responded to a stimulus that was unattended both in terms of spatial

and feature-based attention (since the attended direction was 180 deg away from the direction presented to the neuron). As a consequence, when comparing the neurons' responses depending on whether attention was directed towards or away from the RF, the response difference is likely due to both attended spatial location and attended motion direction. In the remainder of the article, we will refer to this as to the spatial condition (SC). In contrast, task-related response differences not explained by SC (responses to the same spatial location and the same motion direction in the speed- and color-change task) will be referred to as the task condition (TC).

Following motion onset, monkeys had to attend the cued location and feature dimension and to signal detection of the target event (either a speed or a color change) by releasing the lever within 150 ms to 750 ms after the stimulus change. Target events occurred pseudo-randomly between 660 ms and 5500 ms after motion onset. Prior to these changes, up to three distractor events may have occurred, all of which had to be ignored. These distractor events consisted of a change in the currently relevant feature dimension at the uncued location, and/or a change in the irrelevant feature dimension at the cued and/or the uncued location. Their number and sequence varied pseudo-randomly. These trials increased the attentional demand for the monkeys and allowed us to verify that they were following the cue instructions. Throughout the trial and until 300 ms following the lever release, monkeys had to keep fixation within a circular eye window of 2 deg diameter, centered on the fixation point. To support selective attention to the relevant feature dimension (instead of more global attention to any change at the attended object), the speed-change task and the color change task were presented block-wise. The task order was alternated between recording sessions. Within a block, the two spatial conditions of each task type were fully interleaved. We aimed to collect 25 successful trials for each of the four experimental conditions during which the speed change at the RF location was the first change event. This was behaviorally relevant only in the attend-in condition of the motion task, but irrelevant during the color task and the two attend-out conditions. Because they allowed comparing the different attention conditions in response to identical visual stimulation, only these trials entered data analysis. About 30% of all trials were catch trials. These were disregarded for analysis.

Data analysis

Data were analyzed using Matlab R2011b and later releases (The MathWorks, Natick, MA), using both in-built and custom-made functions. Spikes were detected and sorted semi-automatically as previously described in detail (Galashan et al. 2011). Spike thresholds were set by four times the median of the absolute values of the high-pass filtered signal (Quiroga et al. 2004), where applicable, otherwise by three times the signal's SD. Occasionally, these thresholds had to be corrected manually. Preferred motion direction and significant direction tuning of the spike-sorted data were estimated offline using a response reliability approach (Grabska-Barwińska et al. 2012).

We collected data from 303 units, for which we obtained a sufficient visual response (> 1 SD above spontaneous activity and > 10 Hz) and at least 10 trials per experimental condition (mean: 25.1). 61 (20%) of these were excluded from data analysis due to slow electrode drifts over the course of the session. Electrode drifts were identified based on lab notes during recordings and careful visual inspection of the data, as well as by semi-automated procedures taking the mean FR over the course of the session into account. From the 243 remaining units, another 56 were not analyzed because they did not fulfill all of the following inclusion criteria: i) behavioral performance in both tasks above 75% (14%), ii) significant direction tuning (5%), iii) deviation between stimulating and preferred motion direction below 90 deg (3%). The final dataset consisted of 187 units gathered in 130 recording sessions. For 116 of these units, their preferred direction was within 15 deg of the stimulating motion direction (mean deviation: 7.1 deg), estimated by offline analysis of the spike-sorted data. For the remaining units, preferred and stimulating motion direction differed between 15.4 – 72.5 deg (mean: 30.9 deg, $N = 71$). All results derived from the entire database hold true if considering only units stimulated within 15 deg of their preferred motion direction.

Spike-density functions (SDF) were calculated within a 100 ms time window, shifted by 1 ms and smoothed by a Gaussian kernel (σ = 20 ms). Population responses were computed by subtracting each neuron's mean baseline activity from its response, normalizing the response to the mean FR of all conditions during the period 400 ms prior to the speed change, and averaging over the normalized responses of all individual units. Modulation indices (MI) were defined as:

$$MI = \left(\overline{FR}_{cond1} - \overline{FR}_{cond2}\right) / \left(\overline{FR}_{cond1} + \overline{FR}_{cond2}\right)$$

Cond1 and *cond2* relate to each unit's pool of trials from the speed change and the color-change task, respectively, for investigating task-specific response differences (Task condition index, TCI), and, analogously, to each unit's pool of trials from the attend-in and attend-out conditions for investigating the combined effect of spatial and direction attention (Spatial condition index, SCI).

Response latencies were calculated as the point in time at which the transient FR increase following the speed change reached 75% of its maximal peak (Galashan et al. 2013). Peak responses were required to occur between 20 and 300 ms after the speed change. Latencies were only calculated for units responding with a significant FR increase to the acceleration of the motion stimulus in each of the four experimental conditions (Wilcoxon signed rank, $\alpha < 0.05$, $N = 87$). To investigate whether systematic differences in response latencies were independent from the magnitude of the transient speed-change response, we performed a rate-matching procedure by randomly searching for combinations of 10 trials per unit having the same transient peak rate in each of the two conditions to be compared (e.g. same peak rate in the speed and color task with attention allocated towards the RF). We found such trial combinations for 84 – 86 out of the 87 neurons with significant post-change transients in each experimental condition.

Trial-to-trial variability was measured by calculating the Fano factor (FF, mean normalized variance of spike counts) in successive, non-overlapping time windows during the 250 ms prior to the speed change. Window width varied between 5 ms and 125 ms, increased stepwise by 1 ms. For each width, the FF is reported as the mean of all windows. To investigate whether FF effects depended of FR differences between conditions, we performed another rate-matching procedure by searching for groups of 10 trials per experimental condition and unit for which the mean absolute FR did not differ by more than 1 Hz. This was done for successive, non-overlapping 50 ms windows during the 250 ms period starting before the speed change. For each of the windows, we found such trial combinations for at least 174 of 187 units, and 182 neurons were considered for the statistical analysis of the pre-change epoch, during which FRs were relatively stationary.

Spike-count correlations (SCC) were computed for 38 pairs of simultaneously recorded units, using the same integration windows as for the FF. We only considered units recorded at different electrodes. For each pair, the raw spike counts were converted to z-scores, and the SCC was calculated as the Pearson correlation of z-scores across trials. Since this measure is sensitive to outliers, we excluded data segments which were above 3 SD of the mean of a given window and unit.

To investigate whether response differences between the four experimental conditions depended on the similarity between the neurons' preferred features and the actual stimulus properties, we extracted the 50% of neurons from our database for which stimulus motion direction and speed were least optimal. To this end, we first calculated the deviation Δ_ϕ between stimulus direction ϕ_{stim} and a unit's preferred direction ϕ_{pref} as their absolute difference:

$$\Delta_\phi = \left|\phi_{pref} - \phi_{stim}\right|$$

For speed preference, we considered the transient FR change following the speed-up of the stimulus as an indicator for the mismatch between stimulus speed and preferred speed. Large positive transients only occur for neurons with a preferred speed clearly above the stimulating speed before the change (Traschütz et al. 2015), thus indicating neurons with a speed preference substantially deviating from the speed of the stimulus. The transient's amplitude for each neuron was calculated by dividing the mean FR during the 250 ms after the speed change by the mean FR during the 250 ms before the speed change, taken from the attend-in speed task:

$$T_A = \overline{FR_{post}}/\overline{FR_{pre}}$$

For the identification of neurons with non-matching feature preferences, neurons were ranked according to both their Δ_ϕ value and their T_A value. We then sorted all neurons by the sum of their ranks and distributed them to two groups of 'units with least-matching tuning' and 'remaining units' by splitting across the median.

To quantify the amount of explained variance for the relevant response variables (time, spatial condition, task condition, and interaction of spatial and task condition) and to reconstruct the time course of task-specific response modulation, we performed

demixed principal component analysis (dPCA) (Brendel et al. 2011; Kobak et al. 2016). Demixed PCA was run using the original Matlab code as provided by the authors (https://github.com/machenslab/dPCA). In contrast to standard PCA, dPCA considers the data labels such that principal components depend on stimulus and task parameters, and allows demixing of data with arbitrary combinations of parameters. In our experiments, these parameters correspond to the stimulus-dependent neuronal response over time *T*, the two spatial conditions *SC*, and the two task conditions *TC*. The number of available data points *X* can be thought of as a *SC*-by-*TC* dimensional trajectory of length *T* in *N*-dimensional space, where *N* corresponds to the number of recorded units. By considering the labels of each data point, dPCA decomposes *X* into independent parts to estimate the variance attributable to one of the parameters *T*, *SC*, and *TC*. Thus, X_T captures the variance due to stimulation over time, independent from spatial and task condition, while X_{SC} captures the variance due to spatial condition that cannot be explained by X_T. In turn, X_{TC} describes the variance due to task conditions that cannot be explained by time and spatial condition, and $X_{SC/TC}$ describes the variance due to interaction between spatial and task condition that is not explained by the previous parameters. Since dPCA requires the same number of time bins *T* for all trials, the steady-state response between 200 ms after motion onset and 200 ms before the speed change was re-stretched to 260 time bins for each trial (cf. Kobak et al. 2016). For the shortest trials, this conformed to the original SDF resolution of 1ms/bin; for the longest trials each bin represents the SDF over a period of 4.4 ms. After re-stretching, each trial was described by a vector of 910 bins, lasting from motion onset to 250 ms after the speed change. To avoid overfitting, dPCA on each of the datasets was performed by adding a regularization term λ, as described in Kobak et al. (2016).

Statistics

Statistical analysis was performed using non-parametric tests (balanced Friedman test, two-sided Wilcoxon signed rank test). Confidence intervals (CI) were obtained by bootstrapping the data with 5000 re-samples using the bias-corrected and accelerated percentile method (Efron and Tibshirani 1994; DiCiccio and Efron 1996). For dPCA, periods of significant classification were computed by 100 iterations of stratified Monte Carlo leave-group-out cross-validation, as implemented in Kobak et al. (2016).

Behavioral task and performance

Monkeys were trained on two variants of a feature-change detection task, and neuronal processing in area MT was investigated as a function of task requirements, attended

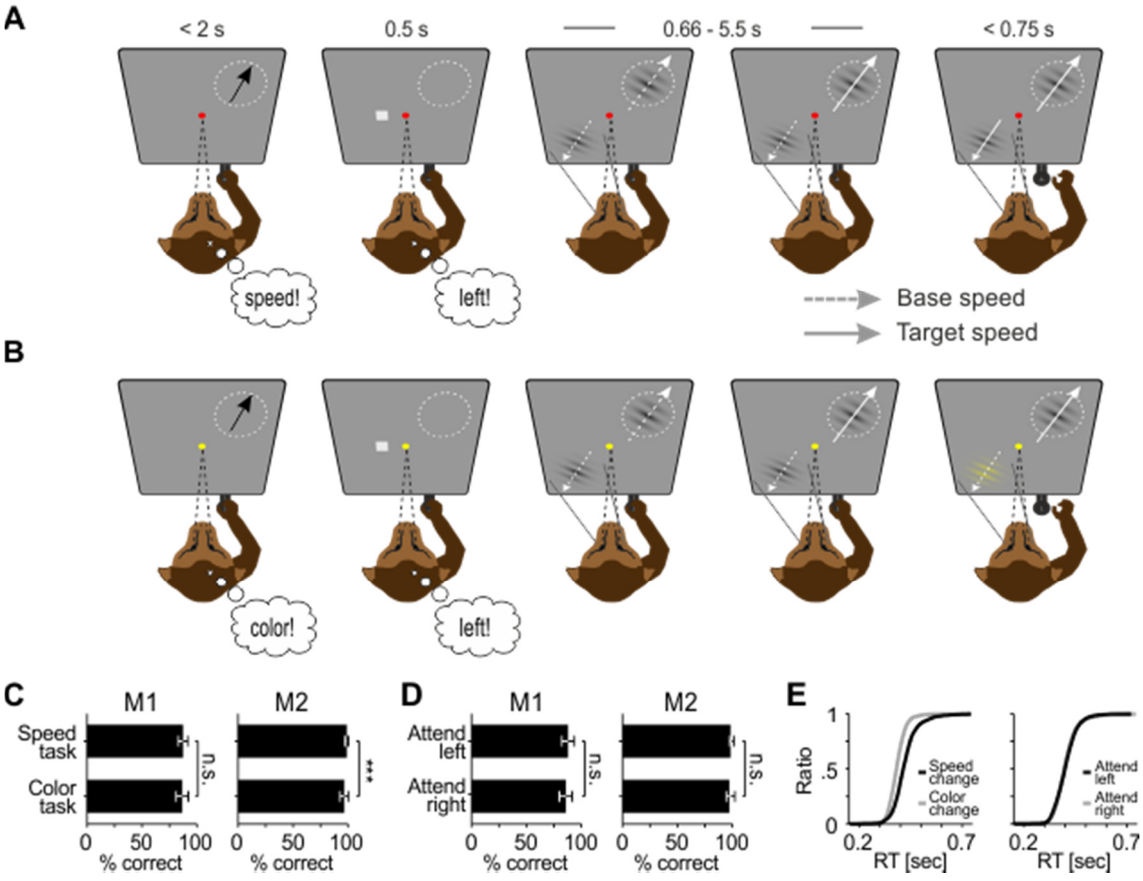

Figure 2 Behavioral paradigm and performance. A and B: Example trials of the speed-change task (A) and the color-change task (B). Task type was indicated by the color of the fixation point. Monkeys were required to detect a change of either the speed or the color at the cued location and to ignore any other change. Fixation had to be kept until 300 ms after releasing the lever (see Material and Methods for detailed information). Circle, RF of the recorded neuron; black arrow, preferred direction; White dashed arrow, motion direction at base speed; white straight arrow, motion direction at increased speed; thin dashed line, gaze direction; bold dashed line, direction of spatial attention. Note that visual stimulation is identical across tasks until the first change (here: RF stimulus speed-up, fourth panel from left in both tasks), and only this period was used for data analysis. C and D: Mean performance (correct responses/sum(correct responses, false alarms, misses)) of monkey M1 and M2 regarding task type (C) and spatial condition (D). Note that with attention directed to the RF stimulus, the monkey attended towards the preferred motion direction of the recorded neuron, while with attention away from the RF it attended a motion direction 180 deg opposite to it. E: Cumulative reaction time distributions of all trials, sorted by task type (left panel) and spatial condition (right panel).

motion direction, and spatial deployment of attention (Figure 2 *A* and *B*). In both variants of the task, stimuli consisted of two grey Gabor patches with inherent motion. One Gabor was placed inside the RF of the recorded unit while the other one was inversely mirrored across the fixation point. The monkeys' task was to detect either an instant 100% speed change or a sudden isoluminant color change to yellow. Each trial started with the appearance of a fixation point, indicating the task type by color (yellow: color task, red: speed task), followed by a spatial cue to signal target location (0.5 s). With a delay of 0.5 s, the two Gabors appeared simultaneously and started to move 0.2 s later. The Gabor within the RF moved approximately in the preferred direction of the recorded unit, and the other one moved in opposite direction. Color and speed changes occurred at pseudo-random points in time 0.66 s to 5.5 s after motion onset. They had to be ignored by the monkeys unless they were cued. The rationale of this 2*2-design was to implement two different task conditions that direct attention either towards or away from the motion domain, at a location inside or outside the neuron's receptive field (RF). Because of the opposite motion directions, the RF stimulus was unattended in terms of both spatial location and motion direction when monkeys attended outside the RF, allowing to investigate an experimental condition for which FSG does not apply. The speed- and the color-change task were presented block-wise and the order of blocks was balanced over recording sessions, while spatial conditions were fully interleaved. Monkey 1 performed both tasks with 87% accuracy, with no statistical difference between tasks (Friedman test, $\chi^2(1) = 0.88$, $P = 0.35$, $N = 53$). Monkey 2 made extremely few errors and performed the speed and the color task with 99% and 97%, respectively, which nevertheless was statistically different ($\chi^2(1) = 15.03$, $P < 10^{-3}$, $N = 77$) (Figure 2C). For neither monkey there was a significant performance difference with respect to the attended location (both animals $\chi^2(1) < 2.77$, $P > 0.096$) (Figure 2 *D*). Regarding reaction times, monkeys detected color changes significantly quicker than speed changes ($\chi^2(1) = 121.94$, $P < 10^{-27}$, $N = 130$), with color change detection leading by 31 ms on average (Figure 2 *E*). This is to be expected, due to the faster sensory processing of color, and in line with the processing time differences previously described (Arnold et al. 2001; Linares and López-Moliner 2006; Moutoussis and Zeki 1997). Attending towards or away from the RF yielded no significant difference between RT distributions ($\chi^2(1) = 0.05$, $P = 0.82$). Overall alertness was tested by calculating the time interval between fixation

point-onset and trial initiation by lever press, assuming that increased or reduced alertness would lead to accelerated or delayed trial initiation, respectively. M1 initiated trials equally fast in both tasks (488 vs. 475 ms, $Z = 1.17$, $P = 0.117$), while M2 was slightly slower in the speed task (631 vs. 610 ms, $Z = 2.86$, $P = 0.004$). No changes in trial initiation time were observed during the course of the recording sessions (linear regression fits for both monkeys and tasks, all $F < 3.61$; all $P > 0.06$). Taken together, the behavioral data show no, or only minor, non-systematic differences regarding both task type and attended location/direction.

Task-specific firing rate modulation

We investigated task-related modulations of MT responses by comparing neuronal activity depending on whether motion was relevant or irrelevant for the task. Visual stimulation was identical across tasks until the first feature change (Figure 2 *A* and *B*), such that for each of the two spatial conditions neuronal activity is expected to be the same in the speed and the color task, unless dependent on task requirements. Specifically, for attention directed to the RF, the motion direction of the attended Gabor usually matched, or was close to, the preferred direction of the recorded neuron. If FBA spreads to task-irrelevant target features (Katzner et al. 2009), the recorded neuron should receive about the same attentional gain in both tasks. In turn, for attention directed to the stimulus outside the RF, the motion direction of the attended Gabor is about 180 deg away from the stimulating, preferred motion direction of the ecorded neuron. Under this condition, the neuron should receive no motion direction-related gain in any of the tasks (Martinez-Trujillo and Treue 2004). Yet, for many of the recorded neurons we found a significant response difference between tasks, both with attention directed towards or away from the RF stimulus. Figure 3 provides two examples. For the single-unit shown in Figure 3 *A* (with responses aligned to motion onset), recorded from monkey M1, FRs were considerably higher when the monkey performed the motion task as compared to the color task, even during the attend-out condition, when attended motion direction was opposite to the motion inside the RF. Likewise, the multi-unit shown in Figure 3 *B* (with responses aligned to the speed change), recorded from monkey M2, was more active in the speed task throughout the period before the speed

change as well as during the transient response following the speed-up of the RF stimulus, again independent of the spatial focus of attention and attended motion direction. In all trials contributing to these SDFs, the speed change was the first change event, i.e. visual stimulation was identical across the four experimental conditions. In addition to this task-specific response difference, neurons were more active when attention was directed towards the RF. Note that the difference between the two spatial conditions reflects the combined effect of spatial and feature-based attention, since the Gabor outside the RF moved opposite to the preferred motion direction of the recorded neuron.

The units shown in Figure 3 *A* and *B* are representative of the population of MT neurons (187 units, M1: 24 single units, 46 multi-units, M2: 57 single units, 60 multi-units), calculated as the mean of the normalized, baseline-corrected responses of individual units. In both spatial conditions, FRs were consistently higher in the speed task than in the color task (Figure 3 *C*). This task-specific response difference was of smaller magnitude than the difference between spatial conditions, but evident throughout the trial, affecting the steady-state response during stimulation with base speed as well as the transient response representing the speed change. Neurons responded strongest during the attend-in condition of the speed task and weakest during the attend-out condition of the color task. Statistical testing was carried out by a non-parametric ANOVA applied to the collapsed data of three 250 ms test-epochs (grey-shaded areas in Figure 3 *C*, referring to the sustained response after the motion onset transient, the sustained response before the speed change, and the transient response following the speed change). Both the factor task condition and the factor spatial condition had a highly significant influence on the FR of the MT population (Friedman tests, task: $\chi^2(1) = 11.85$, $P < 10^{-3}$; spatial condition: $\chi^2(1) = 86.59$, $P < 10^{-19}$). Individual testing of the single epochs confirmed this finding (Friedman tests, all $\chi^2(1) > 5.34$, all $P < 0.0209$). To test whether response differences between tasks depended on the spatial condition and, likewise, differences between spatial conditions depended on task, we compared the firing rates between the tasks and spatial conditions separately (Figure 3 *D*). Significant response differences between the two spatial conditions were evident in both tasks

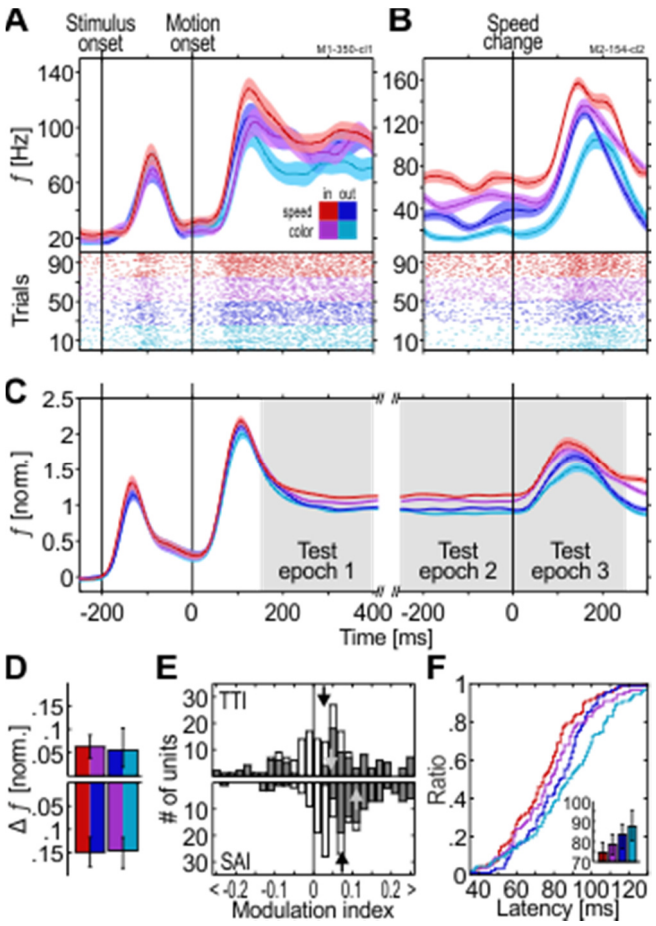

Figure 3 Task-specific modulation of firing rates. A and B: Spike density function (SDF) and corresponding scatter plot of two example units. Color scheme indicated by the inlet in (A) is used throughout the article. In, attend inside RF; out, attend outside RF; speed, detect speed change; color, detect color change. In the scatter plots at the bottom of the SDFs, each mark represents the time of a single spike. For illustration purposes, trials were sorted by condition. C: Population SDF (N = 187) during all trial periods in each of the four conditions. Shaded areas: SEM. D: FR difference between conditions. Top, task effect (TCI); bottom, combined effect of spatial and direction attention (SCI). Left and right color in each bar indicate the attentional conditions that were subtracted from each other. E: Distribution of TCIs (top) and SCIs (bottom). Open bars, all units; gray bars, significantly modulated units. Black arrows, median AIs of all units; Gray arrows, median AIs of significantly modulated units. F: Cumulative distribution of response latencies during test epoch 3. Inlet: median latencies; error bars, 95% CI.

(Wilcoxon signed rank test: both $Z > 8.81$, $P < 10^{-17}$), and a significant task effect was evident for the attend-in condition ($Z = 3.78$, $P < 10^{-3}$). More importantly, however, we found significantly higher FRs in the speed task for attention directed outside the RF, i.e. to a motion direction opposite to the stimulating, preferred direction of the neuron ($Z = 3.12$, $P = 0.0018$). This effect was evident also if restricted to the mere population of single units ($Z = 3.23$, $P = 0.0012$, $N = 81$), as well as for the individual animals (M1: all $Z > 2.15$, all $P < 0.0313$, $N = 70$; M2: all $Z > 2.31$, all $P < 0.0206$, $N = 117$). Thus, neuronal responses where consistently higher in the speed task, independent of both the spatial

location of attention and the relation between the attended motion direction and the neurons' preferred motion direction.

We next investigated how many of the individual units carried the task-specific response difference seen in the population. We found that 55% of all units had significantly different FRs between tasks (Friedman tests, $P < 0.05$), and 71% of these were more active in the speed task. To further test the sign and strength of this modulation, we converted the firing rate differences into a modulation index for response differences dependent on task condition (TCI), ranging from -1 to 1. The TCI is positive for neurons having higher activity during the speed task (see Material and Methods). Collapsed over the three 250 ms time epochs, the median TCI of the entire population was 0.031 (significantly modulated units only: 0.059), and the distribution of index values was significantly greater than zero (Wilcoxon signed rank test, $Z = -3.65$, $P < 10^{-3}$) (Figure 3 *E,* upper panel). The median TCI of the individual epochs 1 - 3 was 0.011, 0.037, and 0.03, respectively, and all distributions were significantly different from zero ($Z < -2.3$, $P < 0.0217$), independent of whether the monkeys started with the speed or the color task ($Z < -2.091$, $P < 0.0365$). For comparison, we also calculated an index for the spatial condition (SCI). 57% of all neurons had a significantly modulated SCI, and 92% of these were more active during the attend-in conditions. The collapsed median SCI of all neurons was 0.07 (significantly modulated units only: 0.106) (Figure 3 *E*, lower panel), and the median SCI of the individual epochs was 0.049, 0.075, and 0.076. All distributions were significantly different from zero ($Z < -6.74$, $P < 10^{-10}$).

Task-dependence of neuronal latencies

As seen from Figure 3 *B* and *C*, firing rate increments following the speed change of the RF stimulus not only differed in amplitude, but also seemed to vary in latency. Recently, we and others have shown that response latencies are significantly modulated by spatial attention (Sundberg et al. 2012; Galashan et al. 2013; Khayat and Martinez-Trujillo 2015) and closely correlate with reaction times (Galashan et al. 2013; Traschütz et al. 2015). Hence, because psychophysically reaction times for speed changes are faster in a speed task than in a color task (Wegener et al. 2008, 2014), we hypothesized that MT response latencies to speed changes will depend on task conditions as well, and will be shorter if

speed is behaviorally relevant. We therefore analyzed the latency of the transient FR increase in response to the speed change (test epoch 3, cf. Figure 3 *C*) of all neurons for which their speed tuning promoted an identifiable response peak in each of the four conditions (N = 87). Cumulative latency distributions were in line with our previous result on the influence of spatial attention (Galashan et al. 2013), and revealed an attention-dependent leftward-shift of the curves in the speed task, both with attention directed to the RF and away from it (Figure 3 *F*). In the attend-in conditions of the speed and the color task, the median latencies were 75 ms and 79 ms, respectively, and in the corresponding attend-out conditions, they were 84 ms and 88 ms, respectively (Figure 3 *F*, inlet). A Friedman test on the factors task and spatial condition revealed a significant influence of each factor (task effect: $\chi^2(1) = 5.08$, $P = 0.0242$; spatial condition: $\chi^2(1) = 14.3$, $P < 10^{-3}$). *Post-hoc* Wilcoxon signed rank tests confirmed the task effect both with attention directed towards the RF and away from it, and also confirmed the combined influence of spatial and direction attention on MT neuronal response latencies for both tasks (all $Z > 2.14$, all $P < 0.0326$). To further investigate whether this latency reduction is a native effect of attention, or, alternatively, a consequence of higher firing rates during the post-change response, we rate-matched the transients of the four experimental conditions (see Material and Methods). Yet, latencies in the four comparisons (task-dependent effect inside and outside RF, spatial condition effect in speed and color task) were still significantly different (Wilcoxon signed rank tests, all $Z > 1.97$, all $P < 0.04$, N = [84 85 86 85]). This result suggests that, like spatial attention (Galashan et al. 2013), task-dependent, dimension-based attentional modulation forces a leftward shift of the latency distribution within the speed task, independent of differences in the magnitude of the speed change response.

Task requirements and neuronal variability

Because the signal-to-noise ratio of a population of neurons depends on both signal strength and variability, we next investigated neuronal response fluctuations. We calculated the Fano factor (FF) of each unit, and the spike-count correlation (SCC) of 38 simultaneously recorded pairs of units. Because independent and correlated response variability fluctuates on a range of time scales, both FF and SCC depend on the width of

the integration window over which spikes are counted (Smith and Kohn 2008). To obtain an unbiased estimate, we used multiple window sizes (5 ms to 125 ms bin width, increased stepwise by 1 ms).

We applied this analysis to the last 250 ms prior to the speed change (during which FRs were relatively stationary). Both the FF and SCC varied significantly as a function of behavioral condition (Figure 4 *A* and *C*). For example, for a window size of 50 ms we found significantly different FFs between tasks both for attention directed towards or away from the RF (Wilcoxon signed rank tests, $Z > 2.29$, $P < 0.0222$, $N = 187$). Likewise, the SCC of both spatial conditions was significantly smaller in the speed task ($Z > 2.94$, $P < 0.0033$, $N = 38$). Testing other window sizes demonstrated that the statistical outcome of the FF was consistent among most widths below 100 ms, indicating a reduced trial-to-trial variability in the speed task (Figure 4 *B*). For the SCC, statistical differences were found for the majority of integration windows, independent of the spatial condition (Figure 4 *D*). For comparison, we also compared the two spatial conditions and found a corresponding and very robust influence, in line with previous results on spatial attention(Cohen and Newsome 2008; Cohen and Maunsell 2009; Galashan et al. 2013). FF differences were highly significant ($Z > 5.1$, $P < 10^{-4}$) for all window sizes, and SCC results were consistent among most windows (Figure 4 *B* and *D*). The combination of spatial and direction attention had a stronger influence on the FF than the task type, but

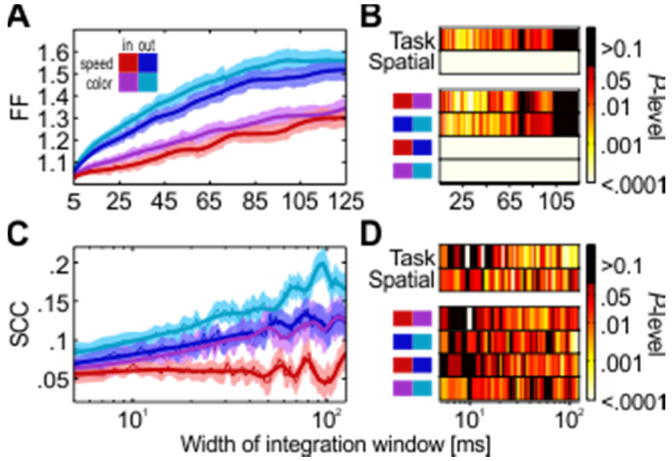

Figure 4 Variability of responses depending on attentional condition. A and B: Fano Factor of spike counts for integration windows between 5 ms and 125 ms width (A), and color-coded P-values for Friedman tests (top rows) investigating the factors task and spatial condition, and Wilcoxon tests (bottom rows) comparing single conditions (B). Color coding ranges between P-values of 10^{-4} and 10^{-1}. Larger and smaller values are colored black and white, respectively. C: Spike-count correlation of 38 pairs of simultaneously recorded neurons for different integration windows. D: Statistical outcome for different integration window widths. Conventions as in B.

their effect on the SCC was about equally strong. We also tested whether the FF modulation was mainly due to differences in FR, or alternatively, independent from these. We applied a mean-matching procedure to five non-overlapping 50 ms time windows and estimated the FF for an integration window of 50 ms. FFs were smaller during the speed task (Friedman test, $\chi^2(1) = 4.77$, $P = 0.029$, $N = 186$) and for attention directed to the RF ($\chi^2(1) = 33.21$, $P < 10^{-8}$). *Post-hoc* tests revealed a significant task effect inside the RF (Wilcoxon signed rank, $Z = 2.37$, $P = 0.0177$), but not so for attention directed away ($Z = 1.08$, $P = 0.2821$). The modulation between spatial conditions was significant in both tasks ($Z > 4.22$, $P < 10^{-4}$). Thus, the task-dependent reduction in trial-to-trial variability occurs independent of changes in FR, yet presumably restricted to the task-relevant visual stimulus.

Relation between feature preference and magnitude of response modulation

The various analyses described earlier provide evidence for a robust influence of the specific change detection requirements on various parameters of the neuronal population response in MT. The finding of a significant, task-dependent response difference when the RF stimulus was unattended in terms of both spatial and feature-based attention (attend-out conditions) suggests a top-down signal to area MT that is affecting neurons independent from the similarity between attended and preferred motion direction. To further test this hypothesis, we applied a control analysis to investigate whether the strength of this dimension-based modulation relates to the neurons' specific tuning properties, or alternatively, is independent from these. Since stimulus direction sometimes deviated from the neurons' preferred direction (mostly due to paired recordings) and stimulus speed was not matched to the neurons' speed tuning properties, we isolated those units for which the stimulus was least matching with their tuning preferences. To this end, we sorted all neurons according to i), the difference Δ_ϕ between their preferred motion direction and the actual stimulus direction (Figure 5 *A* and *B*), and ii), the size of the transient T_A following the speed change (to identify neurons for which the speed before the change was clearly away from their preferred speed, see Material and Methods) (Figure 5 *C* and *D*). Based on this, we ranked all neurons according to their Δ_ϕ value and to their T_A value, and used the sum of these

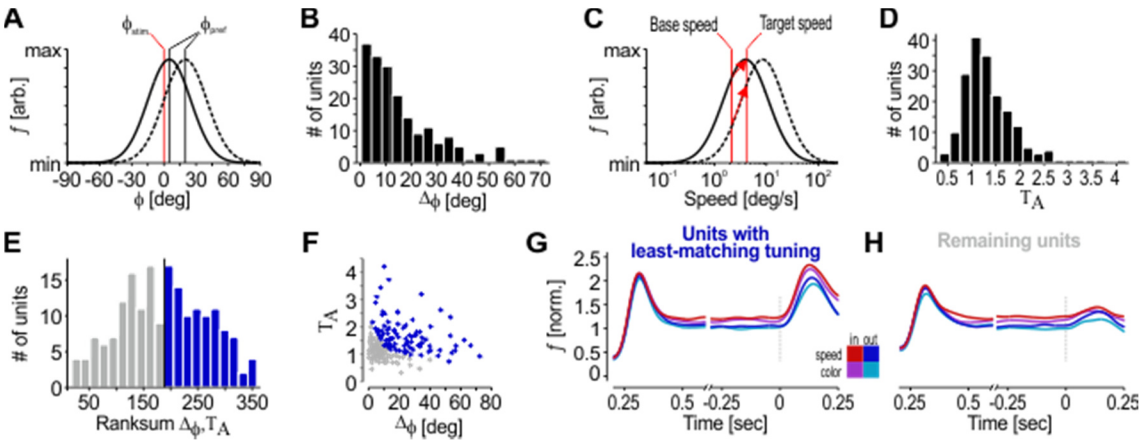

Figure 5 Influence of motion and speed preference on task-dependent response modulation. A: Sketch of two direction-tuning curves with small and larger deviation between preferred direction ϕ_{pref} (black vertical lines) and stimulus direction ϕ_{stim} (red line). B: Distribution of neurons depending on the absolute deviation ϕ_{pref} - ϕ_{stim}. C: Sketch of two log-Gaussian shaped speed-tuning curves. Straight black curve, speed-dependent responses of a neuron for which the base speed of the stimulus (straight vertical red line) is close to preferred and target speed (dashed vertical red line) is preferred; Dashed black curve, speed-dependent responses of a neuron preferring higher speeds; red arrows, vectors indicating the FR increase for a jump from base to target speed, as expected from each neuron's speed tuning. Note that the to-be-expected FR change of the sub-optimally driven neuron is about twice the size of the well-driven neuron. D: Distribution of transients with different amplitude, as expressed by the ratio between the post-change response and the pre-change response (test epochs 3 and 2 in Figure 3). E: Distribution of ranksum values after sorting all neurons according to the deviation between preferred speed and stimulus speed, and to their transient's amplitude, split by median (dashed black line). Blue bars indicate the 50% of neurons with the highest ranksum, indexing units with least-matching tuning properties regarding the actual stimulus properties. F: Combination of Δ_ϕ and T_A values for all units. Blue dots indicate the neurons with highest ranksum. G, H: Population responses of neurons with highest ranksum (units with least-matching tuning) (G) and lowest ranksum (remaining units) (H).

ranks to identify the 50% of neurons with the least-matching tuning (N = 93) (Figure 5 *E* and *F*). The population SDFs of these neurons reveal the same pattern in firing rate differences as the entire population (Figure 5 *G*), with significant FR differences regarding both task type (Friedman tests: $\chi^2(1) = 6.76$, $P = 0.009$, $N = 93$) and spatial condition ($\chi^2(1) = 72.87$, $P < 10^{-16}$, $N = 93$). Post-hoc Wilcoxon tests confirmed the results for both the task effect in the two spatial conditions ($Z > 1.97$, $P < 0.049$), and the modulation between spatial conditions in the two tasks ($Z > 5.41$, $P < 10^{-7}$). For comparison, we also investigated the group of remaining neurons, consisting of many units with best-fitting direction tuning and likely also some neurons with appropriate speed tuning (Figure 5 *H*). As to be expected from the main analyses, both the effect of task type (Friedman tests: $\chi^2(1) = 12.1$, $P < 10^{-3}$, $N = 93$) and spatial condition ($\chi^2(1) =$

74.23, $P < 10^{-17}$, $N = 93$) were significant, confirmed by post-hoc testing (Wilcoxon signed rank tests, all $Z > 1.99$, all $P < 0.048$). Yet, these effects had about the same strength as for the least-matching neurons. The median TCI was 0.031 and 0.034 for the least-matching and the remaining units, respectively, and the median SCI was 0.075 and 0.077. A statistical analysis did not reveal significant differences between the TCI and SCI distributions of the two pools of units (Wilcoxon ranksum tests, $Z < 0.56$, $P > 0.57$), but all distributions were significantly different from 0 (Wilcoxon signed rank test, all $Z > 2.66$, all $P < 0.008$). As a further control, we separately investigated the task effect for the 50% of neurons with the largest deviation from preferred direction (highest $\Delta\phi$), and the 50% of neurons with the largest deviation from preferred speed (highest T_A values), and again found a significant task effect in both cases (Friedman tests, 50% highest $\Delta\phi$: $\chi^2(1) = 5.5306$, $P = 0.018$, $N = 93$; 50% highest T_A: $\chi^2(1) = 5.8429$, $P = 0.0156$, $N = 93$), confirmed by post-hoc tests (Wilcoxon signed rank test, all $Z > 2.25$, all $P < 0.024$, $N = 93$). Thus, in line with the main result of a significant task effect in response to stimuli unattended in terms of both spatial location and motion direction, also the sub-class of neurons with the least fitting tuning properties (regarding either direction or speed, or the combination of both) showed a significant task-dependent modulation.

For both of the tuning-sorted groups, we next investigated how much variance of the response can be explained in terms of task parameters, and performed demixed PCA (Brendel et al. 2011; Kobak et al. 2016). Demixed PCA (dPCA) seeks to capture the maximum amount of variance by a minimum number of parameters, and allows to reconstruct the time course of spike trains as a function of these parameters (see Material and Methods). Based on 20 components, dPCA explained 82% and 90% of the total variance in the two groups, which was not too much below standard PCA (95% and 97%). For both groups, most of the variance (76 – 84%) was explained by the stimulus' time course (from motion onset to 250 ms following the speed change), independent of condition (Figure 6 *A* and *B*). Due to the large transient after the speed change, this was higher in the group of neurons with the least-matching tuning (Figure 6 *C* and *D*). The spatial conditions (combining both spatial and direction attention) explained 7 and 11 % of the variance, and task conditions explained another 6 and 9%. The remaining variance was due to the interaction between spatial and task conditions (3 and 4%). Apart from the condition-independent components, reconstructed neuronal responses (Figure 6 *E*

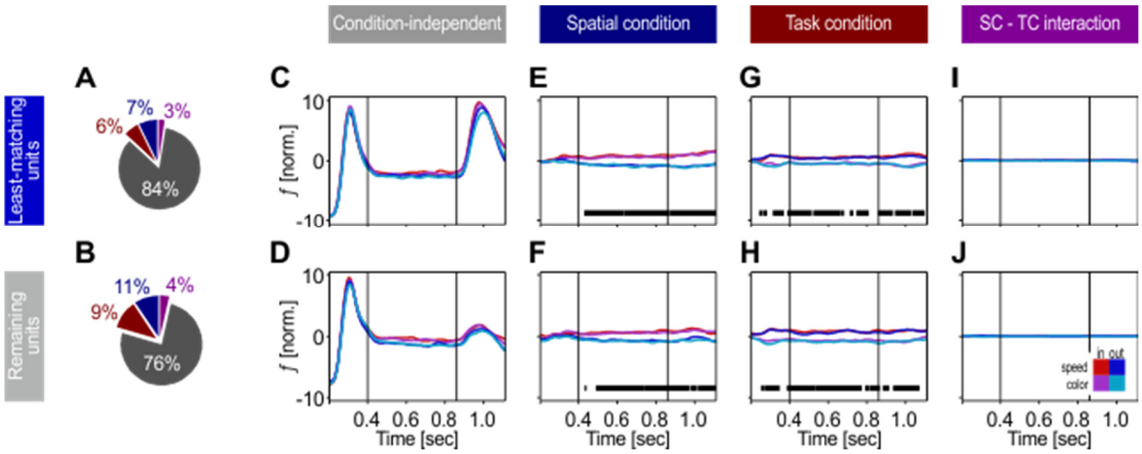

Figure 6 Amount of explained variance as a function of stimulus and task parameters. A, B: Percentage of explained variance for 50% of units with least-matching tuning (A) as compared to the remaining 50% of units (B), estimated by dPCA. Colors in pie plots correspond to variance explained independent of condition (grey), by spatial condition (blue), task condition (red), and interaction between spatial condition and task (purple). C, D: Reconstructed spike trains showing explained variance essentially independent of experimental condition, due to visual stimulation. E, F: Reconstructed spike trains showing explained variance due to spatial condition, G, H: task condition, and I, J: interaction of spatial condition and task. Black lines indicate periods of significant classification.

– *J*) where very similar for both tuning groups. Independent of the sorting criteria, the spatial condition was significantly classified after the firing rate reached a steady state level, about 200 ms after motion onset, and during the remaining response period (Figure 6 *E* and *F*). Explained variance by task type allowed for significant classification of the task during the entire trial period, starting already during the initial motion onset transient and lasting until the end of the response (Figure 6 *G* and *H*). This difference in time course for classifying the spatial and task conditions does not necessarily represent a difference in the underlying mechanism but may be due to the difference in cueing (task condition lasted for a block, spatial condition was cued at the beginning of each trial). However, the dPCA results show that a significant amount of variance is explained by task type even when the tuning to the stimulus is clearly sub-optimal. In summary, both the result of the attend-out condition (for which the attended motion direction and preferred motion direction of the recorded neuron deviated by up to 180 deg) and the analysis of mean responses and amount of explained variance of neurons with sub-optimal tuning suggests that the task effect is independent of the similarity between the attended and preferred features, supporting the hypothesis of a dimension-based modulation of response properties due to the specific demands of the task.

Modulation of spontaneous activity

We finally asked whether this dimension-based facilitation of MT responses depends on the presence of visual input, and therefore analyzed the spontaneous activity before onset of the spatial cue. During this epoch, monkeys already knew the task type due to the color of the fixation point, but not the to-be-attended motion direction of the upcoming target. We found that FRs in the speed task were 8.3% higher than in the color task (Friedman test, $\chi^2(1) = 43.46$, $P < 10^{-10}$, $N = 187$), while no such difference showed up if the same trials were sorted according to their later spatial condition ($\chi^2(1) = 1.97$, $P = 0.16$). We then investigated whether this baseline shift affected neurons differently, depending on their tuning (Figure 7). However, neither in the speed nor in the color task there was any statistical difference between the units with the least-matching tuning and the remaining units (Kruskal Wallis tests, both $\chi^2(3) < 1.42$, $P > 0.23$), but for both tuning groups the across-task comparison revealed a highly significant baseline shift (Wilcoxon signed rank tests, all $Z > 2.89$, all $P < 0.0038$). This indicates that MT received an early, general boost targeting neurons independent of their tuning in the speed task, and suggests that baseline activity in MT is actively adjusted as a function of task requirements.

We also tested whether this difference in baseline activity can account for the significant response differences during evoked responses, and subtracted the spontaneous activity in a condition-specific manner, i.e. we set each condition to the same baseline level. Yet, this procedure did not eliminate the task-dependent modulation seen in the population SDF during visually evoked responses (Friedman test, $\chi^2(1) = 4.27$, $P < 0.039$, $N = 187$;

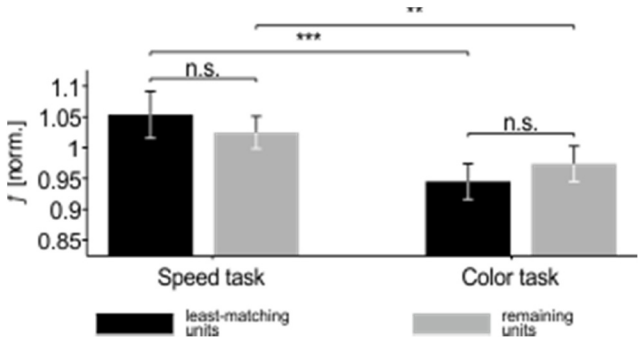

*Figure 7 Normalized spontaneous activity depending on direction and speed-tuning preferences. Errors bars, 95% CI; *: P < 0.05, **: P < 0.01, ***: P < 0.001; n.s.: not significant.*

post-hoc Wilcoxon signed rank tests for attention inside and outside RF: $Z > 2.3$, $P < 0.021$). Thus, although baseline activity is adjusted according to task requirements, task-dependent differences in the evoked response do not constitute a pure reflection of an early baseline shift but get significantly amplified during later visual processing.

Discussion

Location-independent, feature-directed attention plays a crucial role in everyday life. A considerable amount of our knowledge about its neuronal mechanisms has been gained by experiments examining the processing of feature attributes, e.g. a specific color hue or motion direction (Treue and Martínez Trujillo 1999; McAdams and Maunsell 2000; David et al. 2008) and several models of visual attention built on attribute-specific top-down modulations (Corchs and Deco 2004; Wagatsuma et al. 2013). A key finding of FBA studies in area MT is that attending to a specific motion direction facilitates the response of those neurons in area MT well-tuned to that attended attribute, while it does not modulate, or even suppresses, the response of neurons with a clearly different tuning (Martinez-Trujillo and Treue 2004). These works constituted an important step forward in understanding the neuronal mechanisms by which the brain modulates information processing according to the behavioral requirements. Yet, there is another line of evidence suggesting a presumably more general modulation of neuronal responses when attending a specific stimulus feature. In a neuroimaging study requiring attention to either color or speed, both the baseline and stimulus-evoked BOLD signal were found to be enhanced in areas V4 and MT, respectively, depending on task requirements (Chawla et al. 1999). Because the signal increase was evident in MT even when subjects were presented with a stationary stimulus at the beginning of a speed trial, and in V4 when they were presented with a monochromatic stimulus at the beginning of a color trial, the authors concluded a task-dependent change of the attentional set, making those neurons more sensitive that process the relevant feature dimension. Similarly, in several visual search experiments, Müller and colleagues found that both reaction times and error rates benefit from a feature dimension-match between a preceding cue and the to-be-searched item. Interestingly, if the cue also matched the target's feature attribute they did not find a further improvement of behavioral performance (Akyurek et al. 2010; Gramann et al. 2010; Töllner et al. 2010). These behavioral data were accompanied by cue dimension-related modulations of the event-related potential (ERP), which were evident both in the early component of the ERP indicating differences in attentional set, and in a later component reflecting a sustained, feature dimension-related attentional modulation. Finally, in a recent EEG experiment we were able to disentangle the influence of dimension- and attribute-specific attentional effects

(Gledhill et al. 2015). Using a delayed match-to-sample task we found that a match in the feature dimension between a pre-cued, upcoming target stimulus and a spatially unattended, task-irrelevant stimulus is associated with a stronger negativity during the selection negativity-period (representing an event-related measure of feature selection (Anllo-Vento and Hillyard 1996; Torriente et al. 1999)), as compared to a stimulus defined in the non-attended dimension. A match in the feature-attribute provided an additional modulation on top of the dimension-based modulation, coming with longer latency and restricted to occipito-parietal electrodes.

The neurophysiological results described in the present study are well in line with these human psychophysical, EEG, and imaging studies, suggesting that task-specific, dimension-based effects of feature-directed attention are reflected by an attention-dependent weighting of the cortical module most sensitive to process the attended feature dimension. Besides an increase of response rates in the motion task (both with and without visual stimulation), MT neurons showed reduced trial-to-trial fluctuations and reduced spike-count correlations, and faster change transients when motion was behaviorally relevant, regardless of both the spatial focus of attention and the similarity/dissimilarity between the attended and the recorded neurons' preferred motion direction. Our analyses showed that i) the task-specific FR differences during both baseline and evoked responses are independent from the neurons' specific direction or speed preferences, ii) the differences in the evoked response rate exceed the differences during baseline, and they still are of significant magnitude after full elimination of baseline-related FR differences, iii) the task-specific latency shortening of change transients is independent from both spatial attention and the relation between the attended and the stimulating motion direction, as to be expected from psychophysical results (Wegener et al. 2008, 2014), and iv) the differences in response variability and in response latency cannot be accounted for by differences in the firing rate, as they were evident also after rate-matching. Taken together, the results provide evidence for the notion of an attention-dependent, feature dimension-based weighting of visual processing at the neuronal level, and they provide mechanistic insights into earlier reports from human studies in support of an early dimension-based modulation of the attentional set and lasting modulatory processes influencing the processing of the behaviorally relevant stimulus (Chawla et al. 1999; Gramann et al. 2010).

Comparison to other neurophysiological studies investigating task-specific components of visual attention

At the level of single cells, two recent studies addressing motion processing as a function of task requirements did not find corresponding experimental evidence (Katzner et al. 2009; Chen et al. 2012). When recording from neurons in area MT, Katzner et al. (2009) investigated attentional modulations in a speed and in a color task, with an experimental paradigm similar to the one used in the present study. In accordance with our results, they found that spatial attention increases MT firing rates even if color was the anticipated change feature. Yet, the FSG-related response difference between attending a preferred vs. a non-preferred motion direction was of the same size irrespective of the task. The authors concluded that response modulation by both FBA and spatial attention occur independent of specific task requirements. Their results match the predictions of, and experimental findings from, object-based attention studies, proposing that attending a specific feature of a target object facilitates the processing of other, non-attended features of that object (Duncan 1984; O'Craven et al. 1999; Blaser et al. 2000; Rodríguez et al. 2002; Schoenfeld et al. 2003; Berkes and Davidson–Hunt 2007; Wannig et al. 2007; Ernst et al. 2013). Another MT study required monkeys to make a saccade into one of four previously trained directions in response to either the color or the motion direction of a briefly presented grating stimulus (Chen et al. 2012). In 25% of the trials, the saccade direction for indicating the color was congruent with the motion direction of the grating, but in 75% of the trials it was incongruent, requiring the animal to focus on the task at hand to provide the correct response. Yet, only 22% of MT neurons showed significantly different responses between tasks, and of these, some were more active during the direction task, and others were more active during the color task.

Despite methodological differences, including experimental paradigms, visual stimulation, and data analysis, we consider one major difference in the experimental design to be important to understand the proper conditions under which the visual system facilitates or suppresses the processing of an entire feature dimension. In both former studies, monkeys had to frequently switch between motion and color trials, while in the present study they were required to engage in one type of task for several

dozen trials. A strong engagement in one specific task type (and hence, strong attention to one specific feature dimension) is, however, more likely to occur if this task is performed for a prolonged time, as compared to frequently switching between tasks. This interpretation is in line with psychophysical investigations using similar task and stimulus conditions as in the present neurophysiological experiments (Wegener et al. 2008). In this study, subjects were required to respond to any speed or color change as fast as possible. When they were given a feature dimension cue of 75% validity, they responded very quickly to the indicated change, but much slower if the change occurred in the unattended feature dimension, regardless of the spatial focus of attention. In contrast, if they were given an object cue without specific information on the feature dimension most likely to change, reaction times were in-between the previous distributions, i.e. they were slower as compared to the previously attended feature dimension, but faster as compared to the previously unattended dimension. These data indicate that strongly attending to one feature dimension may go along with the suppression of processing in another dimension, preventing the spreading of attention to other, irrelevant features of the selected object, thereby increasing behavioral performance in response to the attended feature. Similar results on the suppression of non-attended object features have been obtained by several other research groups (Fanini et al. 2006; Nobre et al. 2006; Cant et al. 2008; Polk et al. 2008; Serences et al. 2009; Taya et al. 2009; Xu 2010; Freeman et al. 2014). As such, a possible reason for the different results on the task-dependency of MT responses is that monkeys were more strongly focusing on the feature relevant for the current task block in our experiments.

Results cannot be explained by feature-similarity gain

Our finding of a task-specific response facilitation when the attended motion direction was opposite to the stimulating, preferred motion direction within in the RF indicates that feature-directed attention cannot fully be accounted for by FSG, which constitutes the current and most influential mechanistic explanation of FBA. This conflict does not arise from a general incompatibility with FSG (since FSG may co-exist with the task-specific modulation we here describe, cf. Gledhill et al. 2015), but because by concept FSG can hardly account for the response differences as found in our experiments.

Specifically, because Gabors were moving in opposite directions, the dissimilarity between preferred motion direction inside the RF and attended motion direction outside the RF was maximal, providing a condition for which attentional facilitation based on similarity cannot apply. Under such circumstances, response rates of the recorded neurons are not expected to be enhanced but rather suppressed (Martinez-Trujillo and Treue 2004). Our findings, therefore, suggest an additional attention mechanism that does not depend on the specific tuning properties of the neurons, which may act in concert with FSG.

A possible concern to this interpretation of a tuning-independent modulation, however, arises from the following assumption: If it was possible to solely attend the speed but not the direction of the target Gabor, FSG may only facilitate the response of neurons tuned to the attended speed. If, in addition, this modulation would be stronger in the speed task than in the color task, and if a significant portion of our neurons would be tuned to the stimulus speed before the change, then the observed task-specific response differences could be interpreted within the FSG framework.

We argue, however, that this interpretation is unlikely and does not explain the discrepancy between previous findings on FSG and the results of the current study. First, this alternative interpretation still depends on a task-specific response difference. As explained earlier, the effect of FSG was found to not vary between tasks, such that FSG is interpreted to address all those feature-specific neurons that process the attended object (Katzner et al. 2009). Thus, even if most of our neurons preferred the speed prior to the change, based on the findings of Katzner et al. (2009) FSG would have the same effect in both tasks. This conclusion is not supported by our results. Second, the task-specific response difference affected neurons independent of their speed preferences. Although we had no detailed speed-tuning data available, large positive transients in response to an increase unambiguously indicate neurons for which the attended speed before the change is clearly away from their preferred speed. Restricting the analysis to these neurons with the least-matching tuning properties, either based on their preference to only speed, or on their combined preference to both speed and direction, still revealed significant response differences between tasks (Figure 5 and 6). Third, task-dependent response differences were present in the absence of visual stimulation, and

both of the subgroups with different tuning preferences showed a higher baseline activity during the speed change task (Figure 7).

An additional, conceptual argument is that a selective facilitation of only those neurons well-tuned to the speed before the change hardly supports change detection. In a speed-change task, neurons tuned to the attended speed are the poorest change detectors within the population of speed-tuned neurons (Traschütz et al. 2015). Because they respond to their preferred speed, any change in this speed, be it an acceleration or a deceleration, results in a reduction of their response. Due to the log-Gaussian shaped speed tuning curves of most MT neurons (Lagae et al. 1993; Nover et al. 2005), these transients have rather small amplitudes even for noticeable changes, which tend to average out in the population (Traschütz et al. 2015). In contrast, neurons for which the attended speed is on the rising or falling part of their tuning curve respond with significant FR changes even to small changes in speed, and preserve the sign of the speed change (acceleration or deceleration) over a large spectrum of speeds. Experimentally, we recently showed that the response of a population of neurons with heterogeneous speed tuning profiles (such as the population response we measured in the current study) is mainly carried by such neurons, having a preferred speed away from the stimulating speed (Traschütz et al. 2015, Figure. 4). Hence, suppressing the response of these neurons while facilitating the response of neurons with a preference to the attended speed hardly serves to improve change detection. We hypothesize that the same argument applies for other principal stimulus features (as e.g. motion direction) as well, because a substantial part of the population transient following a feature change is carried by the fraction of neurons not well-tuned to the feature preceding the change, due to the fact that the change occurs on the flank of their tuning curve (i.e. on its most sensitive part).

Mechanistic implications for feature-directed attention

In our previous EEG experiment (Gledhill et al. 2015), we found that feature dimension-specific attentional effects emerged at frontal electrodes and then moved over to parieto-occipital electrode sites over visual cortex. In the present study, the first noticeable difference between the speed- and the color task was a global shift in the

baseline activity of MT neurons, prior to stimulus onset, suggesting an adjustment of the attentional set (Corbetta and Shulman 2002). In line with the EEG findings (Gledhill et al. 2015), a possible source for such task-related top-down modulations of visual cortical activity is the prefrontal cortex (PFC) (Miller and Cohen 2001). Neurons in monkey PFC have a different degree of motion- and color sensitivity depending on the behavioral relevance of either feature, and color- and motion-selective neurons cluster in different parts of the PFC (Lauwereyns et al. 2001). Lesions to the lateral PFC impair shifting of the attentional set to another perceptual dimension (Dias et al. 1996). Therefore, a task-dependent increase in baseline activity may constitute an attention-related biasing signal from attentional control areas to specialized visual modules, as previously proposed (Chawla et al. 1999; Driver and Frith 2000).

Although baseline shifts are not sufficient on its own to induce attention-related response differences during the evoked response (Fannon et al. 2008), and do not predict the magnitude of attentional modulation (McMains et al. 2007), they often precede both spatial and feature-based attentional modulations in visual cortex (Luck et al. 1997; Chelazzi et al. 1998; Chawla et al. 1999; Kastner et al. 1999; Shulman et al. 1999; Reynolds et al. 2000; Lee et al. 2007). In line with this, we found that both the effects of task and spatial condition were not dependent on the baseline increase observed during the pre-stimulus epoch, but had a significant magnitude after subtraction of spontaneous activity, even if done for each of the four behavioral conditions separately.

Taken together, the current data show that directing attention between motion and color of a stimulus causes (at least under the task- and stimulus conditions of our experiment) a task-specific, dimension-based attentional modulation of neuronal activity. Unlike FSG, this modulation is not only affecting the neurons well-tuned to the attended stimulus but all neurons in the cortical module sensitive to process the attended stimulus dimension. Yet, future work on feature-directed attention is needed to properly understand the task conditions forcing tuning-dependent and/or tuning-independent response modulations in visual cortex, and whether and how the underlying mechanisms may co-exist or even depend on each other.

Acknowledgements

The authors acknowledge support by Peter Bujotzek, Sunita Mandon, Deniz Parmuk, Ramazani Hakizimana, and Katrin Thoß regarding various aspects of the study.

Chapter III: Phase shifts of cross frequency coupling predicts reaction time

Authors: Bastian Schledde, Detlef Wegener

Affiliation: Brain Research Institute, Center for Cognitive Sciences, University of Bremen, P.O. Box 33 04 40, 28334 Bremen, Germany

Author contributions: D.W. and B.S. designed research; B.S. performed experiments; B.S. analyzed data; B.S. and D.W. interpreted results of experiments; B.S. prepared figures; B.S. drafted manuscript.

Publication: Schledde B, Wegener D. Phase shifts of cross frequency coupling predicts reaction time. *In prep.* 2019.

Abstract

In an ever-changing sensory environment with plentiful information, cortical processing prioritizes relevant information for conscious perception. Selective attention, a process that achieves information prioritization leads on a behavioral level to a decrease in perceptual thresholds and to a reduction in reaction time (RT) to changes of visual stimuli. Recently, we found that evoked transient firing rate responses of motion processing neurons in area MT occur earlier in trials that result in fast RT (Galashan et al. 2013) . Simultaneously, mean firing rates preceding the transient response remained unchanged and were not predictive of RT. Utilizing a feature change detection task we now investigated the processes that precede transient responses and found a physiological correlate of RT that is not captured by average spiking activity. We conducted electrophysiological recordings in two macaque monkeys from area MT and V1 while the animals were trained to covertly attend a drifting grating and react to an abrupt acceleration of the motion signal. We measured cross frequency correlations (CFC) by means of phase-amplitude coupling (PAC) previous to a target speed change occurring within the receptive fields of pairs of MT-V1 neurons. Low gamma band amplitude (35 Hz) of the local field potential (LFP) in one area was temporally modulated along the phases of an alpha band (8-16 Hz) oscillation of the LFP in the other area. We found that gamma amplitude was preferentially locked to a specific phase of the alpha oscillation and crucially, the identity of this “preferred” phase was shifted between RT groups. Between animals, preferred phases were different but were consistently modulated as a function of RT. Using the spiking activity simultaneously recorded in area MT we reproduce and approve the original finding of (Galashan et al. 2013) and show that transient responses are slower and smaller in amplitude for slow RT as compared to fast RT trials. We show that the specificity of CFC has a direct relation to the perceptual performance of the animal and, based on the characteristic of ensuing transient response, that it may be essential for MT neurons to express fast and salient output signals. Both, the relation of intracranial CFC to RT and the finding that the specific phase of PAC has a functional relevance for visual perception are novel and introduce important insights to the research of visual processing in the cortex. The results promote current models of selective attention that incorporate the temporal

modulation of local gamma synchrony as a mean of long range coordination of feedforward signal transmission.

Introduction

Humans as well as non-human primate behavior is based on a constant flow of external sensory evidence. For fast and efficient behavior sensory information prioritization that enters conscious perception is imperative. Selective attention, a process that achieves information prioritization leads on a behavioral level to a decrease in perceptual thresholds and to a reduction in reaction time (RT) to perturbations of visual stimuli (Posner 1980; Pashler and Sutherland 1998; van der Heijden 2003). Correspondingly, neurons in motion processing middle temporal area MT (Maunsell and Van Essen 1983; Mikami et al. 1986) typically increase firing rates with spatial attention (Lee and Maunsell 2010; Galashan et al. 2013; Schledde et al. 2017). Firing rates of area MT neurons have been shown to correlate with behavioral choice (Britten et al. 1996), are at least as sensitive to a motion signal as the perceptual performance of the subject (Parker and Newsome 1998) and are fundamental for the conscious perception of motion (Newsome and Pare 1988). While MT neurons are highly direction selective (Movshon and Newsome 1996) their response to onset or changes of visual stimuli result in fast transient increases in firing rate that correspond to the perceptual visibility of the stimulus (Price and Born 2010; Traschütz et al. 2012).

Recently, it has been shown that the latency of transient responses in area MT towards an abrupt acceleration of a motion stimulus decrease with spatial attention. Transient responses evoked by the behaviorally relevant stimulus change were also faster if the trial resulted in shortened RT (Galashan et al. 2013). Crucially, the authors found that mean firing rates preceding the stimulus acceleration were identical for groups of different RT. It thus remains unknown what mechanism accompany sustained firing that enable neurons to respond with distinct subsequent transient rate increases. The fact that firing rate modulations that accompany RT fluctuations and that accompany different attentional routing are similar, suggest that the same or similar neuronal mechanism may be underlying.

Neural oscillations play a central role for information prioritization or routing. Attention dependent routing was suggested to be mediated by synchronizing oscillatory activity, mainly in the gamma band (>30 Hz) of downstream neuronal pools (Kreiter 2001, 2006, Fries 2005, 2015; Taylor et al. 2005; Womelsdorf et al. 2006b; Bosman et al. 2012;

Grothe et al. 2012) or by decreasing low frequent oscillatory amplitude (<25 Hz) for reduced local inhibition (Snyder and Foxe 2010; Bonnefond and Jensen 2012; Jensen et al. 2012, 2015; Capilla et al. 2014; Bonnefond et al. 2017) or decorrelation of common neural noise (Cohen and Maunsell 2009; Mitchell et al. 2009; Khayat et al. 2010). However, oscillations in different frequency bands of the local field potential (LFP) often interact with each other, a phenomenon that is reflected in cross frequency correlations (CFC). Evidence for a critical role in attention dependent processing of CFC has recently been shown between monkey visual areas V1 and V4 (Bosman et al. 2009, 2012), between anterior cingulate and prefrontal cortex (Voloh et al. 2015), within area MT (Esghaei et al. 2015) and between distributed cortical areas of the human neocortex (Canolty et al. 2006). Although there are differences in the interpretation of the specific role of CFC (Bonnefond et al. 2017) its functional relevance for multiple cognitive functions including multi-item sequencing, encoding (Hyafil et al. 2015), attentional sampling (Landau and Fries 2012; Fries 2015; Landau et al. 2015) and for the long-range coordination of local activity (Canolty and Knight 2010; Bonnefond et al. 2017) is evident.

We hypothesized that cross frequency coupling as a mean of coordinating gamma band synchrony between area MT and its major input source area V1, exhibits a correlation to RT that may not be captured by mean firing rates.

We recorded in area MT and its direct predecessor V1 and quantified inter-areal CFC by means of phase-amplitude coupling (PAC). We found that gamma amplitude is coupled to the alpha phase measured in MT and V1 and that the preferred phase of the coupling is predictive of the RT. The transient response to the stimulus of the recorded MT population was, similar to the finding of Galashan et al. (2013), characteristic for the resulting RT.

We conclude that the low frequent oscillations in the brain coordinate local neural assemblies to activate at distinct phases and that the quality of perception and neuronal sensitivity depend on the specific phase to which local activity is locked.

Materials and Methods

Electrophysiology

We conducted electrophysiological recordings in two adult male monkeys (*Macaca mulatta)* in area MT and area V1. All procedures concerning the surgery, animal care and experimentation comply with the regulations of the Animal Welfare Act issued by the Federal Government of Germany. Conditions during all surgeries were strictly aseptic and surgical procedures are detailed in (Wegener et al. 2004).

Electrode insertions to the middle temporal area (MT) were conducted through a custom-made recording chamber above the middle temporal sulcus. Position and coordinates for electrode penetrations were estimated using structural magnetic resonance images. Neurons in area V1 were recorded via a semi-chronic recording devices, with up to 6 electrodes simultaneously (Galashan et al. 2011). We used tungsten microelectrodes (0.8–5 MΩ, 125-µm shank diameter; Frederic Haer, Bowdoin, ME) for intra-cranial recordings. Neurons in area MT were identified by the high proportion of direction-selective responses, the depth of the recording site and receptive field size/eccentricity ratio (Maunsell and Van Essen 1983; Desimone and Ungerleider 1986). Similarly, we identified neurons in area V1 by the size of the classical receptive field in V1 (Hubel and Wiesel 1974) and their selectivity to specific orientations (Hubel and Wiesel 1968, 1974; Gur et al. 2005). The positioning of the electrodes was determined by manual inspection of the visually evoked spiking response and subsequent validation with an automated mapping procedure (Drebitz et al. 2019). Eye movements were monitored using custom made eye- tracking devices with a spatial resolution of 0.2°.

Raw electrode signals were amplified and sampled at 25 kHz. Line noise was eliminated by subtracting a template of artificial signals that consistently lock to the phases of a simultaneously recorded 50 Hz line signal. Local field potentials (LFP) were obtained using a bidirectional low pass equiripple FIR filter (pass frequency: 300Hz; stop frequency 500 Hz) and decimated to a sampling frequency of 1kHz. Spikes were detected by thresholding the band pass filtered raw electrode signal (bidirectional band pass equiripple FIR filter; pass band: 0.7 – 5 kHz) by either four times the median of the

absolute signal divided by 0.67 (Quiroga et al. 2004) or by three times the standard deviation of the signal. Spike wave forms were stored in 32 bins spanning 1.28 ms and were initially automatically clustered (Harris et al. 2000) and subsequently merged and labeled manually resulting in artifact- free multi-unit activity.

Task and visual stimulation

Animals performed in two variants of a feature-change detection task. In both tasks the animals had to covertly attend a high-contrast drifting Gabor inside the receptive fields of the recorded neurons. We only used data from a condition during which the animals were trained to detect an abrupt acceleration of the drifting Gabor (Figure 9). Trials were initiated by depressing a lever while maintaining central fixation. After an initial delay of 1050 ms, the animals were spatially cued towards to target position for 700 ms. Two Gabor stimuli appeared 250 ms after cue offset and started drifting after another 200 ms. One Gabor was presented inside the RF of the recorded neuron and motion direction was matched to the preference of the recorded MT neuron. The other Gabor was placed in the point-reflected position in the opposite hemi field and moved into the anti-preferred direction. Following motion onset, a series of distractor or targets event could occur. Targets comprised of a 100 % acceleration of the motion speed and distractors were introduced as either color changes at the cued or un-cued position or motion accelerations at the un-cued position. Behavioral responses to the target event were allowed in a time interval from 150 ms to 750 ms after the speed change. Trials were terminated after 300 ms following a correct response, late responses or responses to a distractor event. The behaviorally relevant speed changes could occur in a random time interval after the motion onset between 660 – 5500 ms. For trials that went into analysis the target speed change was the first change to occur at any position on the presentation monitor and thus visual stimulation was identical across trials and conditions.

Stimuli were presented on a 22-inch CRT monitor and consisted of two high-contrast Gabors with a spatial frequency of 2 cycles/°. A detailed description of the task and visual stimuli is reported in (Schledde et al. 2017).

Phase amplitude coupling

Probability density functions. For the estimation of cross frequency coupling we computed probability density functions (PDF) of the amplitude of a high frequent signal relative to the phase of a low frequent signal. For the calculation of the PDFs each LFP trace of a given trial was filtered with a second order two-pass Butterworth filter (Oostenveld et al. 2011) in a specified frequency band. Subsequently we determined the analytical signal by applying the Hilbert transform. The analytical signal was then used to obtain either the phase or the amplitude of the signal. Before filtering and the Hilbert transform we cut each trial before stimulus acceleration and appended 1 second of randomly drawn data from the same trial at the end of the trial. In that way the filter and Hilbert transform are not corrupted by non- stationary events in the data or edge effects. For a given phase supplying signal, e.g. alpha band filtered LFP in MT, the phases were binned into 18 bins. During the same time of a given phase bin, the absolute value of the Hilbert transform of a given amplitude supplying signal, e.g. gamma band filtered LFP in V1, was averaged. Subsequently the average amplitude values were normalized to the total amplitude across bins. The resulting function can be understood as a histogram of average amplitude across phase-bins and resembles a PDF like distribution (Tort et al. 2010). PDFs were calculated across groups of trials (e.g. 33% fastest trials in a session) by concatenating the time interval of interest of each trial.

Modulation Index. We used Tort's modulation index (Tort et al. 2010) that estimates the deviation of the observed amplitude distribution across phase bins *P* from a uniform distribution *U*. The deviation is quantified by the Kullback–Leibler (KL) distance given by:

$$D_{KL}(P,U) = \sum_{j=1}^{N} P(j) log \left[\frac{P(j)}{U(j)}\right].$$

The modulation index (MI) is the normalized KL:

$$MI = \frac{D_{KL}(P,U)}{\log(N)}$$

where *N* is the number of phase bins. Small MIs indicate a lack of cross frequency coupling and approaches a uniform distribution of amplitude across phase bins at *MI* = 0. MIs increase with increasing differences between *P* and *U* where *MI* = 1 if P is a Dirac-like function and amplitudes are non-zero in only one phase bin.

Comodulogram. For the construction of the comodulogram we filtered the phase supplying signal with a bank of low frequent pass band filter from 4 to 20 Hz in 1 Hz steps and the amplitude supplying signal from 25 to 100 Hz in 5 Hz steps. In order to avoid low frequent bias, filter band width were kept variable and were defined as ±1/3 of the center frequency (Aru et al. 2015; Voloh et al. 2015). Filter width growth for phase supplying signals was capped at ± 3.5 Hz in order to avoid very large filter band width. Plotting followed a linear 10 step interpolation in both dimension. In the main analysis MIs used in the comodulogram were obtained from the average PDF across the population of neuronal pairs. Subsequent analysis was focused on the animal specific region of interest in cross frequency space. Filtering and subsequent analysis steps were re-calculated, this time using the specified low frequent pass band and pass band width while keeping the original pass band width for the amplitude signal.

Surrogate data. Surrogate data was constructed using a trial-shuffling method that reshuffles trial identities of the amplitude providing signal. The original phase signal and the reshuffled amplitude data is then used for each surrogate PDF. Surrogates thus represent chance-level PAC given the identical time course of visual stimulation and without disturbing the phase dynamics within trials. We used 500 resamples to achieve an approximation of the chance level PDF.

Circular statistics. Circular measures such as the preferred phase and distribution statistics were performed using the *CircStat* toolbox for Matlab (Berens et al. 2009). Preferred phases for each pair's PDF were obtained by the amplitude weighted mean angular direction of the PDF (*circ_mean*). Tests for non- uniformity of the PDFs were performed using the Rayleigh test (*circ_rtest*). Multi-sample tests on the phase distributions were performed using a non-parametric test for equal medians, a circular analogue to the Kruskal-Wallis test (*circ_cmtest*). We corrected for multiple comparisons by correcting for the false discovery rate (FDR) using the Bonferroni- Holm Method (Holm 1979).

Spiking activity

Spike density functions. Spike density functions (SDF) were computed by counting spike times with a 1 ms resolution and convoluting each trial with a Gaussian of 100 ms length and a sigma of 10 ms. Each site's SDF was corrected for its spontaneous activity measured in an 800 ms time interval before the spatial cue and in absence of any visual stimulation.

Speed Change Index. We calculated a speed-change index (SCI) to quantify the evoked firing rate response towards the acceleration of the motion speed. The index is calculated by

$$SCI = \frac{MI_{post} - MI_{pre}}{MI_{post} + MI_{pre}},$$

where $MI_{post/pre}$ are the mean firing rates in the 250 ms following and preceding the speed change, respectively.

Amplitude and latency. We utilized a novel approach to quantify the differences between transient responses to counteract a concern with conventional latency estimation that uses a simple thresholding procedure. Often transient responses, when evaluated on few trials, may have very different shapes. For example, a transient can be

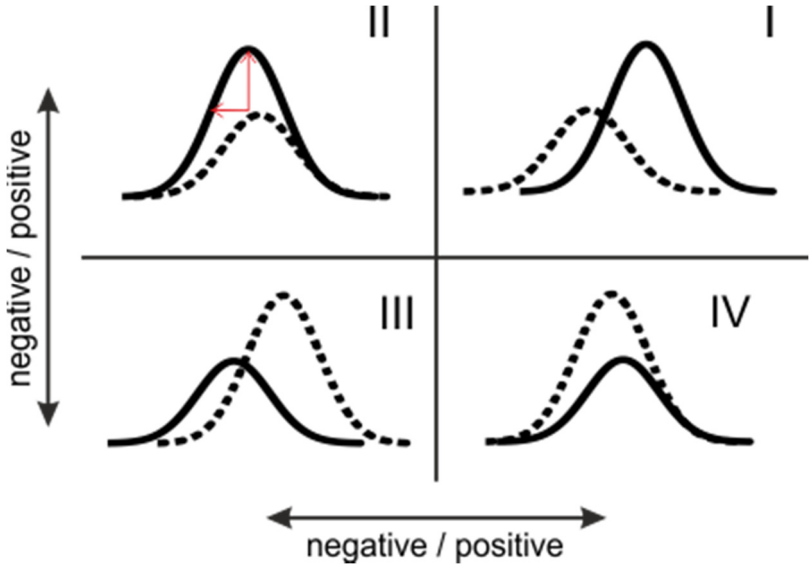

Figure 8 Time shifts and amplitude shifts quantify the difference between a test transient (solid line) and a reference transient (dashed line). Each of the four quadrants display one possible relationship between a test and a reference transient.

large in amplitude but will have a longer latency than a much smaller transient if a threshold relative to the peak amplitude is used. However, at the point in time when the small transient reaches its maximum, the larger transient response exhibits higher firing rates and will therefore have a higher and earlier impact on post-synaptic neurons than the smaller transient response. Our novel method characterizes latency modulations and amplitude modulations always between two transients while incorporating the above stated case. Differences in the characteristic in transient firing rate changes were quantified by determining the amplitude and time differences between two points at the rising flanks of the shape of two transient responses (a test transient and a reference transient). In a first step the point in time at which a test transient is maximal (t_{p1}) is determined. Amplitude shifts are given by the difference between the peak of the test transient and the amplitude value at t_{p1} of the reference transient. In a second step time shifts are obtained. In case of a positive amplitude shift (Figure 8, quadrant I-II) time shifts are calculated as the time difference between peak of the reference transient (t_{p2}) and the point in time (t_{r1}) at which the amplitude of test transient first reaches the peak of the reference transient. In case of a negative amplitude shift (Figure 8, quadrant III-IV) time shifts are calculated between t_{p1} and the point in time at which the reference amplitude first reaches the peak of the test transient (t_{r2}). In that way, negative time shifts always represent leading test transients and positive amplitude shifts always higher amplitudes for the test transient. In the main text, transients resulting from the group of fast trials were always used as test transients and references transients came always from the slow RTF.

Statistics. Statistical differences for mean firing rates, the amplitude and time delay modulations were obtained via the non-parametric Wilcoxon signed rank test. Correction for multiple comparisons was done by correcting for the false discovery rate (FDR) using the Bonferroni- Holm Method (Holm 1979).

Trial-to-trial correlation

In order to detect the linear relationship between the preferred phase of the cross frequency coupling to reaction time we utilized the Jackknife correlation (JC) method that allows to relate trial wise fluctuation of the mean angular direction of PAC and mean

firing rate to RT (Richter et al. 2015). The logic of this method is to calculate each measure across the entire population of pairs while rejecting a single trial from the population. This is repeated until each trial was discarded once. Subsequently the variations along these leave-one-out repetitions (Jackknife resamples, JCR) are correlated. For the correlation between a circular measure and a linear measure (e.g. preferred phase and reaction time) we used the circular-linear correlation from the *CircStat* toolbox (*circ_corrcl*) while for the correlation of mean firing rate and RT we used Spearman's correlation coefficient. P-values were obtained by randomly reshuffling JCRs of one measure before correlation. This was done 1000 times and the p-value was obtained by counting the incidences that showed higher correlation values as the observed correlation coefficient.

Results

Exclusion criteria and behavioral performance

Data was considered for analysis if the animals performed sufficiently well in the task and we excluded sessions with a performance below 70%. The resulting average performance for animal I was 99.49 % (S.E.M. 0.13) and for animal II 87.29 % (S.E.M. 0.71).

We recorded from a total of 162 (animal I 69; animal II: 93) recordings sites in area MT and a total of 440 (animal I: 228; animal II: 212) recordings site in area V1. The phase-amplitude correlation analysis is based on a total of 1208 (animal 1: 580, animal 2: 628) paired recordings, excluding 16 pairs for animal II for which we did not record enough trials (minimum of 10 trials) in the attend-in condition. Spikes were extracted from the MT recording sites and we obtained 66 mutli-units from animal I and 90 from animal II. For the firing rate analysis, we applied two more exclusion criteria in order to select only neurons that exhibit a sufficient stimulus driven sustained activity and a sufficient transient increase evoked by the speed change (see Methods, Spiking activity). We required a minimum mean firing rate in the pre-change interval of 10 Hz (N: animal I: 46; animal II: 73) and a positive speed change index (N: animal I: 50; animal II: 60) for each recorded multi-unit. This amounted to a total of 36 multi-units for animal I and 55 multi-units for animal II. To compensate for the loss of data by these exclusion criteria we pooled the data of both animals and evaluated firing rates based on 91 multi-units.

Behavioral Task

The experimental paradigm we utilized (Figure 9) was previously used in another study (Schledde et al. 2017) investigating firing rate modulations in two feature change detections tasks. In both tasks the animals had to covertly attend a high-contrast drifting Gabor inside or outside the receptive fields of the recorded neurons. In this study, we made use of only one task for which monkeys had to detect a 100 % acceleration (speed change) of the inherently moving target grating and ignore other color or speed changes that could occur throughout the trial. In the following we will only consider the trials

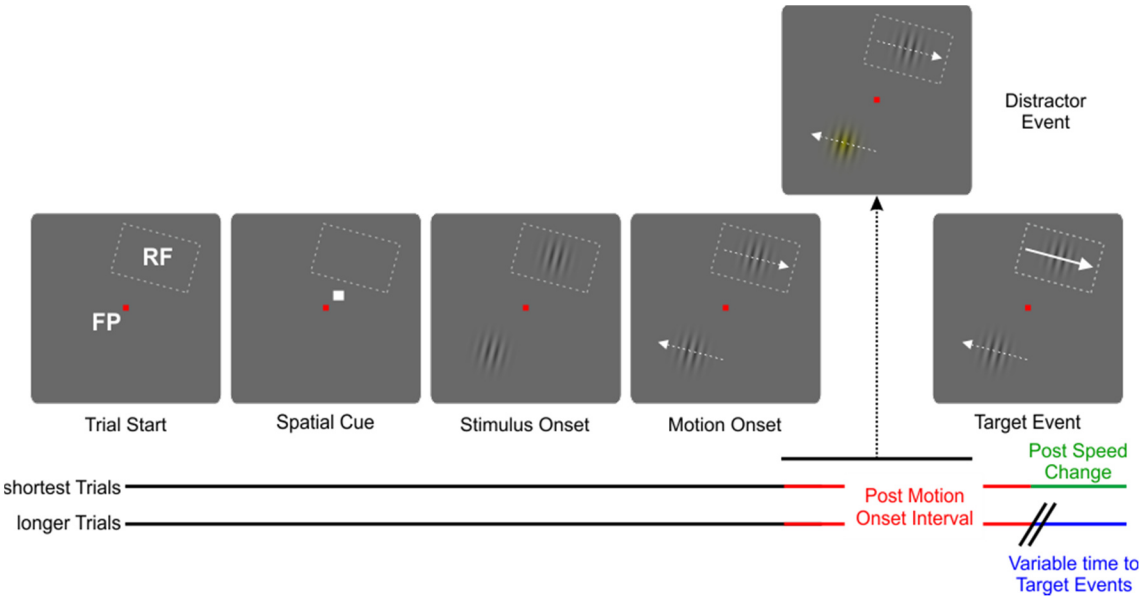

Figure 9 Experimental paradigm. Monkeys were trained on a feature change detection paradigm. Trials were initiated by depressing a lever while fixating on a central fixation point. Following an initial delay period of 1050 ms a spatial cue was presented for 700 ms indicating the position of the target event. Static Gabor gratings appeared 250 ms after cue offset and started moving intrinsically after another 200 ms. After motion onset a series of distractor or targets event could occur. Target events in this task were 100 % acceleration of the motion speed and distractor events were either color changes at the cued or un-cued position or speed changes at the un-cued position. Monkeys could respond to the target event in a time interval from 150 ms to 750 ms after the speed change. Trials ended either after another 300 ms delay after the correct responses, late responses or responses to a distractor event. Target speed changes could occur in a random time interval after the motion onset between 660 – 5500 ms. We only analyzed trials during which the target speed change was the first event to occur at any position, thus recorded neurons underwent identical visual stimulation across trials and conditions.

that required the animal to react to a stimulus change inside the receptive field (RF) of the recorded neurons and will refer to this condition using the term "attend-in condition". Target speed changes could occur in a random time interval between 660 – 5500 ms after stimulus onset. We only analyzed trials for which the first change at any position was the target speed change inside the RF and in the speed changes of these trials occurred maximally after 1540 ms relative to stimulus onset.

Reaction time and firing rate modulations

In an identical experimental setup we have shown in a previous study that firing rates of MT neurons are not predictive of RT in the interval directly preceding the speed change but transient evoked response were correlative of RT (Galashan et al. 2013). As a first

step we quantified mean firing rates and transient responses of the neurons in MT in order to reproduce, validate and extend the previous finding in our spiking data. We pooled trials of the attend-in condition (mean *N*: Animal I: 17.62; Animal II: 20.36) for each recording site into 3 groups of similar RT. We choose 3 fractions (33% fastest (RTF I), medium (RTF II) and slow (RTF III) RTs) because this segmentation allowed for enough data within a fraction and gave some resolution across RTs. We made sure that for each recording site the same number of trials went into each RT fraction (RTF), excluding median RT trials to equalize trial numbers. In his way we eliminate bias due to session wise variations. This amounted to an average number of 5.49 (6.46) trials for each RTF and recording site. In Figure 10 A the cumulative reaction times of the three groups are shown for both animals. Because very long behavioral response delays indicate a lack of attentiveness we decided to exclude RTs larger than 500 ms although during the experiment we allowed the animal to respond within 750 ms. Consequently, cumulative functions are cut off at 500 ms. For animal II RT distributions are broader resulting in larger shifts between RT fractions than for animal I.

In Figure 10 B the spike density function (SDF) of the time course across the trial is displayed. Stimulus onset and the following motion onset expectedly evoked transient increases in firing rate of MT neurons. After approx. 260 ms subsequent to the motion onset firing rates reached a sustained level that was maintained throughout the trial until the ensuing transient response to the speed change. The SDF in the right panel resulted from re-segmenting the trials locked to the speed change. We investigated mean firing rate in two periods of interest. In both, the post-motion interval (460 – 860 ms after motion onset) and the pre-change interval (the 400 ms preceding the speed change) mean firing rates between any of the reaction time fractions (RTF) were not statistically different (Wilcoxon singed rank, Post Motion: RTF I vs. RTF II, $p = 0.523$, $Z = 1.358$; RTF I vs RTF III, $p = 0.729$, $Z = 1.358$; RTF II vs. RTF III, $p = 0.729$, $Z = -0.598$, Pre-change: RTF I vs. RTF II, $p = 0.575$, $Z = 0.965$; RTF I vs RTF III, $p = 0.368$, $Z = 1.543$; RTF II vs. RTF III, $p = 0.575$ $Z = 1.062$, p- values corrected for multiple comparison, Figure 10 C and D).

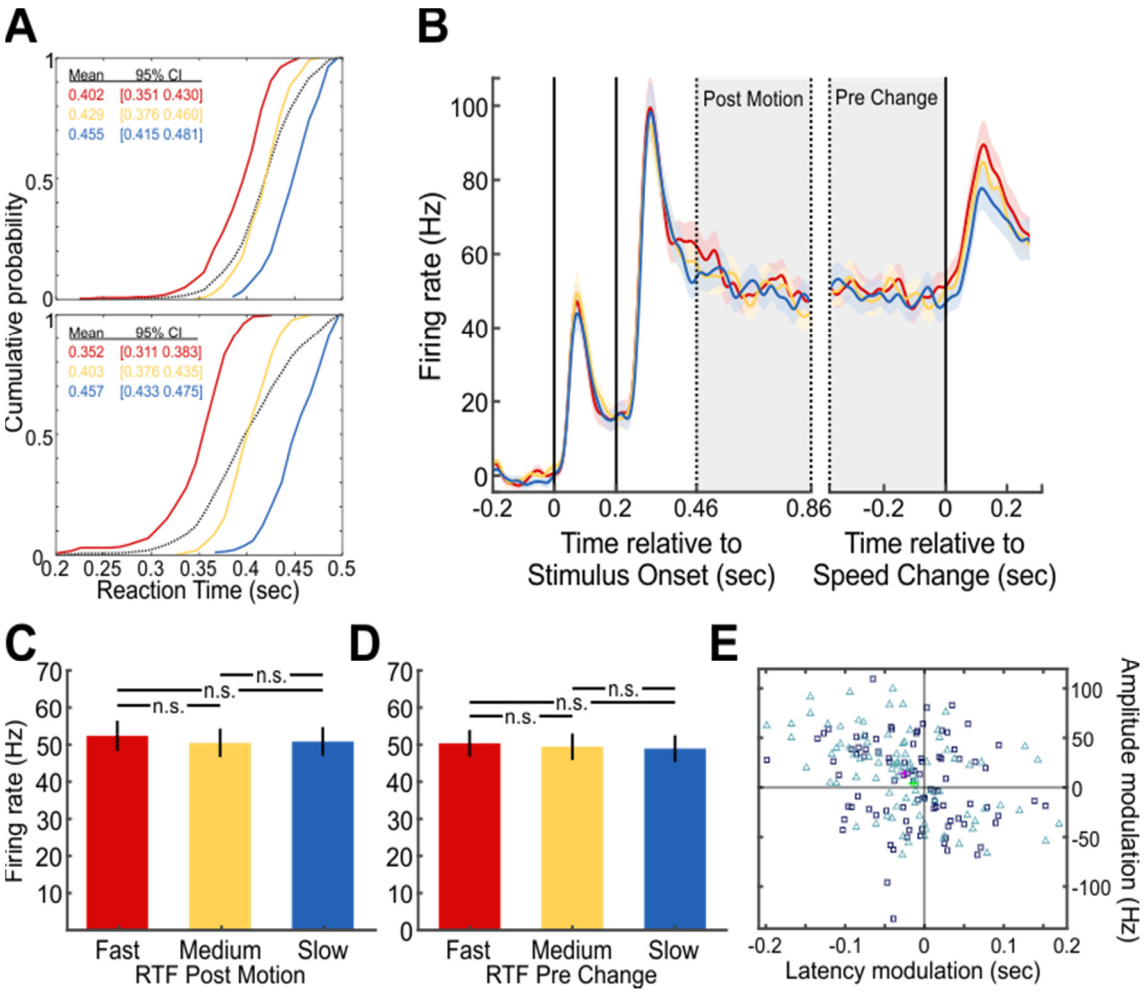

Figure 10 Reaction time distributions and firing rate analysis. ***A*** *Reaction time distributions of the two animals (top panel: anima I; bottom panel: animal II). Cumulative reaction time distributions, mean and 95 % confidence intervals are shown. Reaction times (RT) above 0.5 sec were excluded from analysis.* ***B*** *Time course of the baseline corrected spike density functions (SDF) are shown locked to the Stimulus onset (left) and relative to the target speed change (right). Colors indicate the RTF according to the distributions in* ***A****.* ***C*** *Average mean firing rates of the 3 RTFs in the post-motion interval. Error bars indicate S.E.M., n.s. mean no significant difference.* ***D*** *Same as in* ***C*** *but data is taken from the pre-change interval.* ***E*** *Display of latency and amplitude modulations. Triangles represent unit-wise modulations between RTF I and RTF III and squares represent unit-wise modulations between RTF I and RTF II. The center of the purple and green crosses represent the mean latency/amplitude modulation (purple for RTF I vs. RTF III; green RTF I vs. RTF II), the extent of the crosses represent S.E.M.*

We applied a novel method to quantify the characteristic of the ensuing transient response. In short, we calculated the time difference and amplitude difference always between a test and reference transient (see Methods). In our case test transients always come from the faster RTF and reference transients originate from slower RTF. The method encompasses a concern in latency estimation if latency is determined by a simple threshold relative to the peak amplitude. Negative latency modulations always represent leading test transients and positive amplitude modulations always represent

higher amplitudes of the test transient. In Figure 10 E the latency and amplitude modulations of the two comparisons (RFT I vs. RFT II black, RFT I vs. RFT III, blue) are displayed. Each entry represents the paired comparison within each recording site, for which only few trials were used. However, both comparisons result in negative latency shifts and positive amplitude shift of the population (mean and 95% CI of the mean, comparison 1: green, comparison 2: red) and the majority of recording site cluster in the upper left quadrant. The comparison between RTF I vs. RTF II and RFT II vs. RFT III however, did not reveal a significant modulation for latency modulations, although comparison RTF I vs. RFT II show a statistical trend (Wilcoxon signed rank, RTFI vs. RTF II, p = 0.095, *Z* = -1.982, RTFII vs. RTF III, p = 0.245, *Z* = -1.161, corrected for multiple comparisons) but the latency modulations between RTF I and RFT III were significant (Wilcoxon singed rank, p = 0.001, *Z* = -3.571, corrected for multiple comparisons). Likewise the comparison of amplitude modulation became significant for the comparison between RFT I and RFT III (Wilcoxon signed rank, RFT I vs. RFT II, p = 0.312, *Z* = 1.009; RFT II vs. RFT III, p = 0.054, *Z* = 2.212; RFT I vs. RTF II, p = 0.009, *Z*= 2.936, corrected for multiple comparisons). Here also the comparison between RTF II vs. RFT III only slightly failed to reach significance. Disregarding the comparisons involving smaller RT differences we show that large RT differences are accompanied with distinct differences in latency and amplitude of a transient response towards a behaviorally relevant stimulus change.

Modulation of phase amplitude coupling

In line with previous studies (Womelsdorf et al. 2006b; Galashan et al. 2013) we found that mean firing rate during sustained activity does not undergo the same trial-wise fluctuation as RT. However, it has been shown that the phase-synchrony of local gamma band activity in area V4 is not only a correlate of spatial attention but also modulates as a function of RT during sustained activation (Womelsdorf et al. 2006b). We hypothesized that the interaction of low and high frequent oscillation may play a fundamental role in coordinating gamma oscillations between areas involved in the processing of the attended stimulus. Such a temporal coordination of gamma spindles may be a direct prerequisite for the emergence of gamma synchrony between areas, as gamma spindles

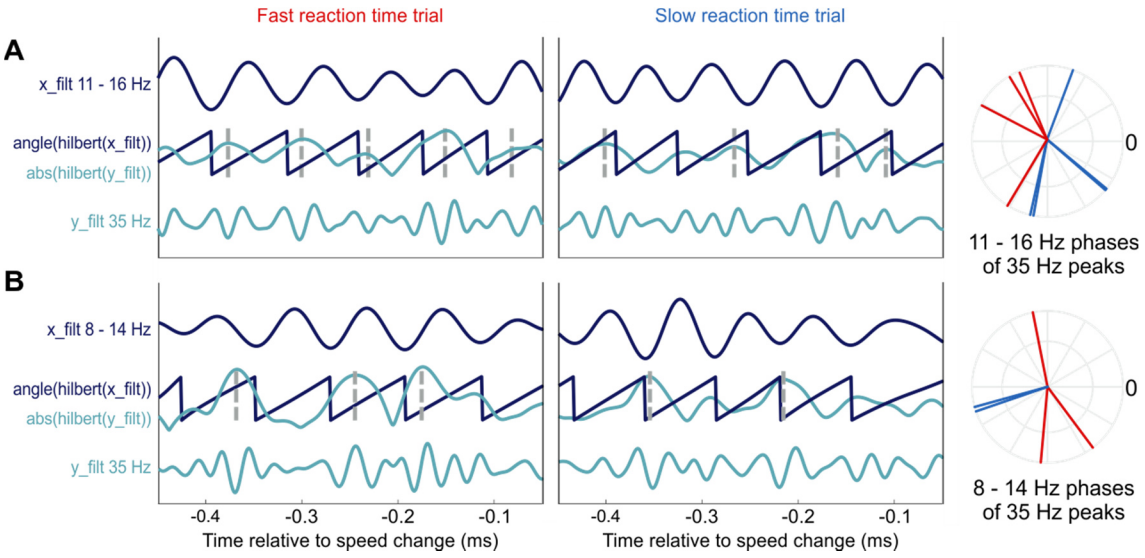

Figure 11 Example trials of animal 1 (A) and animal 2 (B). The x_filt traces display the phase supplying raw signal that was filtered in a designated alpha frequency band. Traces of the y_filt signal display the gamma band filtered raw signal at 35 Hz. Phase and amplitude traces are displayed in between the two filtered raw signals. Phases were obtained by extracting the angle of the analytical signal (Hilbert transform) and amplitude were given by the absolute value of the analytical signal. Vertical dashed lines designate the time of the gamma amplitude peaks. For fast RT trials these peaks fell into different phases of the alpha oscillation for both animals. The individual directional unit vectors at the time of gamma amplitude peaks are displayed on the right side.

need to temporally align in order to become phase-locked (Bonnefond et al. 2017). Therefore, we investigate whether and how a low-frequent oscillation might coordinate gamma spindles across areas along the motion processing stream in visual cortex and quantified cross-frequency-correlations (CFC) between area MT and area V1. Both phase and amplitude providing signals were recorded in area MT and area V1 simultaneously, while the two signals that were correlated came always from two distinct areas. Cross-frequency correlation was therefore measured between area MT and V1. Initially, we observed that low-gamma amplitude measured at one electrode was higher at distinct phases of an alpha band oscillation measured at a separate electrode. The example trials in Figure 11 depicts the relationship between the phase of the alpha oscillation and the amplitude of the gamma signal in the interval directly preceding the transient speed change. Fast RT trial gamma peaks fell into phases of the alpha oscillation that were shifted away from the phases at which gamma peaks occurred in slow RT trials (polar plot in the right panel of Figure 11). Such a relationship between a low frequent oscillation and a high frequent amplitude can be quantified via phase-amplitude coupling (PAC). PAC was measured by binning the low frequent phases and calculating

the probability density of the gamma amplitude within each bin (see Material and Methods).

Theoretical (Zhang et al. 2012; Onslow et al. 2014) and experimental studies (Courtin et al. 2014; Voloh et al. 2015) suggest that a reset of low frequent phase may casually trigger the locking of high frequent spindles to specific phases of the low frequent oscillation i.e. phase resets may initiate PAC (see Discussion). In our experimental design the speed change could occur at largely varying stimulus onset asynchronies (SOA). Speed changes of trials that went into analysis occurred between 0.66 – 1.54 seconds after the onset of intrinsic motion of the stimulus. Across trials and during the time interval immediately preceding the speed change, the progression of phases relative to phase resets that were observed at stimulus/motion onsets (see Suppl. Figure 1), could vary anywhere between 7.6 cycles to 17.7 cycles of the observed alpha band oscillation. Given the dissipation of phases over time, we assumed that a precise estimation of the preferred phases of PAC is most consistent over trials and neural pairs during a time interval that is close to and at constant temporal distances to the phase reset. Thus we choose to investigate a time interval ranging from 460 ms to 860 ms after the stimulus onset during which firing rates returned to a sustained and stationary level. This interval is confined to the 400 ms previous to the first possible speed change of all trials. Our initial observation indicated that the amplitude of a high frequent oscillation in one area

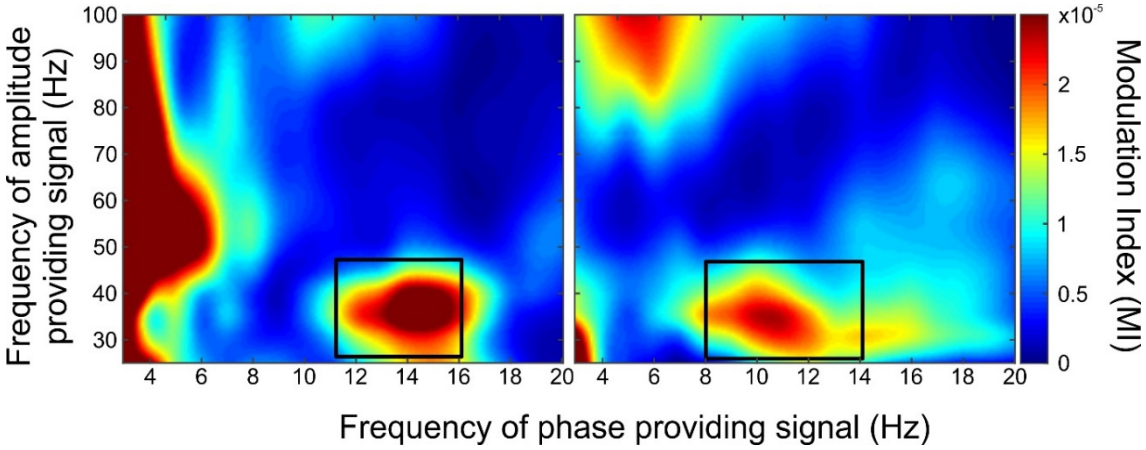

Figure 12 Comodulogram of animal I (left) and animal II (right). Cross frequency correlations were estimated via the modulation index (see Material and Methods)). Low frequencies were scanned from 4 to 20 Hz in 1 Hz steps with a variable band width of ±1/3 of the center frequency that was limited to a filter bandwidth of ±3.5 Hz. High frequencies were scanned from 25 to 100 Hz in 5 Hz steps using the same choice band width rule (see Methods). Regions of interest (ROIs) are located within the black rectangles.

is coupled to the phase of a low frequent oscillation in the other area when both neuronal populations process the attended stimulus. In order to find the particular frequency pair at which phase and amplitude are correlated we scanned the low and high frequent components for phase-amplitude correlations across various frequencies (see Material and Methods). Due to the short time interval and the length of the low frequent cycle, data for each recording pair was sparse. Therefore we pooled PDFs across the population of recorded neuron pairs and constructed the comodulograms on the population PDFs.

We used all available trials from the attend-in condition for the construction of the modulation index (MI). The MI quantifies the deviation of the PDF along the low frequent phases from a uniform distribution (Tort et al. 2010, but see methods) and thus indexes the strength of coupling between phase and amplitude. The resulting comodulogram in Figure 12 peaked for both animals in the alpha range at a low gamma range. MIs were also high at other frequency bands. PDFs of these frequency pairs were, however non-sinusoidal and therefore challenging regarding the interpretation of the underlying ongoing amplitude modulation. We defined animal specific regions of interest (ROI) that roughly locate within the alpha band (animal 1: 8 – 14 Hz; animal 2: 11 – 16 Hz) for phase providing signals and a low gamma range (35 Hz) for the amplitude providing signal (black rectangles in Figure 12). PDFs resulting from these frequency pairs were sinusoidal and consistently peaked at either peak or close to the through of the alpha oscillation. All subsequent analysis is based on these ROIs.

We tested for significant phase amplitude correlation of the defined ROIs by producing 500 shuffled resamples (see Material and Methods) and counted the number of resulting MIs that were larger than the observed MI. For all groups in both animals we found that the MIs of population PDFs were significantly larger than their population surrogates (animal I, all groups, $p <= 0.001$; animal II, all groups, $p <= 0.001$). We found that this correlation in the population was carried by a large fraction of the neuronal pairs. By using the same resamples we calculated for each neuronal pair the significance of cross frequency correlation for each RT fraction and recorded pair and found that 46.33% for animal I and 47.93% for animal II of pairs showed significant correlation between phase and amplitude in at least one of the RT fractions. Furthermore, the

origin of the phase or amplitude providing signal was not biased towards a specific area. For the fraction of pairs with significant correlation the number of phase providing signals originating from area MT was 131 for animal I and 128 for animal II and from area V1, 160 for animal I and 150 for animal II.

Gamma amplitude peaked at different phase bins for the 3 RTFs. Population PDFs of the RTFs are shown in Figure 13 A & B. For both animals PDFs for the slow RTF were shifted towards the through of the alpha oscillation while for fast RTFs the preferred direction was closer to the peak.

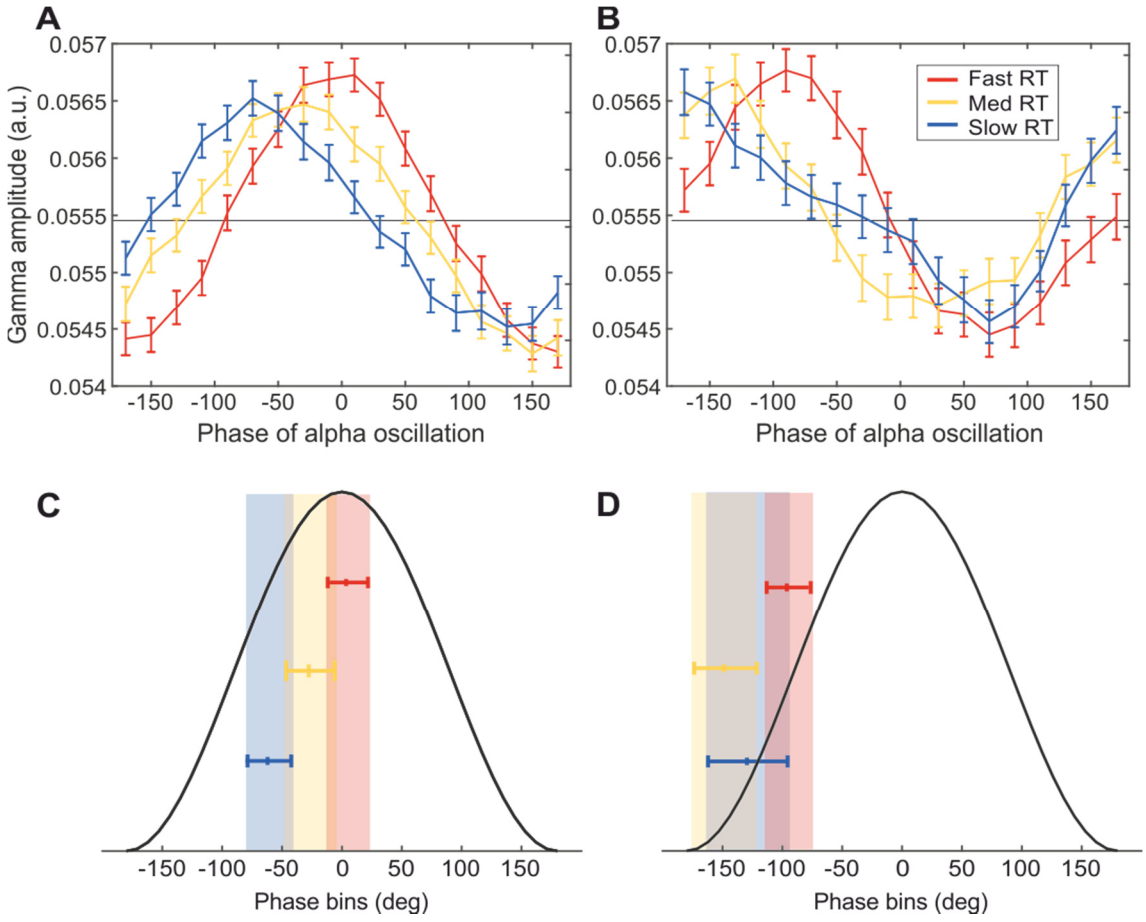

Figure 13 Gamma amplitude as a function of alpha phase and preferred phases of PAC. Population probability density functions of gamma amplitude as a function of the alpha phase. Alpha phases were binned in 18 non-overlapping bins and mean gamma amplitude was calculated for each bin. For each recorded pair gamma amplitude within each bin was normalized to the total amplitude across bins, resulting in a probability density (PDF) like function across phase bins. PDFs were calculated for each RTF within each session. Mean PDF across the population of neuronal pairs are shifted between RT for animal I (**A**) and animal II (**B**). Error bars represent S.E.M. **C** & **D** display the average angular direction and 95 % CI (shaded area) of the population PDFs. For comparison the full cycle of the alpha phase is shown as the black solid line.

We calculated the preferred phases as the amplitude weighted mean angular direction of the PDFs from each neuronal pair. In Figure 13 C & D the mean and 95 % confidence intervals of the population PDFs mean direction for each RT group are displayed. For both animals mean preferred phases of the three groups were distributed along the cosine of the alpha oscillation (black solid line). Preferred phases of the fast RT group clustered closer to the peak with a mean of 3.82° and a 95% CI of [-11.49°, 19.14°] for animal I and a mean of -100.18° and a 95% CI of [-117.09°, -83.27°] for animal II. The medium RTF cluster further away from the peak with a mean phase of -28.79° and a 95% CI [-47.56°, -10.04°] for animal I and a mean of -155.28°, 95% CI [-180.18°, -130.39°]) for animal II. Likewise the slow RTF is shifted to the through of the oscillation with a mean of phase of -64.81° and 95% CI [-81.47°, -48.14°] for animal I and a mean -135.03°, 95% CI -167.92°, -102.13°] for animal II.

We applied a Rayleigh test to the distribution of preferred phases of each RT group and found that all differ significantly from a uniform distribution around the circle indicating that the mean and confidence intervals are a meaningful characterization of the distributions of preferred phases (Rayleigh test, animal I, all groups, $p<0.001$; animal II, all groups $p < 0.01$, corrected for multiple comparisons).

Finally, we applied a non-parametric multi-sample test to the preferred direction estimated for each neuronal pair. For animal I all preferred directions are significantly shifted between all RTF (multi-sample test for equal medians, animal I: RTF I vs. RTF II, p 0.032; RTF I vs. RTF III, $p < 0.001$; RTF II vs. RTF III; $p= 0.030$). For animal II preferred directions between the fastest and medium RTF were significantly different, while the fastest and slowest RTFs show a only a trend to significantly shifted preferred directions (multi-sample test for equal medians, animal II: RTF I vs. RTF II, $p = 0.002$, RTF I vs. RTF III, $p= 0.0917$, RTF II vs. RTF III, $p = 0.8602$, corrected for multiple comparisons).

Preferred phases clustered around different mean phases for the two animals. For animal I mean phases were closer to the peak of the alpha oscillation and for animal II these were closer to the through. We were interested whether there are animal specific differences in the recording or positioning of the electrodes that are able to explain these differences. The measured phase that can be extracted from the LFP is arbitrary and only interpretable if the position of the recording site relative to the sinks and

sources in the cortical layer are known. However, we do not know the exact positioning of the electrode recordings sites but we can estimate differences in the recording between animals by comparing the observed phases at the prominent stimulus onset phase resets (Suppl. Figure 1). In Suppl. Figure 2 the phase distributions of both animals at maximal phase concentration following the stimulus onset are displayed. Mean phases of these distributions were offset by 119.72°. Since visual stimulation was identical between animals the offset indicates that other factors involving the recording technique, e.g. positioning of the recording electrode are capable of explaining the differences between preferred PAC phases.

The post motion time interval is temporally close to the prominent stimulus/motion onset related perturbations of the LFP (see Suppl. Figure 1). It is therefore possible that temporal modulation of gamma spindles is a direct consequence of the input modulations. In order to control for this possibility we calculated the time delay of the gamma peaks occurring in the post-motion interval relative to stimulus onset. Similarly, we obtained the phases of the alpha oscillation at time of the gamma peak. If gamma responses are evoked by the stimulus or motion onset, the temporal delay of gamma peaks should be locked to the stimulus onset and should show less variation as compared to the alpha phases at the time of the gamma peak. However, if gamma is locked to the alpha phases the opposite should be true. In Figure 14 the standard

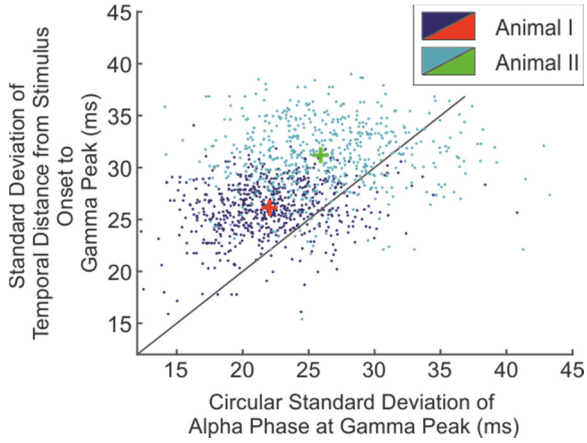

Figure 14 Variance of the location of gamma peaks relative to Stimulus Onset vs. alpha phase. On the ordinate the circular standard deviations of alpha phases at the time of gamma peak within the first full cycle of the alpha phase are plotted. The temporal delay from stimulus onset to the gamma peak are plotted along the abscissa. Crosses represent the mean of both animals. Variation for both animals is larger for the stimulus delay times in comparison to the phase variations.

deviation of alpha phases and delay periods are plotted for each recorded neuronal pair. We restricted the delay of the maximal gamma amplitude to the first full alpha cycle in order to restrain variability of both measures to the same time interval. Variation for the temporal delay between stimulus onset and gamma peaks is significantly higher as compared to the variation of alpha phases at the time of the gamma peak (both animals, Wilcoxon signed rank, p<= 0.001, animal I: Z = -16.92, animal II: Z = -16.30). We therefore conclude that the measured gamma responses are more closely locked to the alpha phases and phase-amplitude coupling does not occur as a secondary effect to the evoked responses.

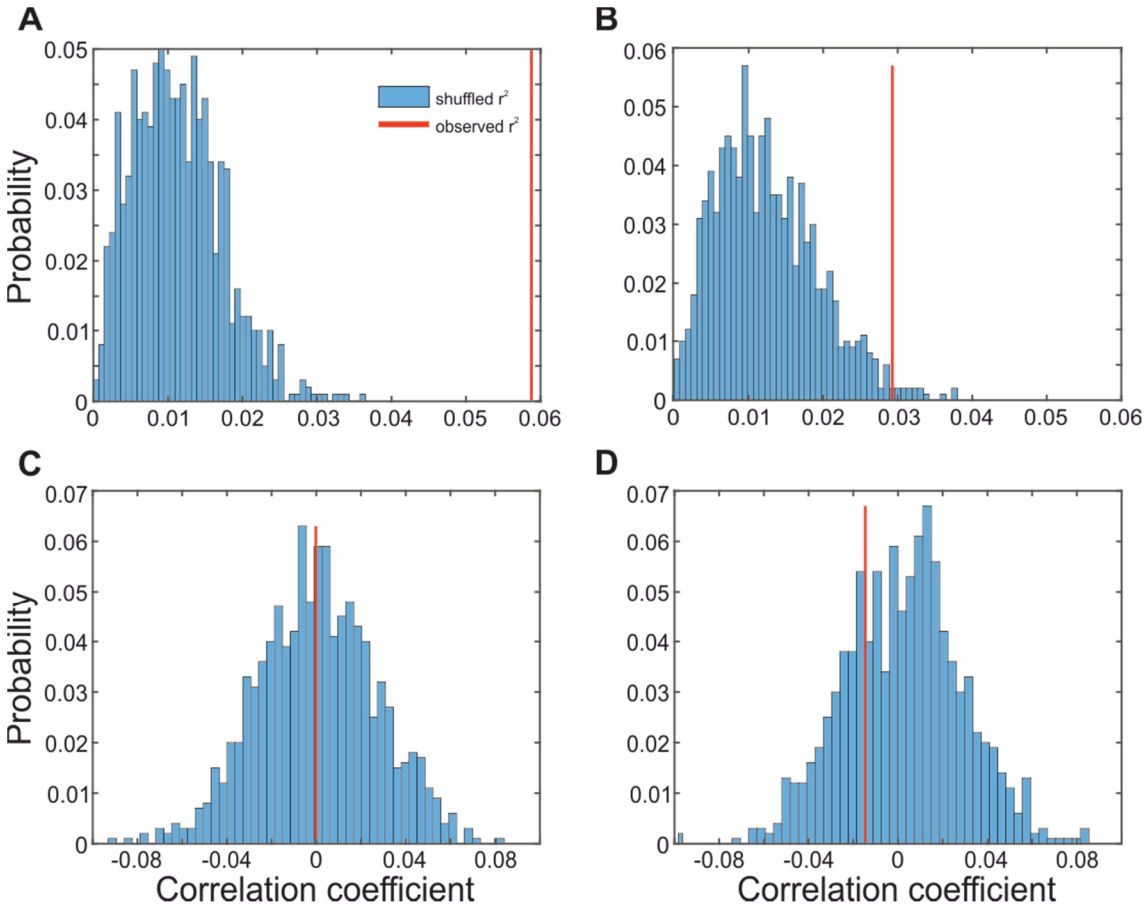

Figure 15 Visualization of the Jackknife correlation statistic. In all panels the histogram shows the distribution of correlation coefficients resulting from the correlations between the randomly shuffled Jackknife resamples of RT and the non-shuffled Jackknife resamples of either mean preferred phase (top) or mean firing rate (bottom). The histograms resemble chance-level distribution of the Jackknife correlations. Red vertical lines are centered on the Jackknife correlation coefficient that was actually observed in the data (non-shuffled data). ***A*** *Trial-wise correlation between RT and mean preferred phases of the population of recording pairs for animal I,* ***B*** *the same for animal II.* ***C*** *Trial-wise correlation of RT and mean firing rates for animal I,* ***D*** *the same for animal II.*

Sorting and binning RT is, under some circumstances, not the ideal method to investigate correlations between measures that are calculated across multiple trials (PDFs are calculated across multiple trials to compensate for short data intervals). For example, the number of RTFs and their location relative to the total distribution of RT may be suboptimal to illuminate modulations of PAC relative to RT. We applied a trial-by-trial correlation between RT and preferred phases in order to overcome these limitations (Jackknife correlation, see methods). In short, we used all except one of the trials of all recorded pairs and calculated the resulting population PDF and its preferred coupling phase. Likewise we computed the mean RT of the involved trials and repeated this procedure until each trial was discarded once. The resulting resampled values for RT and preferred phase (jackknife resamples) were correlated using a circular-linear correlation coefficient (Berens et al. 2009). Subsequently, we randomly shuffled RT resample identities and calculated the correlation with the non-shuffled preferred phase resamples to obtain a chance-level estimation of the circular-linear correlation. This procedure was originally used for a trial wise estimation of spectral coherence and has been shown to precisely recover correlations based on conventional trial-by-trial correlation in simulated data (Richter et al. 2015).

We found that for both animals variations in preferred phase correlated significantly with the variations in mean RT of the jackknife resamples (Figure 15 **A** & **B**, animal I: $p <= 0.001$; animal II: $p = 0.015$). Likewise we calculated the Jackknife correlation with the spiking data of the involved MT neurons in the post-motion interval. In line with our observation of equal mean firing rate in the post-motion interval, the Jackknife correlation did not reveal any significant relation between firing rate and RT (Figure 15 **C** & **D**, animal I: $p = 0.511$; animal II: $p = 0.723$).

Discussion

Our results show that local gamma amplitudes lock to specific phases of alpha oscillation in a remote area and that the identity of the preferred coupling phase is predictive of the following RT in that trial. PAC was measured between area MT and area V1, thus the temporal coordination of local gamma band spindles occurs across subsequent areas in the dorsal visual processing pathway. Modulations in inter-areal PAC is accompanied with reduced latencies and increased amplitudes of responses to the behaviorally relevant event in fast RT trials. At the same time we observed a lack of correlation between firing rates preceding the speed change and RT. Therefore, the current results go beyond mere sustained mean spiking activity and elevate the importance of inter-areal cross frequency coupling with regard to the perceptibility of visual stimuli.

We found that the modulating range is approximately within conventional alpha bands but gamma amplitudes were maximal at different alpha phases for the two animals. However, data of both animals showed a clear shift of preferred phases between fast and slower reaction time trials. We take this as an indication that the precise low frequent phase at which gamma spindles occur are functionally relevant for the successful and effective coordination of local feedforward gamma band synchrony. In addition we show that this coordination of gamma spindles does not lead to an increase or decrease of mean firing rates in the downstream area MT. These firing rates are measured across multiple cycles of the modulating frequency band and any rate specific differences may not surface on these timescales. However, we show that the output signals generated in area MT in response to the behaviorally relevant stimulus do relate to RT. Thus, the data suggest that the precise coordination of remote gamma spindles to optimal alpha phases may enable MT neurons to express fast and high-amplitudic transient responses.

Functional interpretation

A mechanistic role of phase specific coupling between a low frequent modulating band and local gamma band amplitude may indeed play a crucial role in visual attention as proposed by a current model of selective gating (Bonnefond et al. 2017). Local gamma

activity may be aligned in a phase specific manner between areas by means of a common low frequent oscillation (e.g. alpha band). Such temporal long-range coordination may be fundamental for inter-areal gamma band synchrony mediating feedforward stimulus routing (Kreiter 2001, 2006; Taylor et al. 2005; Womelsdorf et al. 2006b; Bosman et al. 2012; Grothe et al. 2012). A prerequisite for gamma-band phase-synchrony is that gamma spindles across different areas occur at similar time intervals. This coordination may well be mediated by means of phase-amplitude coupling (Canolty and Knight 2010; Bonnefond et al. 2017). Our results corroborates such interpretation by the finding that local gamma band spindles during presumably ineffective stimulus routing (slow RT trials) occur at phases that may be less optimal for stimulus processing as compared to fast RT trials where gamma amplitudes are maximal at presumably optimal alpha phases. While phase specificity of the coupling remains ambiguous in our data we show that the neural sensitivity, as indexed by the ensuing transient spiking response, adheres to the perceptual sensitivity and follows the phase specificity of PAC. These findings are in particular compliant with a recent finding that investigated PAC in pre-frontal cortex. In this study PAC was quantified with pairs of neurons in anterior cingulate (ACC) and pre-frontal cortex and between theta phase (5-10 Hz) and gamma amplitude (35-55 Hz). Using an attentional paradigm they could show that PAC indexed correctly executed trials or supposedly successful orientation of spatial attention. Interestingly, preferred phases of PAC during hit trials were earlier and confined to a narrower range along the theta cycle as compared to miss trials. Although, this was not a significant modulation, the data indicates a functional and attention dependent role of the specific preferred phase of PAC (Voloh et al. 2015). Aside from this study and up to our knowledge we show for the first time a significant shift of preferred PAC phases that relate to the efficacy of attention dependent stimulus processing as indexed by the respective RT of the trial. This interpretation is furthermore supported by the finding that alpha phase is instrumental for the initiation of broad-band population level activity and that deviations from preferred alpha phase result in variation in the behavioral RT. In this study (Coon et al. 2016) four human subjects, implanted with subdural electrode arrays performed in a modified Posner cueing paradigm in which subject had to detect the onset of a visual stimulus as quickly as possible. The onset of broad gamma band responses to the onset of visual stimulation was estimated trial-wise at several stages

of the visual processing hierarchy and the resulting mean response delays expectedly accumulated along the hierarchy. Broad-band population level onsets were preferentially locked to the through of an accompanying alpha oscillation. Crucially, for electrodes with high alpha power deviations of this relationship resulted in increasing RT of the trial. For slow trials, population onsets were biased towards the falling slope of the alpha through while for fast RT trials onsets tended to arrive during the through. Furthermore, they showed that the variability of onset times increases with mean onset latency suggesting that temporal onset variance accumulates across subsequent processing nodes amounting to behavioral RT. Although the phase relationships between our animals and in comparison with this study are not consistent, our result also indicate that the phase relationship between gamma band activity and alpha phase are predictive of RT. In line with the conclusions of Coon et al. (2016) we propose that behavioral RT is dependent on the relationship of the population feedforward oscillatory activity (represented as gamma amplitude in our study) to an ongoing modulating alpha oscillation.

Evidence that phase-amplitude coupling is involved with the allocation of attention comes from a further study that investigated the inter-areal gamma amplitude modulation in the human fronto-parietal attention network (Szczepanski et al. 2014). Using ECoG signals from subdural electrode arrays in epilepsy patients they investigated the allocation of visuo-spatial attention in a spatial-cueing paradigm. They found that the strength of delta/theta phase to high gamma (HG) amplitude coupling was stronger in trails resulting in fast RT than in trials resulting in slower RT if attention was directed to the contralateral hemi field relative to the modulated electrodes. Although the finding is different to ours in that the strength of PAC is correlative of RT, they show that the inter-areal coordination of local gamma activity is important for attention dependent processing of visual stimuli. Whether or not they also find differences in the preferred phase of coupling is not stated in the article but given our findings and the results of Voloh et al. (2015) this is likely.

Specificity of phase-amplitude correlation

Phase-amplitude coupling in humans and non-human primates has been observed at various frequency pairs for which the most prominent modulation of gamma amplitude was often found to be confined to theta (4-10 Hz) range (Canolty and Knight 2010; Bosman et al. 2012; Voloh et al. 2015). However, the dominant modulating frequency has also been suggested to be task and regional specific. For example, alpha-gamma PAC has been observed in magnetoencephalography (MEG) using posterior alpha (Osipova et al. 2008) and human nucleus accumbens (Cohen et al. 2009). Furthermore, high frequent amplitude can be modulated by multiple frequency bands and the composition of correlated frequencies may vary according to task demands. For example, gamma modulations were shown to be dominated by an alpha oscillation during a visual task whereas in an auditory task, theta was the predominant modulating frequency (Voytek et al. 2010). Similarly, the frequency specificity of PAC may vary with difficulty and the modulating frequency may shift from high to low theta ranges with increasing memory load (Axmacher et al. 2010). The functional role of the specific modulating frequency band is, to date, not clear and mechanistic explanations has been put forward for different modulating timescales. For example the theta band has been suggested to be an underlying rhythm that determines the rate of attentional sampling throughout the visual field (Fries 2015), whereas the alpha band was associated with a common structure that enables long range coordination of local gamma band synchrony (Jensen and Mazaheri 2010; Jensen et al. 2012; Bonnefond et al. 2017).

Gamma power of local field potential has been suggested to contain local stimulus information in area MT and V4 in a frequency band above 40 Hz (Liu and Newsome 2006; Grothe et al. 2012) and in area V1 in a frequency band between 25 – 90 Hz (Henrie and Shapley 2005). In our data the gamma band that is modulated along the phases of the alpha oscillation is relatively low (35 Hz) but confines to a frequency range that has previously been shown to relate to the phases of a lower frequent oscillation in rat (Belluscio et al. 2012) and human hippocampus (Axmacher et al. 2010).

The discrepancy between the conventional stimulus related gamma band and the frequency band coupling to the alpha phase raises the question whether or not these are two functionally distinct oscillatory modes. One study that investigated the gamma

dependent routing of information in the hippocampus found that CA1 neurons differentially couple to other areas or subfields of the hippocampus (Colgin et al. 2009). CA1 units coupled at a high gamma range to inputs of the medial entorhinal cortex and at a low gamma band to neurons in the CA3 subfield. Since both coupled population are associated with different functions the data suggest that gamma synchrony can occur at different frequency components mediating distinct functionality. We cannot disentangle the possibility of functionally distinct high frequent components in our data but suggest that the specificity of the modulated gamma band is specific to the type of the visual stimulation and experimental paradigm.

The relation of phase reset to PAC

The modulation of preferred phases between RT groups we report here occurs subsequent to a prominent realignment of the phases of the modulating alpha oscillation (Suppl. Figure 1). Phase alignment in this case is most probably due to the prominent modulation of the LFP by the salient onset and change of visual stimulation, although we cannot reject the possibility that phase alignment is partially attributable to an attentional modulation. In particular the onset of motion can serve as a temporal cue to start attending the moving grating as from this time on potential target changes can occur, which was not the case previous to this event. However, we cannot disentangle these possibilities, as both stimulus evoked and intrinsic phase resets may occur simultaneously. We can nonetheless, make use of the fact that the measured phases are realigned in order to choose a time interval of interest where PAC and PAC modulation may be consistent over trials and recording sessions as we have done in our analysis. A number of studies suggest that phase alignment of a low frequent oscillation might be vital for the emergence of PAC. In a study that investigates the temporal control of fear behavior in mice it was found that spikes of projection neurons in the dorsomedial prefrontal cortex (dmPFC) were locked to the phases of theta oscillation of LFP in the dmPFC during the presentation of a conditioned fear stimulus. The locking was accompanied by an increase of theta phase alignment of the LFPs compared to state of low fear expression. Moreover, using optogenetic manipulations they casually related theta phase resets and enhanced spike synchronization to the inhibition of parvalbumin

interneurons, which suggest a mechanistic link between theta phase reset and spike synchronization (Courtin et al. 2014). Van Atteveldt et al. (2014) suggested that the integration of relevant sensory stimuli may enter different processing modes. If the relevant stimuli are predictable in time the brain operates in a rhythmic mode during which excitability fluctuates at timescales of lower frequency oscillations. Modulatory phase resets (e.g. due to the occurrence of neuronal input) may synchronize high excitable phases to the anticipated occurrence of the input. Because neural excitability varies according to the phases of the low-frequent oscillation, gamma-range amplitude might synchronize to the high excitability intervals and thus couple to the low frequent oscillation. Furthermore, Voloh et al. (2015a) showed that the successful orientation of spatial attention is indexed by increases of theta-gamma PAC following the attentional cue. Increases of PAC were accompanied with cue induced theta-phase resets and the authors suggested that phase resets underlie a functional remapping in connectivity between the involved cortical areas that synchronizes gamma-activity burst to the theta rhythmic activation periods.

Differences between phase-amplitude relations

The population PDFs of both animals exhibited different phase-amplitude relationships. For animal I gamma amplitude was preferentially locked to the peak of the alpha oscillation whereas for animal II gamma amplitude was maximal closer to the through. Based on the proposed roles of cortical alpha oscillations (Axmacher et al. 2010; Jensen et al. 2012; Van Atteveldt et al. 2014; Bonnefond et al. 2017) we expected gamma amplitudes to be locked to the through of the alpha oscillation as during these phases excitability is highest. However, the phase of intra-cortical recorded local field potentials is dependent on the positioning of the electrode relative to the sinks and sources of the cortical layer. We did not verify the exact positioning of our electrodes within the cortex and thus do not know the exact relation of excitability of the cortical tissue and the phases that we measured. However, even if the positioning of electrode relative to the cortical surface is constant preferred phases of PAC has been shown to vary substantially even between electrodes in individual subjects. Watrous et al. (2015) investigated PAC, in the context of phase-coding, measured at electrodes of human ECoG and found that

on average high frequent amplitudes were most likely to occur at the through of the low frequent oscillation. On individual electrodes however, high frequent amplitude occurred at various low frequent phases. Furthermore, the main finding of the article, phase specific coupling for the representation of specific image categories, was equally likely to occur at any phase across electrodes. Similarly, our main result confines to the observation that preferred phases are shifted between RTF on individual subjects but the phase specificity of coupling was animal specific.

Moreover, the prominent phase reset following stimulus onset resulted in different phases at maximal phase alignment. The observed phase differences of the two distributions is 119.72° (Suppl. Figure 2) a range that approximate the distances between the preferred phases of PAC measured between animals. Whether and how the coupling of gamma amplitude in the post-motion interval is dependent on the preceding realignment of alpha phase is not clear and we do not speculate about this. However, the phase difference at the phase reset between animals suggest that animal specific difference in electrophysiological recordings do exist and because visual stimulation and task requirements were identical between animals alternative explanations with regard to the observed phase differences are less likely.

Conclusion

We show that the gamma band activity is locked to phases of an alpha oscillation that originates in a remote yet locally connected cortical area. The most significant contribution to this article is that the relationship between the phase of the alpha oscillation and the gamma-band amplitude is predictive of the ensuing reaction time of the trial. We were able to show that trial-to-trial variations in RT relate to trial-to-trial variations of the mean angular phase of the phase-amplitude correlation. This observation could be dissociated from mere firing rate modulations and was accompanied with a modulation of the latency and response amplitude of the output signals in area MT. Our data suggest that gamma spindles are coordinated between areas along the phases of a common alpha oscillation and that the efficiency of stimulus processing is dependent on the preferred phase of this coupling. Future work will have to illuminate what the specific role of the alpha phase is, for example whether cortical

excitability is directly relatable to the fluctuations of a low frequent oscillation and whether inter-areal gamma band synchrony is dependent on the specific phases of such fluctuations.

Acknowledgements

The authors acknowledge support by Peter Bujotzek, Ramazani Hakizimana, and Katrin Thoß regarding animal care and Deniz Parmuk, Eric Drebitz and Andreas Kreiter for support during data recording and the design and evaluation of the analysis.

Supplementary Material

Phase reset at stimulus and motion onset

After the offset of the spatial cue the visual stimulation inside the RF of the recorded neurons began with the presentation of static Gabor's followed by the onset of intrinsic motion in the preferred direction of the recorded MT neurons. From the spike density function we know that MT neurons exhibit large transient responses to the stimulus and motion onset. These may be accompanied with stimulus locked perturbations of the LFP in area MT and V1. Furthermore, the start of the motion onset may serve as a temporal cue for the animals to start paying attention to the motion signal of the gratings. It is only after this event that potential target speed changes may occur. As this structure is consistent for all presented trials the animals likely made use of this cue. Both

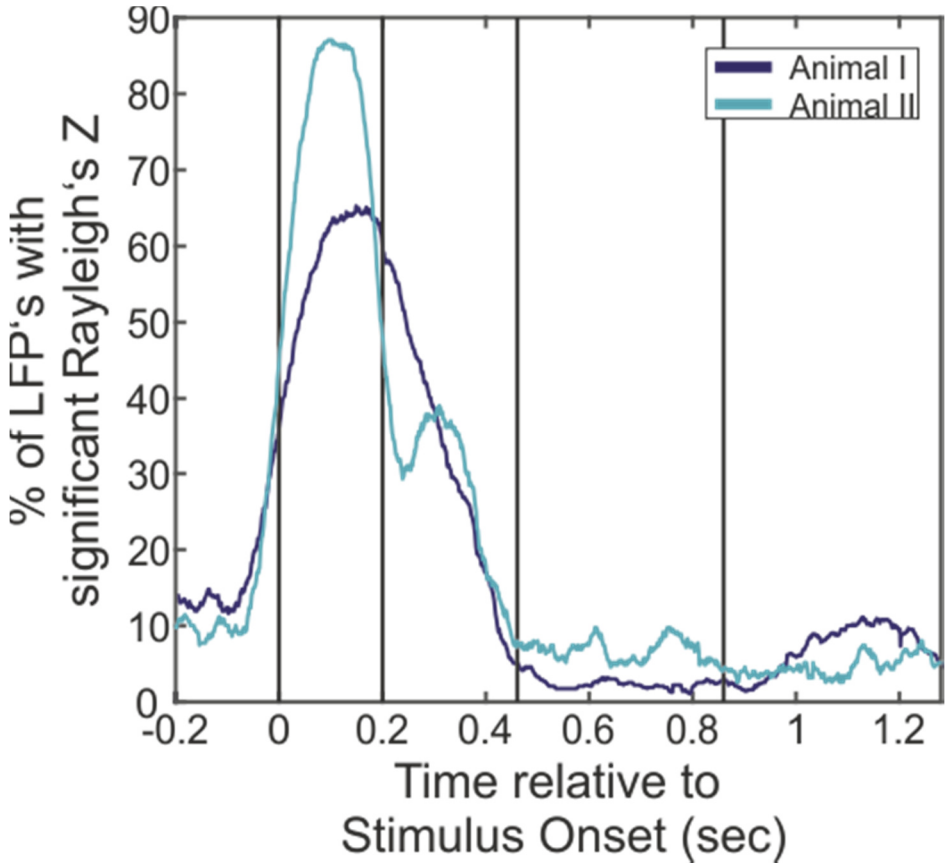

Suppl. Figure 1 Time course of phase concentration across the population of LFP used for the calculation of phase-amplitude coupling. On the ordinate the percentage of LFP that exhibit a significant Rayleigh's Z value (see methods). On the abscissa the time course across the trial is shown. After 0.86 seconds the number of LFP that went into the calculation decreases as the shortest trials end at this time point. Vertical black lines indicate 1. Stimulus onset, 2. Motion onset, 3.-4. the analyzed post motion interval.

attentional onsets (e.g. Voloh et al. (2015b)) and stimulus induced onset (e.g. Coon et al. (2016)) may result in prominent phase resets.

Phase resets in turn are related to the initiation of PAC (see Discussion). In order to choose a time interval during which phase-amplitude coupling is most similar across recorded neuronal pairs and trials, we estimated phase concentration across the time course of the trial. Phase concentration was estimated via the Rayleigh's test for non-uniformity for each time point across the all trials in the attend-in condition. Suppl. Figure 1 the percentage of LFP's that exhibit significant phase concentration ($p <= 0.05$) for each time point is displayed. Prominent phase resets can be observed following

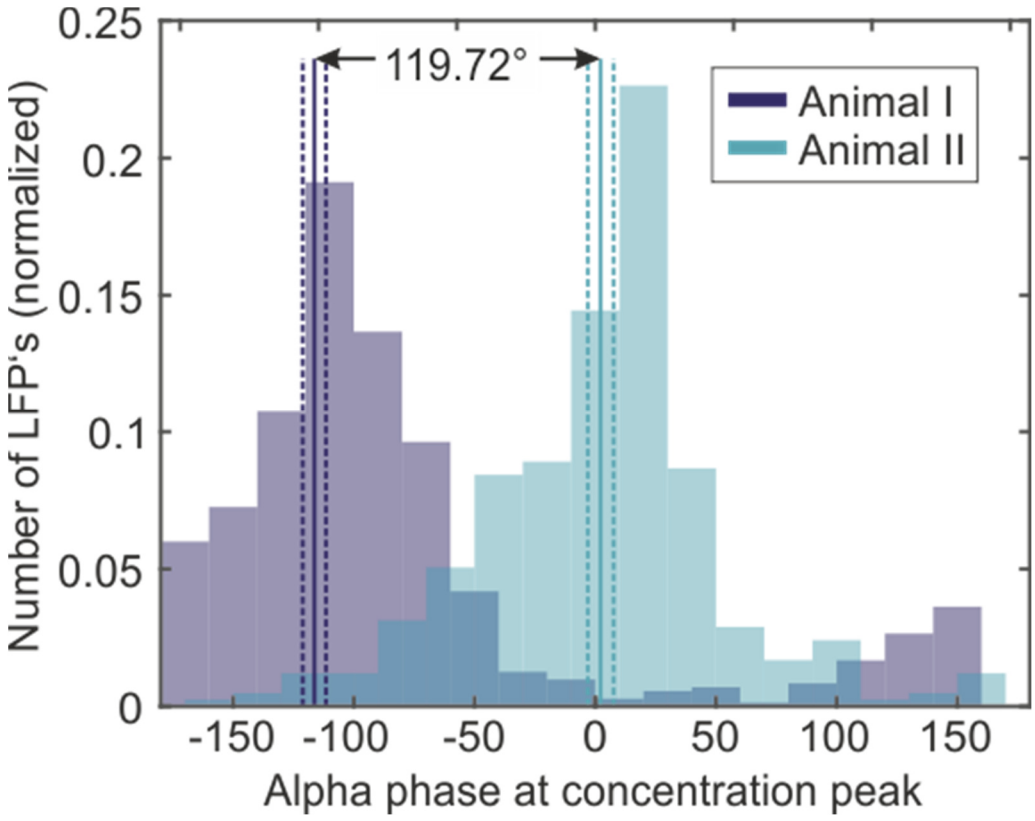

Suppl. Figure 2 Mean angular direction of the alpha phases across the population of LFP's at the peak of stimulus onset induced phase reset. For both animals the distribution (histogram), circular mean (solid lines) and 95 % confidence intervals of the circular mean (dashed lines) of alpha phases at the time point of highest phase concentration (see Suppl. Figure 1 Time course of phase concentration across the population of LFP used for the calculation of phase-amplitude coupling. On the ordinate the percentage of LFP that exhibit a significant Rayleigh's Z value (see methods). On the abscissa the time course across the trial is shown. After 0.86 seconds the number of LFP that went into the calculation decreases as the shortest trials end at this time point. Vertical black lines indicate 1. Stimulus onset, 2. Motion onset, 3.-4. the analyzed post motion interval.) is displayed. These time points closely follow the stimulus onset and designate the time at which most of the LFPs adhere to similar phases, i.e. are reset. Phase distributions are shifted between animals (black horizontal arrow) and the circular distance is 119.72°.

stimulus onset and motion onset. After approximately 400 ms following the stimulus onset phases return to uniform distribution and it is this interval during which also firing rates return to a sustained level of activity. Because PAC may be initiated close to this interval we assumed that the precise estimation of preferred phases are more consistent at this time interval than later in the trial.

Alpha phase at maximal phase resets

In Suppl. Figure 1 we have shown that alpha phases are realigned after the stimulus and motion onsets. Furthermore, the preferred phases of PAC in the main results of both animals are shifted between each other and RTFs cluster around different mean phases. We were interested whether such difference can be attributed to a general parameter in the recording or phase estimation of the low band-pass filtered LFP. In Figure 2 we show the distribution of mean angular phases at the time of maximal phase concentration. Alpha phases for animal I are clustered around a mean of -116.31° with a 95 % confidence interval of the mean of [-120.89°, -111.15°] and for animal II around a mean of -2.29° with a 95% CI [-2.86°, 7.45°]. The distance between the average circular phases is 119.72°. This distance is approximately the same size as the shift of preferred PAC phases between animals. We do not want speculate about the role of the realignment towards a specific phase in the context of phase-amplitude coupling but show that the estimated phases evoked by a constant external event are animal/recording specific and thus may translate into distinct preferred phases in phase-amplitude coupling.

Chapter IV: Optimizing the Yield of Multi-Unit Activity by Including the Entire Spiking Activity

Authors: Eric Drebitz*, Bastian Schledde, Andreas K. Kreiter, Detlef Wegener*

Affiliation: Brain Research Institute, Center for Cognitive Science, University of Bremen, Bremen, Germany

Author Contributions: E.D., A.K., and D.W. designed research, E.D., B.S., and D.W. performed research, E.D. and D.W. analyzed data, E.D., B.S., A.K. and D.W. interpreted results, E.D. and D.W. prepared figures, E.D. and D.W. drafted manuscript, E.D., B.S., A.K., and D.W. edited and approved final version of the manuscript.

Publication: Drebitz E, Schledde B, Kreiter A. K., Wegener D, Optimizing the Yield of Multi-Unit Activity by Including the Entire Spiking Activity. *Frontiers in Neuroscience*, 13:83, 2019.

Abstract

Neurophysiological data acquisition using multi-electrode arrays and/or (semi-) chronic recordings frequently has to deal with low signal-to-noise ratio (SNR) of neuronal responses and potential failure of detecting evoked responses within random background fluctuations. Conventional methods to extract action potentials (spikes) from background noise often apply thresholds to the recorded signal, usually allowing reliable detection of spikes when data exhibit a good SNR, but often failing when SNR is poor. We here investigate a threshold-independent, fast, and automated procedure for analysis of low SNR data, based on fullwave-rectification and low-pass filtering the signal as a measure of the entire spiking activity (ESA). We investigate the sensitivity and reliability of the ESA-signal for detecting evoked responses by applying an automated receptive field (RF) mapping procedure to semi-chronically recorded data from primary visual cortex (V1) of five macaque monkeys. For recording sites with low SNR, the usage of ESA improved the detection rate of RFs by a factor of 2.5 in comparison to MUA-based detection. For recording sites with medium and high SNR, ESA still delivered 30% more RFs than MUA. This significantly higher yield of ESA-based RF-detection still hold true when using an iterative procedure for determining the optimal spike threshold for each MUA individually. Moreover, selectivity measures for ESA-based RFs were quite compatible with MUA-based RFs. Regarding RF size, ESA delivered larger RFs than thresholded MUA, but size difference was consistent over all SNR fractions. Regarding orientation selectivity, ESA delivered more sites with significant orientation-dependent responses but with somewhat lower orientation indexes than MUA. However, preferred orientations were similar for both signal types. The results suggest that ESA is a powerful signal for applications requiring automated, fast, and reliable response detection, as e.g. brain-computer interfaces and neuroprosthetics, due to its high sensitivity and its independence from user-dependent intervention. Because the full information of the spiking activity is preserved, ESA also constitutes a valuable alternative for offline analysis of data with limited SNR.

Introduction

As an early step during analysis of extracellularly recorded signals, the actual spiking response of a neuron, or a group of neurons, usually needs to be separated from the background noise of the recorded signal. A common procedure is to set up an amplitude threshold to the high-passed neuronal signal. This threshold can be set manually or be defined automatically based on statistical likelihood. Frequently used methods for automatic threshold definitions use multiples of the standard deviation of the high-passed signal (Pouzat et al. 2002) or the median of the absolute signal (Quiroga et al. 2004). Amplitude threshold-based spike detection has been proven successful in data with good SNR, but its performance declines significantly with decreasing SNR (Nenadic and Burdick 2005). Other methods such as template matching (Bankman et al. 1993) and wavelet-based extraction of time- and frequency-resolved spike features (Yang and Shamma 1988; Hulata et al. 2002; Quiroga et al. 2004; Nenadic and Burdick 2005) either require a priori knowledge about the spike form, or an extensive amount of processing (Obeid and Wolf 2004). Yet, robust methods for dealing with low SNR data become particularly important with the increased importance of multi-electrode arrays used for large-scale neuronal recordings and brain-computer interfacing (Buzsáki 2004; Lebedev and Nicolelis 2006; Lewis et al. 2015), and other semi-chronic recording techniques (deCharms et al. 1999; Galashan et al. 2011; Mendoza et al. 2016). In contrast to acute recordings with separately controlled microelectrodes, however, the position of array electrodes is fixed, or electrodes are more difficult to adjust. It is hence either impossible or difficult to carefully guide individual electrodes for optimizing a neuron's signal, resulting in highly variable magnitudes of extracellular action potentials (Gold et al. 2006). Additionally, signals of (semi-) chronically implanted electrodes degrade over time, due to local tissue responses (Schwartz 2004; Polikov et al. 2005). Both issues are likely to result in a high number of channels exhibiting low SNR.

Analysis of such data is usually confined to the local field potential (LFP), because thresholding spikes in low SNR responses potentially results in a high number of either false positives or false negatives, depending on the threshold level. Hence, thresholding may have a significant impact on the estimated strength and temporal structure of the

response, and interpretation of such data is problematic. The LFP, on the other hand, represents the integrated neuronal activity in close neighborhood of the electrode and constitutes a sensitive measure of neuronal activity (Liu and Newsome 2006; Katzner et al. 2009). Yet, the LFP reflects the sum of all local transmembrane currents rather than the output signal of the recorded neurons. Analysis of the latter, therefore, requires a reliable method to efficiently segregate stimulus responses from unspecific background noise, particularly at low and medium SNR recording sites. At the same time, there should be no trade-off at recording sites with high SNR when compared to established methods based on thresholding.

We hypothesized that a method introduced in the early 1990s by Eckhorn and colleagues (Eckhorn 1991, 1992; Eckhorn and Obermueller 1993; Brosch et al. 1997) possesses the critical properties to serve as such a reliable signal for detecting evoked responses in low SNR data. This method was invented for analyzing correlated activity at multi-unit recording sites, and is based on a fullwave-rectification of the high-passed neuronal signal (containing the spike information), followed by low-pass filtering. The method delivers a continuous instead of a binary signal, and represents the aggregated spiking activity of neurons located about 50 µm around the electrode's tip (Legatt et al. 1980; Brosch et al. 1997). Its most important advantage is that it does not rely on setting up a threshold but takes all the available spiking information. Because of the final low-pass filtering it should be rather insensitive to random high-frequency noise, making it a highly promising candidate approach for detecting evoked responses when SNR is weak. For the remainder of the paper, we denote this signal as ESA (Entire Spiking Activity).

Since its introduction, ESA has been used as an alternative measure for multi-unit activity by several groups(Dougherty et al. 2015; Self et al. 2016; Drebitz et al. 2018), but many of its important properties are still awaiting quantitative description. The purpose of the present study is to analyze the potential of ESA for increasing the yield of multi-unit recordings at different SNRs, and to quantitatively compare evoked responses based on ESA and thresholded MUA. For the example of receptive field (RF) mapping, we analyze semi-chronic recordings from primary visual cortex (V1) of five macaque monkeys (*Macacca mulatta*), and compare ESA-based RF detection rates with both

conventionally thresholded MUA and the LFP, and further analyze RF size and orientation selectivity between ESA- and MUA-based RFs obtained from the same high-frequency signal. We use two approaches to set the threshold for analyzing MUA: a standard procedure with a fixed threshold for all units, and a second, computationally time-consuming iterative procedure to determine the optimal threshold for each unit individually. The results show that ESA outperformed MUA in both cases, particularly when SNR was low. ESA-based RF detection was almost as sensitive as LFP-based detection, and RF parameters corresponded to those found with thresholded MUA. RF-sizes were slightly larger than MUA-RFs, due to considering all available spiking information, but size differences were consistent over all SNR fractions. Relative orientation sensitivity (i.e. number of sites with significantly biased responses for different orientations) was higher for ESA, while absolute orientation selectivity (i.e. orientation indexes) was slightly attenuated as compared to thresholded MUA. Independent of these differences, the majority of recording sites delivering a RF with both signal types was found to have similar preferred orientations. Thus, ESA constitutes a powerful source of information to be considered when depending on reliable and fast neuronal response detections, such as for (semi-) chronic recordings or BCI-approaches, as well as for increasing the information content of low SNR data for offline analysis.

Materials and Methods

Subjects and Surgical Procedures

Five male macaque monkeys (*Macaca mulatta)* were implanted with custom-made head holders and recording chambers under aseptic conditions and propofol/remifentanyl anesthesia. Four animals (monkeys B, P, V, and F) were implanted with a V1 microdrive array, allowing for bidirectional movement of six semi-chronically inserted electrodes (Galashan et al. 2011). The fifth animal (monkey T) was implanted with a recording chamber located above areas V4 and V1, allowing for bidirectional movement of up to four electrodes. Details on anesthesia, analgesia, and surgical procedures are reported elsewhere (Wegener et al. 2004; Galashan et al. 2011; Schledde et al. 2017; Drebitz et al. 2018). All procedures were in accordance with the Regulations for the Welfare of Experimental Animals issued by the Federal Government of Germany and with the guidelines of the European Union (2010/63/EU) for care and use of laboratory animals, and were approved by the local authorities (Senator für Gesundheit, Bremen, Germany).

Visual Stimuli and Behavioral Task

Data was acquired with an automatic bar-mapping procedure to stimulate the visual field region of interest, similar to the method described by Fiorani et al. (2014). The mapping was performed for different scientific projects not reported here. For the stimulation details that follow, task parameters of monkey T are stated in the text, and deviating parameters of one or more other animals are given in brackets. Visual stimulation was performed on a 20-inch (22-inch) CRT-screen, with a resolution of 1024 x 768 (1280 x 1024) pixels at 100 Hz vertical refresh rate. Monkeys were placed in a custom-made primate chair 90 (80) cm in front of the screen. Appearance of the central fixation point (FP) indicated trial start and animals were given 2 sec to initiate the trial by gazing at the FP and pressing a lever. Following a blank period of 820 (300) ms, a high-contrast bar appeared on screen and moved with constant speed in one of 12 motion directions (separated by 30°), and disappeared at the end of the trajectory. Length of bars (3.2 - 8.2°), motion trajectories (2.5 - 10.75°), and stimulus speed (1.9 – 4.7 °/sec)

varied between animals, recording sites, and occasionally between recording sessions, depending on the spatial area to be covered (16 – 64 deg²). Monkeys were required to keep fixation throughout the trial and to indicate a decrease in FP luminance occurring during a pseudo-random interval between 250 and 1250 ms after bar disappearance, by releasing the lever within a time period from 150 to 750 ms after FP dimming. To ensure that animals stayed alert throughout the trial, FP dimming occurred already during bar presentation in about 10 % of trials. These trials did not enter data analysis. Successive trials were separated by a 2 sec inter-trial interval. Eye position was monitored by video-oculography (monkey T: ISCAN Inc., MA, USA; monkeys B, P, V, and F: custom-made eye tracking system). Correctly performed trials were rewarded with a small amount of water or diluted grape juice. Responding too soon or too late, and eye movements of more than 0.5° (1°) away from the FP caused immediate trial termination without reward.

Data acquisition

Neuronal data was recorded using up to six epoxy- or glass-insulated tungsten electrodes (125 µm diameter, 1-3 MΩ, FHC Inc., Bowdoin, ME, USA). Two different recording setups were used for data acquisition. In the first setup (monkeys B and P), the electrode signal was sampled at 25 kHz frequency, amplified 3000 fold (10 x, custom-made head stage, 300 x, custom-made main-amplifier), and band-passed between 0.7 and 5 kHz for receiving the spike information. For the LFP, the amplified electrode signal was low-passed at 300 Hz and down-sampled to 1 kHz. Hardware-filtered data was then digitized at 16 bit ADC resolution. In the second setup, the electrode signal was amplified using either a custom-made head stage (monkeys V and F), or a wideband preamplifier (monkey T; MPA32I, Multi Channel Systems, Reutlingen, Germany), both with a gain of 10, and a main-amplifier (PGA 64, 1 -5000 Hz, Multi Channel Systems, Reutlingen, Germany) with a gain of 1000. The amplified raw-signal was digitized with a sampling-rate of 25 kHz and a resolution of 12 (monkey T) or 16 bits (monkeys V and F). Electrode signals were referenced either against a low impedance electrode (< 0.1 MΩ) implanted into the frontal skull bone and touching the dura (monkeys B, P, V, F), or against the

titanium recording chamber (monkey T), which was screwed into the bone and touching the dura.

Data analysis

All offline analyses were performed with customized MATLAB-scripts (Mathworks, Natick, MA, USA). As described above, data of monkeys B and P was already band-pass filtered before digitizing. Data of monkeys T, V, and F was filtered offline either between 0.7 – 5 kHz (monkeys V and F) or 0.3 – 12.5 kHz (monkey T) for isolating the high-frequency components (spikes), and low-passed either below 300 Hz (monkeys V and F) or 170 Hz (monkey T) for the low-frequency components (LFP). All offline filters were equiripple FIR-filters, applied in forward and backward direction to avoid phase shifts.

Spike detection for analyzing thresholded MUA was done using the method introduced by

Quiroga et al. (2004), defining the threshold *Thr* as:

(1) $$Thr = a * \text{median}\left(\frac{|x|}{0.6745}\right),$$

where *x* represents the high-passed data of which the median is taken and *a* represents a factor for different threshold levels. This factor was set to $a = 3$ for the standard procedure, and was varied between $a = 2$ and $a = 4$ (in steps of 0.5) for the iterative procedure. To take advantage of the full spike information, no further spike sorting was performed, and all events surpassing the threshold were used (Figure 16 A). Spike times were binned with a resolution of 1 ms and convolved with a Gaussian kernel ($\sigma = 25$ ms) to obtain the spike-density function (SDF).

ESA was calculated on the same high-passed data, but instead of setting a threshold the data was full-wave rectified and low-pass filtered in forward and backward direction (Figure 16 B), and down-sampled to 1 kHz (Legatt et al. 1980; Eckhorn 1991, 1992). To achieve best comparability, low-pass filtering was performed by a Gaussian filter with the same characteristics as used for calculating the SDF. LFP power was calculated by convolving the low-passed signal with complex Morlet's wavelets (Torrence and Compo 1998), as described in more detail elsewhere (Tallon-Baudry et al. 1997; Taylor et al.

2005). The resulting complex coefficients $\tilde{x}$ at time t and frequency f can also be expressed by their amplitude A and phase Φ such that:

(2) $$\tilde{x}(t,f) = A(t,f)e^{i\Phi(t,f)}.$$

Power was calculated by taking the square of the absolute value of $\tilde{x}(t,f)$, divided by the Nyquist-frequency (500 Hz). For each recording site, the power values for each time-frequency bin were normalized by first subtraction of and then division by the mean power spectrum of the spontaneous activity (obtained during the blank period prior to bar onset, excluding the first 100 ms). From this time–frequency representation of the LFP power we extracted the time course of the average power between 40 and 120 Hz.

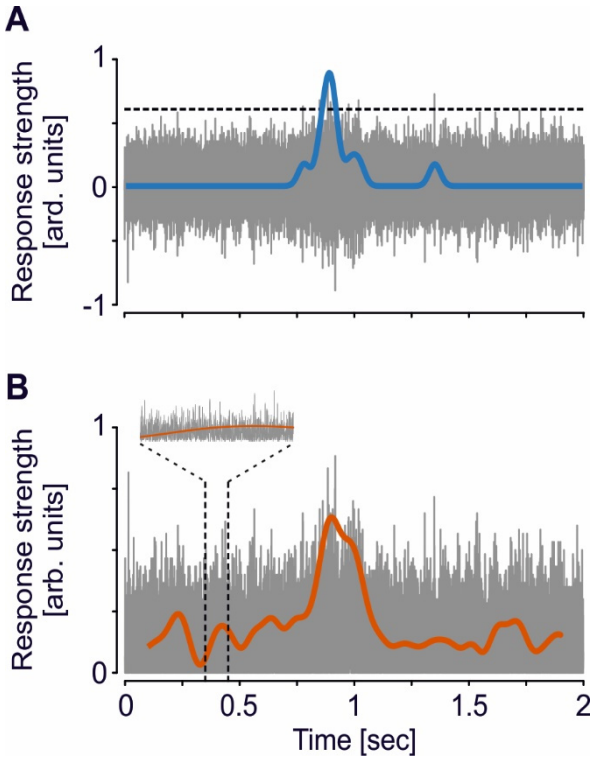

Figure 16 Exemplary trace of a single-trial illustrating analysis of MUA and ESA. ***(A)*** *For MUA, a threshold (dashed line, cf. equation 1) based on the method introduced by Quian Quiroga et al. (2012) was applied to the high-passed signal (grey trace). All events surpassing the threshold were then used for calculating the SDF (blue line).* ***(B)*** *For ESA, analysis is based on the full-wave rectified signal, i.e. the absolute values of the high-passed signal (grey trace), and then low-pass filtered (red line), using the same filter settings as for the SDF. This computation is independent of setting a threshold. Ordinate scaling is identical in both plots, SDF and ESA traces are both upscaled by a factor of 5 for visual purposes. Note that due to line thickness and time span, gaps between adjacent spike events are hardly visible. The inset in (B) shows a time period of 100 ms to illustrate the time course of the rectified signal in more detail.*

Receptive field detection

RF analysis was limited to data having at least five repetitions of each bar direction. To allow for direct comparison between MUA, ESA, and LFP, all data was *z*-transformed according to Fiorani et al. (2014). To this end, we first subtracted the mean spontaneous activity (averaged over all trials and orientations) from the response to a given motion trajectory, and then divided by the standard deviation of the responses to this direction. For the LFP, this was based on the average power in the broad γ-frequency range (40 – 120 Hz). RF-locations were calculated using the back-projection method, which is described in more detail in Fiorani et al. (2014). In brief, for each specific time point mean *z*-transformed responses to each of the twelve motion directions were back-projected to the location and orientation of the bar on screen, to obtain activity maps spanned by the bars' size and path length (see Figure 17, Fiorani et al. 2014). The geometrical mean of the averaged, aligned responses to each of the 12 bar motion directions then provides the merged activity map. To avoid multiplying by values below one, each activity map with a minimum *z*-value < 1 was shifted by an offset parameter R_{off}, given by the difference between the actual minimum value and one. The final merged map was corrected for these offsets by subtracting the geometrical R_{off} mean. We then searched for areas with mean activity higher than half the maximum of all values within the map. Such areas were considered a RF if first, the diameter (recalculated from estimated RF area) was between 0.6° and 2.6°, and second, the average *z*-value was larger than 0.8. Recording sites with low SNR often contained several connected areas in their activity maps with values larger than half of the maximum amplitude. In these cases, we only considered the largest of these areas as RF, if all other areas were smaller than 0.5° in diameter. These rather conservative criteria are more likely to deliver false negatives than false positives. RF size was calculated based on the spatiotemporal resolution of the activity map and the number of entries defining the RF. With the exception of estimating significance of orientation tuning (described below), all other analyses were based on the mean *z*-transformed response within these RF borders, calculated separately for each of the 12 motion trajectories.

Orientation Tuning

For analysis of orientation tuning, we first verified whether a site's tuning was significant ($P < 0.05$), using a method introduced by Grabska-Barwińska et al. (2012) to test the reliability of response differences to different orientations for repeated stimulus presentations. The response in any given trial is represented by the mean, non-transformed activation over the time the bar is passing the RF. In detail, for identifying significantly tuned sites, the full set of n_Φ bar orientations was shown for n_k repetitions, and the average in the complex plane $z_{PO(k)}$ was calculated for each of the repetitions *k*:

(3) $$z_{PO(k)} = \frac{1}{n_\Phi}\sum_\Phi f(\Phi,k)e^{2i\Phi},$$

with $f(\Phi,k)$ representing the neuronal response to each orientation Φ. The angle of $z_{PO(k)}$ delivers the preferred orientation *PO* from each repetition. The vector average $\langle z_{PO}\rangle$ of the normalized vectors $z_{PO(k)}$ for all repetitions can then be calculated by:

(4) $$\langle z_{PO}\rangle = \frac{1}{n_k}\sum_k \frac{z_{PO(k)}}{|z_{PO(k)}|} = \frac{1}{n_k}\sum_k e^{2iPO(k)}.$$

The reproducibility of the preferred orientation r_{PO} is defined as the length of $\langle z_{PO}\rangle$:

(5) $$r_{PO} = \frac{1}{n_K}\left|\sum_k e^{2iPO(k)}\right|.$$

The reproducibility is 1 if the *PO* is equal for all repetitions, and 0 if *PO* values are uniformly distributed on the 0 – 180° range. Significance of orientation tuning was determined by comparing the reproducibility r_{PO} to a probability distribution $P(r_{PO(n_k)})$ obtained from Monte-Carlo simulations under the assumption of a uniform distribution of *POs*.

Sites with significant orientation tuning were used for comparing the tuning between signal types based on an orientation selectivity index calculated by vector averaging(Grinvald et al. 1986). If an average *z*-transformed response to any of the twelve bar directions was below zero, this value was multiplied with -1 and added to each of the twelve response vectors. Neuronal responses $f(\Phi)$ to each of the n_Φ bar directions were represented in the complex plane and averaged:

(6) $\langle z \rangle = \frac{1}{n_\Phi} \sum_\Phi f(\Phi) e^{i2\Phi}$.

The preferred orientation is then given by the halved angle of the average vector $\langle z \rangle$, and the tuning strength by its length $|\langle z \rangle|$.

Statistical Analysis

For each monkey and signal type, the detection ratio *DR* of significant RFs was given by:

(7) $DR = \frac{N_{Signal}}{N_{all}}$,

where N_{Signal} corresponds to the number of significant RFs found for the signal type under investigation, and N_{all} corresponds to the total number of recording sites with a significant RF independent of signal type. Note that for each signal type, each recording site delivered maximally one RF by definition. Statistical analysis of detection rates was done by performing paired ANOVAs on the mean detection rates of each animal and post-hoc testing with Tukey's honestly significant difference (HSD) procedure, correcting for multiple comparisons. Statistical analysis of RF size and orientation selectivity was performed on sites delivering a significant RF for both ESA and thresholded MUA, pooled over all animals, using Wilcoxon signed rank tests. Effect size *R* was calculated by:

(8) $R = \frac{|Z|}{\sqrt{N}}$,

where *Z* is taken from the Wilcoxon test statistics, and *N* represents the total number of samples.

Results

The aim of the study was to assess the sensitivity of the fullwave-rectified, low-passed spiking activity (ESA) for unsupervised detection of visual responses. For directly comparing ESA performance under different SNR conditions with conventionally thresholded MUA and with the LFP, we used a data-set of semi-chronic intra-cortical recordings from area V1 of five macaque monkeys. Data was acquired during an automatic bar mapping procedure. We used two approaches to set the threshold for analyzing MUA-based detection. The first approach (standard procedure) used a multiplication factor of α = 3 for all data (see Material and Methods). The resultant threshold level was found to be quite robust against false positives and false negatives. The second approach used an iterative procedure with multiplication factors of α = 2 to α = 4 (in steps of 0.5) to find the optimal threshold for each individual unit. Although this procedure is time-consuming and requires computing of RF maps for each threshold, it maximizes the yield of MUA-based RF detection. Note, however, that it requires a priori knowledge to distinguish evoked responses from false positives. The final dataset included all recording sites delivering an RF for at least one of the three signals types (standard procedure: N = 653, iterative procedure: N = 656).

Quantitative comparison of RF detection between signal types

We first analyzed RF detection rates for ESA and conventional MUA, based on signal strength and area of activation (see Material and Methods), and compared it to LFP-based detection rates. Figure 17 provides boxplot histograms of the pooled data across signal types for each of the two MUA procedures. ESA delivered an RF at 500 recording sites, which was close to the detection rate of the LFP (N = 570). In contrast, MUA delivered an RF at 337 recording sites using the standard procedure, and at 399 recording sites using the iterative procedure. The latter provides the maximum of RFs to be obtained by thresholding. Table 1 summarizes the number of RFs for each individual animal and signal type. Comparing across animals, ESA-based detection delivered most RFs in three of the five animals, while in the remaining two animals most RFs were obtained using the LFP. Importantly, ESA delivered more RFs than thresholded MUA in each individual animal, regardless of the procedure to set the threshold. Note that this

was true albeit individual animals were recorded for different experimental purposes, using different recording setups and filter settings, and predominant recording layers varied between animals. Thus, the higher detection rates obtained with the ESA signal were not due to specific experimental conditions but a general outcome independent of the specific recording details.

Table 1 Number of detected RFs for individual subjects and signal types. If different between standard procedure and iterative procedure, numbers in brackets refer to the iterative procedure.

		LFP		ESA		MUA	
Monkey	Total *N*	*N*	%	*N*	%	*N*	%
B	130	99	76.2	109	83.9	83 (87)	63.9 (66.9)
F	81 (82)	55	67.9 (67.1)	65	80.3 (79.3)	39 (57)	48.2 (69.5)
P	219	212	96.8	176	80.4	150 (161)	68.5 (73.5)
T	172	166	96.5	118	71.1	65 (80)	37.8 (48.2)
V	51 (53)	38	74.5 (71.7)	32	62.8 (60.4)	0 (14)	0 (26.4)
Total	653 (656)	570	87.3 (86.9)	500	76.6 (76.2)	337 (399)	51.6 (60.8)

We performed the statistical analysis on RF detection rates per thresholding procedure and across animals. For the standard procedure, a 1-way RM-ANOVA confirmed

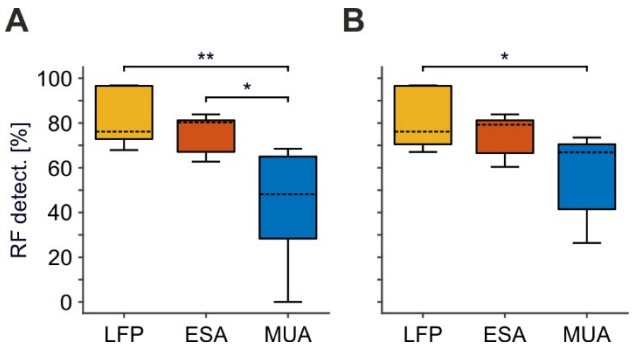

Figure 17 Comparison of RF detection rate between LFP, ESA, and MUA. ***(A)*** *Standard approach for thresholding MUA.* ***(B)*** *Optimized, iterative approach for thresholding MUA to maximize MUA-based detection rate. For each signal type, boxplots are based on detection rates of individual animals. Detection rates refer to the absolute number of RFs detected relative to the number of recording sites with a significant visual activation for at least one of the signals, merged over all animals. Boxes indicates the 25th and 75th percentile, dashed lines indicate the medians, and whiskers indicate the full range of data. Asterisks indicate statistical difference for α < 0.5% (*) and α < 0.05% (**), respectively.*

significant differences between signal-types ($F(2,14) = 9.28$, $P = 0.008$, $N = 5$). Post-hoc Tukey HSD tests showed that the percentage of detected RFs based on ESA was significantly higher than detection rates for thresholded MUA ($P = 0.026$), while detection rates between ESA and LFP were statistically indistinguishable ($P = 0.739$). For the iterative procedure, the difference between ESA- and MUA-based detection now failed to reach significance ($P = 0.113$). Note, however, that also in the iterative procedure ESA delivered considerably more RFs than MUA in each individual animal (mean increase: 25%, range: 9 - 125%).

Dependence of RF detection on SNR

We next investigated detection rates under different SNR conditions. When recording with (semi-) chronically implanted electrodes or electrode arrays, the electrodes' tips are usually not optimally positioned to the neurons in their vicinity, such that spike amplitudes may surpass background fluctuations only marginally. Figure 18 A provides an example of a single trial under such poor SNR conditions. Although there was a significant visual response in the LFP, spike events at this site had very small amplitudes and only a few passed the threshold, calculated based on equation 1 with $\alpha = 2$ (Figure 18 A, top panel). The resultant visual response map, computed over all trials, did not reveal any responsive region in the stimulated visual space based on the thresholded MUA (Figure 18 E, left panel). Full-wave rectification and low-pass filtering the signal, however, revealed a small amplitude modulation during the course of the trial (Figure 18 A, lower panel). Because in the ESA-signal such small modulations can be reliably detected in trials with low SNR, the ESA-based analysis of the same data provided a visual response map with a significant area of activation (Figure 18 F, left panel). A second example from a different monkey is presented in the second-most left panels in Figure 18 E and F. Under conditions of high SNR, on the other hand, both thresholded MUA and ESA reliably isolate the evoked spiking activity from background noise (Figure 18 D), resulting in visual response maps with clearly defined and similar RFs (Figure 18 E and F, middle to right panels). However, when based on MUA, the detected RF regions sometimes appear a little bit noisier and smaller (Figure 18 E and F, middle and second rightmost panels).

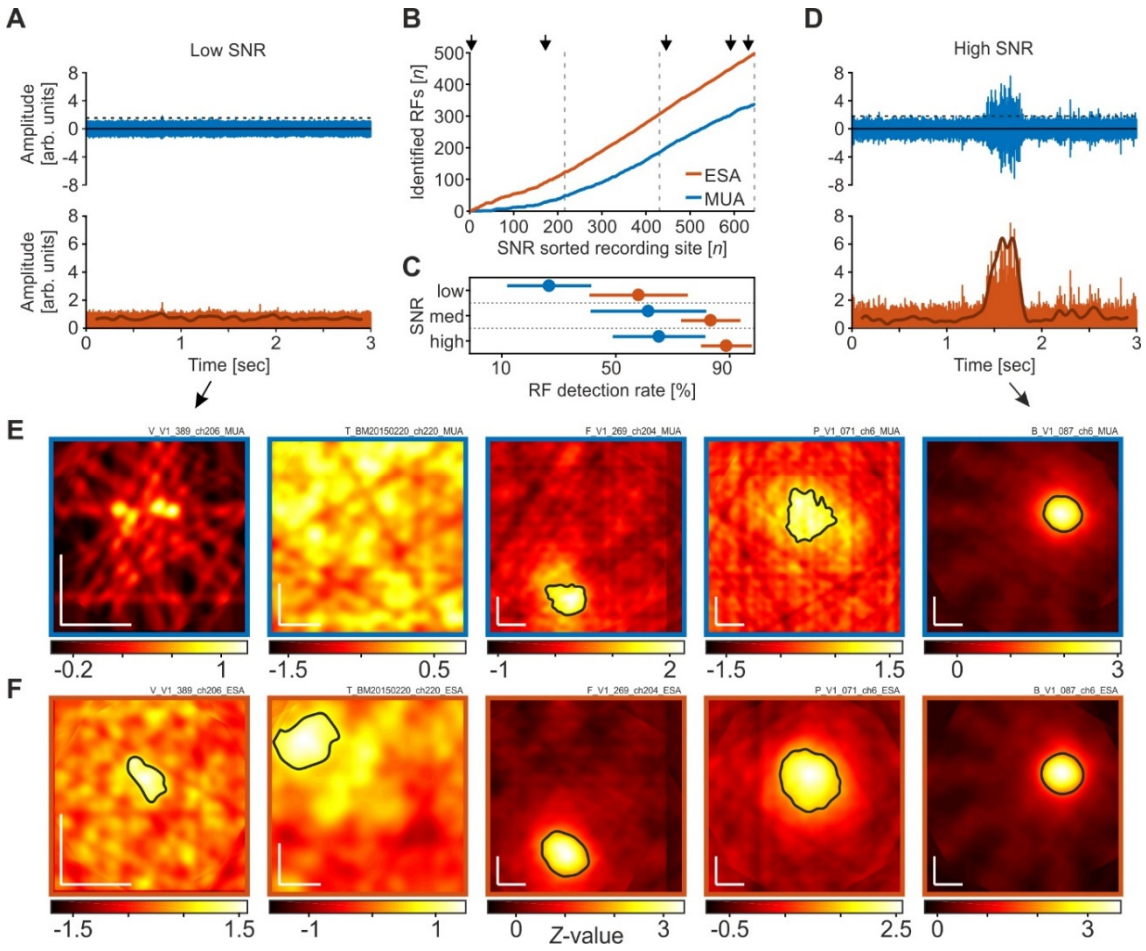

Figure 18 RF detection rates in dependence of signal-to-noise ratio (SNR). ***(A)*** *High-pass filtered neuronal activity with very poor SNR (rank 4 out of 653). The upper panel depicts a single trial in response to a motion direction that reliably modulated the LFP. The dashed line indicates the threshold as calculated over all trials, using the method of Quian Quiroga et al. (2004) with a median multiplication factor of a = 2. Events surpassing the threshold are used to calculate spike density functions. The lower panel shows the same high-passed signal after full-wave rectification. Subsequent low-pass filtering provides the ESA-signal (thick line), revealing a small amplitude modulation during the course of the trial.* ***(B)*** *Cumulative distribution of the number of RFs detected using either MUA or ESA, sorted by SNR. Dashed lines distinguish equally large fractions of recording sites with low, medium, and high SNR, as used for statistical analysis. Arrows indicate the SNR ranks of the five example sites shown in (E, F).* ***(C)*** *Detection rates for low, medium, and high SNR sites, based on the respective detection rates of data from the individual animals, separately for ESA and MUA. Disks and lines indicate mean ± S.D, respectively.* ***(D)*** *Same as in (A), for a recording site with high SNR (rank 632).* ***(E, F)*** *Visual response maps based on thresholded MUA (E) and ESA (F) for the five recording sites indicated in (B). SNR rank increases from left to right. Vertical and horizontal white bars in the lower left corners indicate 1° of visual space. White outlined areas depict significant visual responses (receptive fields). For the two left-most maps in (E) no significant visual response was found with any of the thresholds tested during the iterative procedure. Actual maps were calculated based on a median multiplication factor of a = 2 for setting the threshold. Remaining maps (middle to right) were calculated after thresholding with a = 3.*

To investigate the relation between RF detection rate and SNR in more detail, we calculated the SNR of all recording sites and determined detection rates as a function of

SNR. SNR was calculated by dividing the median amplitude of all spike events surpassing the threshold by the threshold value itself. For reasons of comparability, the threshold was calculated by a multiplication factor of $a = 3$, as applied in the standard procedure. We used the same dataset as before, i.e. we also included those recordings for which we only detected an RF in the LFP to keep the total N constant. Figure 18 B depicts the cumulative distribution of the number of RFs detected using either ESA or MUA, sorted from low to high SNR. Note that at low SNR, the two traces representing ESA and MUA strongly deviate, and even with medium and high SNR, the ESA slope is still steeper than the MUA slope. For statistical analysis, we divided the dataset into three equally large groups of sites with low, medium, and high SNR (indicated by dashed lines in Figure 18 B), and calculated the RF detection rate of each animal and group. Based on ESA, a significant visual response was detected at 59.3%, 84.7%, and 90.2% of recording sites with low, medium, and high SNR, respectively. For thresholded MUA, the corresponding detection rates obtained by the standard procedure were 28%, 62.8%, and 66.5%. A 2-way RM-ANOVA with the factors signal type and SNR revealed a main effect of both factors (signal type: $F(1,2) = 14.87$, $P = 0.0182$; SNR: $F(2,2) = 4.85$, $P = 0.0417$, N = 5), and no interaction ($F(2,8) = 0.018$, $P = 0.548$). Post-hoc Tukey HSD multiple comparison tests showed that at low SNR, ESA-based detection rates were higher than MUA-based detection rates at the 95% confidence level, while the difference in detection rates at medium and high SNR was statistically not significant (Figure 18 C). The iterative procedure delivered equivalent statistical conclusions.

Additionally, because ESA delivered RFs at recording sites where MUA did not (iterative procedure: N = 115), we estimated the likelihood to get a false positive RF detection. This was done by re-shuffling the time bins and labels of the raw PSTH. We then computed visual activity maps as before (cf. section Receptive field detection). The actual number of RFs found with this procedure was zero, indicating a very low likelihood that the additionally detected ESA-RFs consist of a significant number of false positives.

RF size and orientation Tuning

Higher detection rates in data with poor SNR do not necessarily imply that they will provide reliable estimates about the response characteristics of the underlying group of neurons. We therefore investigated the selectivity of ESA and thresholded MUA with respect to the estimated RF size and orientation tuning of the detected units. To get the maximal RF yield, we based this analysis on the iterative procedure for thresholding. Likewise, to obtain the maximal spike information from each unit, we used the smallest threshold that allowed detection of a significant visual response for that unit. Assuming idealized circular RFs, the mean calculated diameter ± S.D. of ESA- and MUA-RFs was 1.6 ± 0.45 and 1.49 ± 0.46°, respectively. For comparison, the size of LFP-RFs was 1.7 ± 0.38° and thus was slightly larger than for ESA and MUA. For statistical analysis, we limited the dataset to those units delivering a significant RF for both ESA and MUA and based the calculation on actual RF areas. ESA-RFs were found to be significantly larger than MUA-RFs (Wilcoxon signed rank test, $Z = 9.84$, $P < 10^{-22}$, $N = 385$, $R = 0.355$) (Figure 19). A Tukey HSD multi-comparison analysis for units with low, medium, and high SNR revealed that the estimated size of both signals increased from low to high SNR (both $P < 10^{-5}$, $N = [30\ 60\ 295]$), but the size difference between ESA-and MUA-RFs did not differ

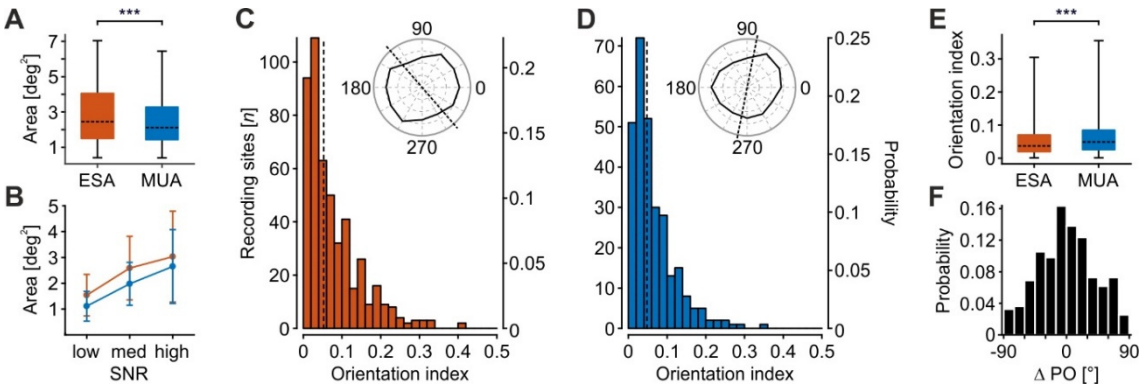

Figure 19 . Comparison of stimulus selectivity between ESA and MUA. ***(A)*** *RF area of recording sites with significant visually evoked response modulation for both ESA and MUA (N = 385). Boxplot conventions as in Figure 17.* ***(B)*** *RF area as a function of SNR for same units as in (A). Error bars indicate S.D.* ***(C, D)*** *Distribution of orientation indexes for ESA (C) and MUA (D). Dotted lines indicate median OI. Polar plot insets show exemplary orientation selective responses at median OI value for either signal type.* ***(E)*** *Direct comparison of orientation selectivity of units with significant orientation-selective responses for both MUA and ESA (N = 275). Box plot conventions as in Figure 17.* ***(F)*** *Signal-dependent difference in preferred orientation (ΔPO) for same units as in (E).*

between SNR groups (1-way ANOVA, $F(2,382) = 2.394$, $P = 0.09$, $N = [30\ 60\ 295]$) (Figure 19).

Orientation selectivity was estimated based on vector averaging the responses to the six bar orientations, according to Grabska-Barwińska et al. (2012). The method labels orientation tuning as significant depending on the reliability of orientation-related responses over trials, but independent of the absolute orientation index (OI). Orientation tuning was considered significant at 97.8% ($N = 489$) of all recording sites with a significant ESA-RF, and at 72.2% ($N = 288$) of all sites with a significant MUA-RF. Figure 19 C and D show the distribution of OI values for the two signal types. Polar plot insets depict two exemplary recording sites with an OI close to the population medians for ESA (0.053) and MUA (0.048). Statistical analysis was performed on units with a significant orientation tuning for both ESA- and MUA-RFs (Figure 19 E). For this subset of sites, MUA turned out to be significantly more orientation selective than ESA (Wilcoxon signed rank test, $Z = 3.8$, $P < 10^{-3}$, $N = 275$), but the effect size was small ($R = 0.162$). Despite this reduction in absolute selectivity, 43% ($N = 117$) of the recording sites had about the same preferred orientation (deviation < 15°) independent of signal type, and 70% ($N = 164$) of recording sites did not differ by more than 30°, i.e. preferred orientation was within the range of two neighboring stimulus orientations (Figure 19 F).

Discussion

Full-wave rectification and subsequent low-pass filtering of multi-unit spiking activity was introduced by Eckhorn and colleagues (Eckhorn 1991, 1992; Eckhorn and Obermueller 1993; Brosch et al. 1997) to improve spectral frequency analysis of correlated activity, and has been used by several groups as an alternative measure for multi-unit activity (Dougherty et al. 2015; Self et al. 2016; Drebitz et al. 2018). Because this method does not involve setting a threshold for cutting spike amplitudes, full information about the neuronal response is preserved. We hypothesized that this way of pre-processing is particularly effective for data with poor SNR. Even if spike amplitudes do not surpass the background, aggregated spike events in the rectified signal will be reflected in the low-passed derivate due to their different temporal structure, while random background fluctuations get attenuated. Thresholding of such small spikes, on the other hand, is likely to result in both false positive and false negative spike events, thus blurring the available stimulus information.

We tested this hypothesis by using data from semi-chronic recordings of primary visual cortex that was acquired during mapping procedures for testing visually evoked activity. The mapping procedures were performed for different research projects having different target layers within V1. In addition, electrodes were located within the tissue for variable time periods (days to weeks to months), and recording details (hardware, filter) varied across animals. This explains the variance in detection rates across animals (Table 1), but more importantly, it shows that the findings of the current study do not result from specific experimental conditions. Instead, the basically same result across animals suggests a general advantage of ESA over thresholded MUA for detecting evoked activity in the high-frequent signal of neuronal responses. Over all SNR fractions, ESA delivered about 50 % more RF estimates than conventional MUA, and was only slightly less sensitive than the broadband-gamma LFP (40 – 120 Hz). This increased detection rate was mainly due to a much higher sensitivity for detecting RFs in low SNR recordings. With the standard procedure, ESA delivered 2.5 times the number of RFs as compared to MUA. Optimizing the yield of MUA-based detection by iteratively applying a series of thresholds to each unit allowed to increase the number of detected RFs in low SNR data by about 60%, but this was still significantly less than ESA-based detection

rates. For medium and high SNR, ESA delivered more RFs than MUA in each individual animal, independent of the procedure, but detection rates for ESA and MUA approximated and were statistically not different over the sample size of five animals.

Average RF size slightly increased from low to high SNR for both ESA and MUA, and ESA-RF size was about 17% larger than MUA-RF size in units delivering an RF with both signals. Yet, this difference was consistent over all SNR fractions, indicating about the same reliability of both signal types. Similarly, ESA-RFs were found to have a slightly smaller absolute orientation selectivity than MUA-RFs, but for 70% of recordings ESA and MUA delivered the same or a very similar preferred orientation. These results support the notion that ESA is a highly sensitive, selective, and reliable signal type significantly increasing the yield of recordings, particularly under conditions that do not allow optimal positioning of electrodes to isolate single units.

Increased sensitivity for detection of evoked responses.

As a rule of thumb, the amplitude of a spike decays as the inverse of the square of the distance to the recording electrode's tip. For example, the voltage amplitude of a spike generated at a soma with 10 to 30 µm diameter will decay by about 90% in 60 to 65 µm distance from the recording electrode tip (Rall 1962; Lemon 1984; Gray et al. 1995). Thus spikes generated at larger distances from the electrode tip get lost in general background noise when not surpassing the threshold, or will be intermixed with noise when threshold is too low. Because of this negative effect on SNR, this introduces a significant limitation for detecting evoked responses. ESA, on the other hand, is sensitive for aggregated spikes even when having small amplitudes, and rather insensitive to random background noise. The resultant signal has a clearly improved SNR, as indicated by the strong increase in the yield of significantly modulated ESA-RFs with low SNR, and even the moderate though insignificant increase in yield for medium and high SNR data.

It is worth to note yet that the division into the three SNR groups is to some extent arbitrary. We divided our dataset into equally large SNR fractions and categorized these as low, medium, and high. Our recordings were obtained from different cortical layers, in many sessions we were primarily interested in the LFP. Thus, only a few data may has

been recorded under truly high SNR conditions, while some of the data representing the high SNR pool might has had a weak absolute SNR in fact. Thus, the slightly higher ESA-detection rates for medium and high SNR may disappear under conditions with overall higher SNR. However, our analyses show that ESA is particularly powerful to detect evoked responses when SNR conditions do not allow to set a legitimate threshold. This is particularly evident when comparing ESA detection rates with the optimized yet much weaker detection rates obtained after iteratively searching for the most appropriate threshold of each unit. Such low SNR conditions may result from larger distances between electrode tips and somata when using permanently implanted probes, or from cell loss, gliosis, or local tissue responses potentially associated with (semi-) chronic recording approaches (Turner et al. 1999; Biran et al. 2005; Polikov et al. 2005; Griffith and Humphrey 2006; Lacour et al. 2016; Salatino et al. 2017), which in turn makes it necessary to exclude single electrodes from further analysis. Here, ESA represents a powerful alternative to conventional thresholding of MUA activity and allows for a strongly increased yield of data, with the additional advantage that its application can be fully automatized.

Stimulus selectivity

Because ESA is a neuronal mass signal and reflects the activity of a local population of neurons, the slight differences in RF size and absolute orientation selectivity may primarily be due to a larger group of neurons underlying the ESA-signal as compared to thresholded MUA. Supèr and Roelfsema (2005) compared direction selectivity, response latency, figure ground segregation, and attentional modulation of ESA (denoted as MUA_E in their article) to single units. In line with our results, the authors found a somewhat reduced direction selectivity but otherwise largely identical response characteristics. Because axonal and dendritic spikes are very small and the time course of postsynaptic potentials is slow, they concluded that ESA is representing the summed action potentials of neurons with a soma in the vicinity of the recording site rather than electrical fluctuations from other sources. This interpretation also explains the increase in RF size and the reduction of absolute orientation selectivity (Figure 19). Because ESA is not discarding spikes below threshold, it integrates over more sources than

conventional MUA, which necessarily results in a somewhat reduced stimulus selectivity. Brosch et al. (1997) specified the effective range of ESA as approximately 50 µm around the electrode tip. Referring to the classical finding that orientation preference of neurons only 25 to 50 µm apart from each other may shifts by about 10° (Hubel and Wiesel, 1974), integration of smaller spikes from more distant somata is likely to explain the reduction in absolute orientation selectivity. In addition to this, the higher sensitivity for small spikes prevents, or at least attenuates the typical sampling bias towards large pyramidal neurons when thresholding spikes. Thus, the ESA database may include a larger diversity of cell types than the MUA database, including cells with larger RFs, smaller orientation selectivity, or different center-surround interactions, as found in different layers of V1 (Sceniak et al. 2001; Ringach et al. 2002; Shapley et al. 2003).

Apart from the slightly attenuated total stimulus selectivity, both the analysis of RF size as a function of SNR and cross-comparison of orientation selectivity across signal types primarily revealed that ESA delivers a reliable estimate of the response properties of the recorded group of neurons. First, although RFs were getting slightly larger with better responsiveness of the recording site (due to the reasons outlined above), this increase was found for both signal types and to equal extent. This indicates that even with poor SNR evoked responses were sufficiently well detected to allow for a reasonable estimation of the response properties of the local set of neurons. Second, the estimated preferred orientations were similar between ESA and MUA for the majority of recording sites. Importantly, the method we used for denoting a cell's response as either significantly or insignificantly being influenced by the orientation of the stimulus relies on reproducibility of responses rather than on absolute orientation selectivity. This diminishes the influence of random singular events for estimating response properties of the recorded group of neurons. The finding that almost 98% of the ESA responses were classified as orientation-dependent (as compared to 72% of the MUA responses) proves the high reliability of the ESA-signal to reveal even a small response bias towards one orientation. Detectability of such biases might be important for different purposes, as e.g. for selecting proper stimulus conditions or improving performance of decoding techniques.

Taken together, full-wave rectification and subsequent low-pass filtering of spiking activity effectively increases the signal's SNR and allows for more reliably detecting evoked responses in data with low SNR. Because no thresholding is applied, ESA considers the full spiking information and allows for reliable characterization of the response properties of the underlying group of neurons when conventional techniques may fail.

Acknowledgements

The authors acknowledge support by Fingal Orlando Galashan, Johanna Barnstorf-Brandes, Hendrik Borgmeier, Emel Erdogdu, Lea Greifenberg, and Deniz Parmuk during data acquisition and analysis, Katrin Thoß and Ramazani Hakazimani for animal care, and Aleksandra Nadolski and Peter Bujotzek for technical assistance.

Chapter V: Complementary Results

In this section, I present results that accompany the investigation presented in Chapter III. The results and methods were not part of the respective manuscript for reasons of readability and relevance for the findings in chapter III. The aim of the following investigation was to reproduce the findings of Galashan et al. (2013) while extending the main results to the spiking activity in area V1 and common correlated spiking activity in area MT. In this investigation I first show that amplitude and latency shifts that relate to reaction time (RT) already exist in area V1 and argue that shifts of transient responses in area MT may be partly inherited and part of an latency accumulation process across visual processing areas. Secondly, I show that shared neural variability is reduced in trails that result in fast RT. I furthermore argue that the reduction of shared neural noise is substantial for an efficient read-out mechanism and therefore decreased RT as its impact on the SNR may be superior to e.g. individual neural noise.

As introduced in Chapter I, area V1 is the major input source to area MT. Given the close relationship of transient firing rate increases and RT in area MT, we hypothesized that transient responses in area V1 might exhibit a similar relationship to RT and that transient firing in area MT might at least partially be inherited from area V1. Area V1 neurons are velocity-selective, with neurons close to the fovea being mostly low-pass and exhibiting a broader velocity tuning with increasing distance to the fovea (Orban et al. 1986). Stimulation velocities in our experiment were adjusted to the RF properties of the recorded MT neurons and V1 neurons were sampled at intermediate distances to the fovea. Thus, we did not expect to find transient responses in area V1 that were as clearly defined as in area MT. However, transient responses to the presented speed change could be observed at individual recording sites enabling a latency and amplitude estimation for a subset of recorded V1 neurons.

The motivation to investigate correlated variability in area MT in relation to RT is twofold: First, as introduced above spatial attention was found to de-correlate spiking activity between simultaneously recorded neurons. Correlated spiking activity was found to occur at timescale of tens of milliseconds and is often maximal at around 100

ms (Mitchell et al. 2009; Schledde et al. 2017). These large timescales suggest that spiking activity is modulated along slow firing rate fluctuations and on a larger spatial extent in the cortex (Mitchell et al. 2009). Single neuron activity that carries visual content and underlies such global firing rate modulations may not be distinguishable from neurons that do not carry relevant information but exhibit the same rate fluctuations. The finding that visual attention tends to de-correlate spiking activity on these timescales (Cohen and Maunsell 2009; Mitchell et al. 2009; Galashan et al. 2013; Schledde et al. 2017) suggests that de-correlation is a means to reduce neural noise, i.e. spiking activity that is not related to the visual content of relevance. If RT fluctuations underlie fluctuations of visual attention, reduction in correlated spiking activity is a plausible candidate correlate of RT.

Second, in Galashan et al. (2013) the authors found that the reliability of the firing pattern of single neurons decreases both with spatial attention and with decreasing RT. This reliability is measured as the normalized trial-to-trial fluctuations of spikes (Fano Factor, FF), counted in time windows of a similar timescale as spike count correlations. The FF is measured at single electrodes across trials. High FF values indicate that the variability across trials with identical visual stimulation is high. A potential interpretation of this finding is that slow fluctuations are not locked to the trial-wise visual stimulation modulate firing rate activity. Across trials, these fluctuations may not align precisely, introducing large variability of firing rates at single time points, i.e. introducing noise to the firing rates. It has been shown that the FF decreases with spatial attention (Cohen and Maunsell 2009; Mitchell et al. 2009; Galashan et al. 2013; Schledde et al. 2017), providing evidence for a possible mechanism to reduce individual neural noise. The interpretation of the origin of individual noise (as measured by the FF) and correlated noise (as measured by the spike count correlations, SCC) is identical, namely that firing rates of neurons are locked to an ongoing slow fluctuation spanning large cortical space and large neural populations. Given the relationship of the reduction of the FF to RT, I hypothesized that spike count correlations will likewise decrease in trials that exhibit fast reaction times.

A number of details concerning the data analysis differ from the analysis used for the original manuscript in Chapter III:

- *Multi-unit estimation.* I was not able to extract distinct single- or multi-unit activity in area V1 based on thresholding the high-pass filtered signal as I have done for area MT. Therefore I made use of an approximation of multi- unit activity via the ESA signal (Complementary Methods; Drebitz et al.,2019), which is essentially the envelope of the full-wave rectified high-pass signal approximating aggregated multi-unit activity. I first show that this signal resembles single-and multi-unit activity in area MT and then proceed to analyze ESA responses in area V1.
- *Database.* The data used for this analysis originates from a larger database as was used for the investigation in Chapter III because substantially more recording sessions were available for single and paired recordings when analyses were restricted to area MT.
- *Reaction time correction.* I found that RT was dependent on the length of the time interval between the motion onset, the start of a stream of potential target events, and the actual target event the animal had to react to. In order to correct for this bias I applied a correction method to the RT distributions of each single session (see Complementary Methods). After the correction, RTs were uniformly distributed across different trial lengths, however main results did not change qualitatively. Therefore we did not correct for the bias in Chapter III.

Modulation of transient spiking response in area MT

Firing rates of 234 multi- and single- units recorded in two animals in area MT were selected and analyzed based on a minimal performance of 70% correct trials in the recording session, a minimum number of 10 recorded trials, and a minimal firing rate during sustained activation of 10 Hz. As shown in Figure 20, at time zero MT neurons respond to the onset of a static Gabor grating with a sharp transient followed by a second transient increase 200 ms later, evoked by the abrupt start of inherent motion. The transients in response to the speed change (right time axis), the change in visual stimulation the animal had to detect and react to, are expressed in strength and occurrence relative to the behavioral reaction time (RT) in the respective group of trials. Trials ending with very fast reaction times (blue, 20% fastest trials) coincide with

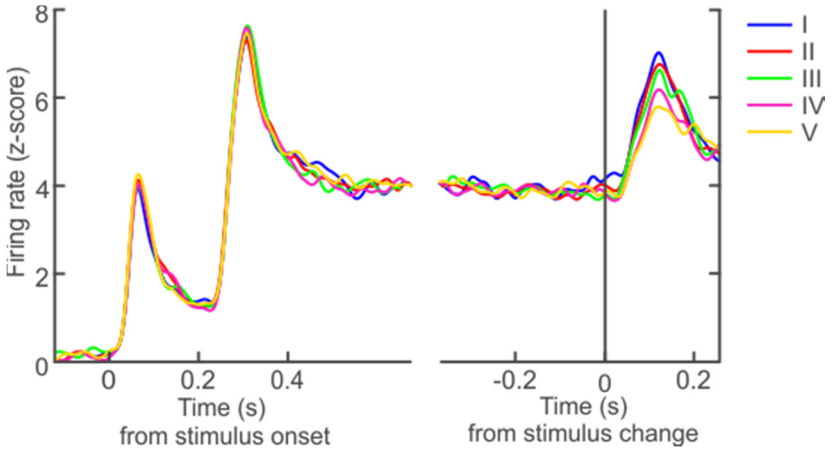

Figure 20 Firing response of MT neurons to the onset, motion and speed change of a moving gabor grating. Five reaction time groups comprise of the 20% of the total number of trials recorded in the same behavioral condition which represent fastest to slowest reaction times in ascending order.

transients with the highest amplitudes, reaching higher amplitudes earlier than in other trials. All five reaction time fractions (RTF) follow the order of their mean reaction time (RTFs: I: 360 ms; II: 392 ms; III: 415 ms; IV: 440 ms; V: 490 ms)

Transient firing rate increases following the speed change were quantified always between two groups of trials. Here we compare the groups with fastest 20% of RT with the groups of 20% slowest RT, such that the time constant describes the difference in latency between the fast and slow group (negative values indicate leading fast trial transients) and the amplitude value describes the difference in amplitude between the peak of the fast group and the value of the slow group at the same point in time (cf.

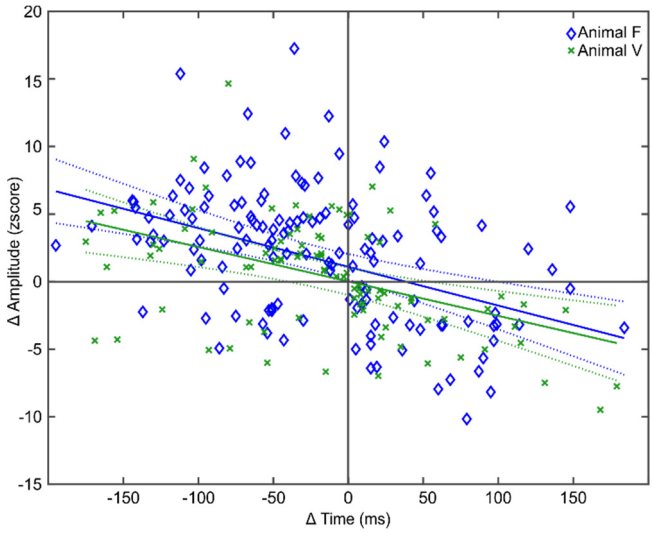

Figure 21 Amplitude and Time shifts between fast and slow group of the two animals. Quadrant I-II display larger amplitudes for the fast group and quadrant II-III display fast transients for the fast group.

Chapter III). We use this approach to quantify differences in transient firing between groups, as they are parameter free and represent the characteristics of the transient response more accurately than conventional (and possibly error prone) latency estimation.

We used as test transients the trial-average transient response of the 20 % fastest trials (5 trials) and the same response of the 20% slowest trials (5 trials) as reference transients. For both animals most of the test and reference transients exhibit the typical characteristic that is indicated by quadrant II and IV representing either faster and higher transient responses or slower and lower transient responses (Figure 21, as indicated by the two regressions). Both time shifts and amplitude shifts are biased towards fast and higher transients for the fast group (significance of a left shift in the time shift distribution, Animal II: $p<0.001$, $N = 137$, t-test; Animal I: $p=0.015$,$N = 96$,t-test; significance of an upshift of the amplitude shift distribution Animal II: $p<0.001$,$N=137$,$Z = 4.1166$, Wilcoxon signed rank; Animal I: $p = 0.21$, $N=96$,$Z = 0.7802$ Wilcoxon signed rank test). A complete Overview of all comparisons are given in Supplementary table 2.

In Figure 22 and Figure 23, firing rate responses of the recorded MT neurons are displayed as the entire spiking activity (ESA, Drebitz et al., (2019)). Response profiles are qualitatively identical to the firing rate estimation using spike times, except for the fact that the amplitude of the second fastest trials exceed the amplitude of the fastest trials. Apart from this, transients are sorted according to the RTF succession. The statistical analysis of amplitude and time shifts revealed significant increase of amplitude and decrease of latency with decreasing RT and thus a clear effect of RT on the characteristics of transient responses (Figure 23 , significance of a left shift in the time shift distribution, Animal II: $p<0.001$, $N = 137$, t-test; Animal I: $p=0.007$,$N = 118$,t-test; significance of an upshift of the amplitude shift distribution Animal II: $p<0.001$,$N=137$,t-test; Animal I: $p = 0.034$, $N=118$,$Z = 1.818$, Wilcoxon signed rank test).

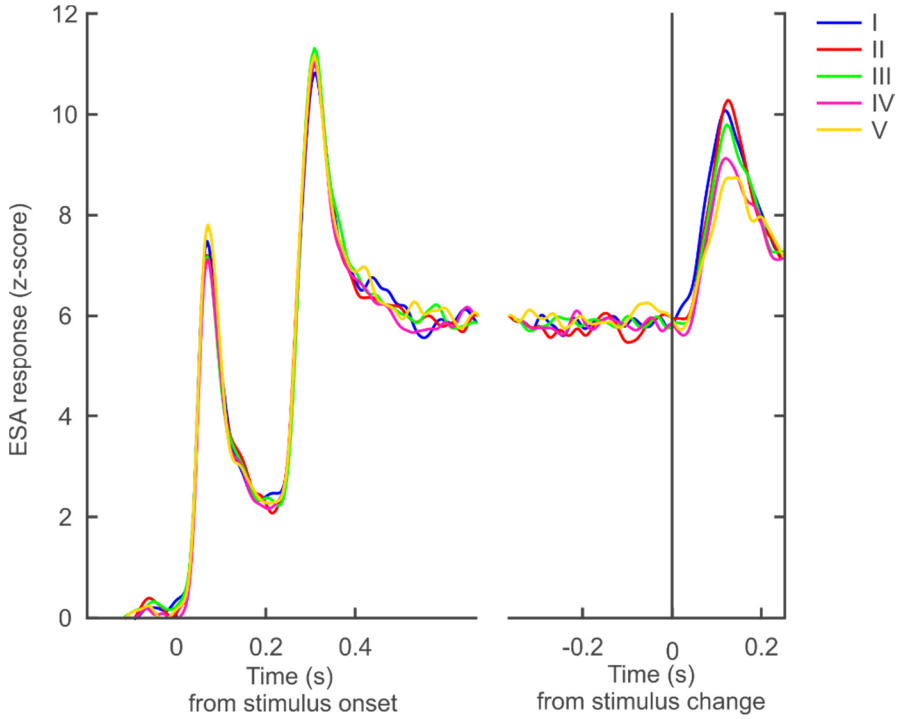

Figure 22 Firing response of MT neurons to the onset, motion and speed change of a moving gabor grating. Firing response of is measured with the entire spiking activity, parameter free measure of multi-unit activity. Conventions follow figure 1.

These amplitude and latency shifts are particularly puzzling because pre-change activity did not reveal any effect between RT groups and thus does not predict differences in transient responses, a discrepancy introduced already in an earlier investigation (Galashan et al. 2013) and subject to the investigation in Chapter III. Average pre-change activity during the 400 ms previous to the stimulus-change does not differ significantly

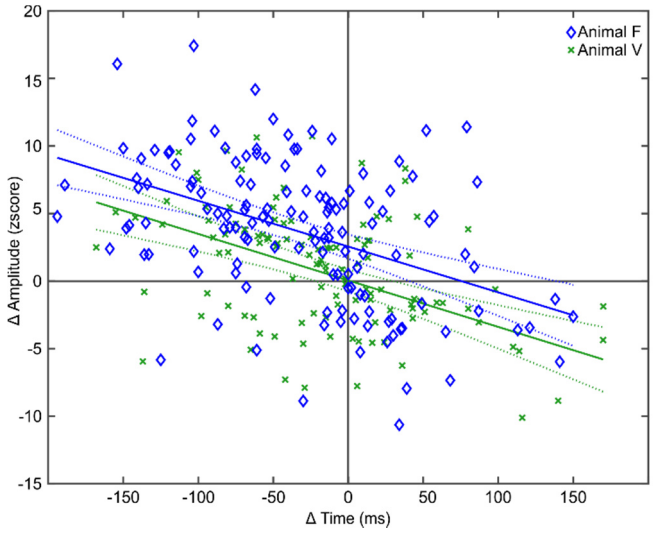

Figure 23 Amplitude and Time shifts of the ESA response. Quadrant I-II display larger amplitudes for the fast group and quadrant II-III display fast transients for the fast group. Conventions follow figure 3.

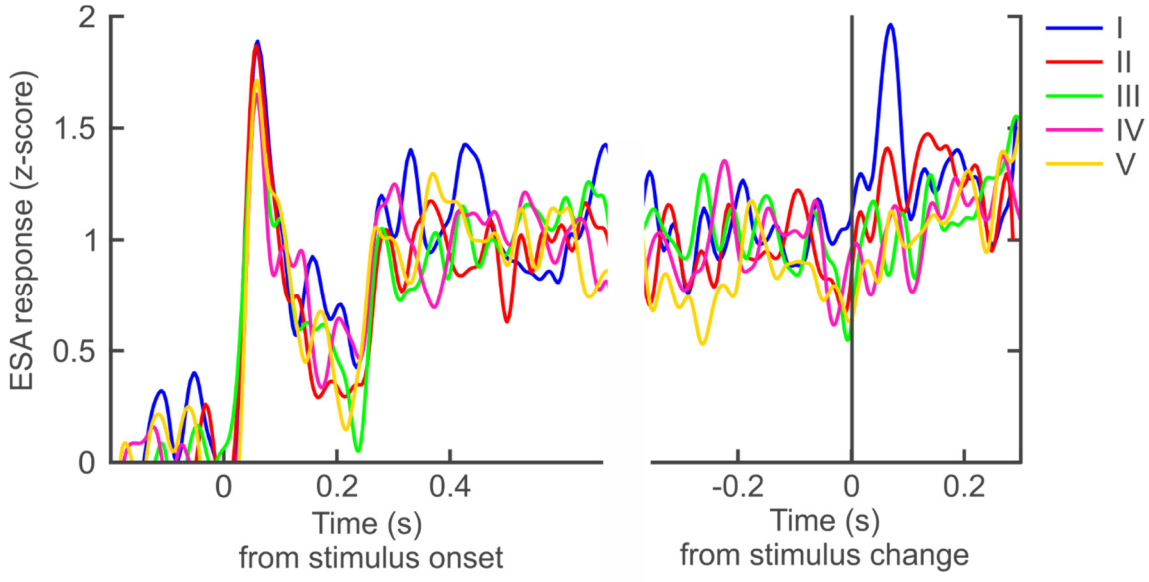

Figure 24 Firing response of V1 neurons to the onset, motion and speed change of a moving gabor grating. Firing response of is measured with the entire spiking activity, parameter free measure of multi-unit activity. Conventions follow figure 1

between fast and slow trials, neither for ESA responses nor for spike rates (significance of the pre-change activity between group I and V: rate, Animal II: p = 0.514, N=137, Z = 0.6521, Wilcoxon signed rank test; Animal I: p = 0.829, N = 96, Z = 0.215, Wilcoxon signed rank test; ESA, Animal II: p = 0.283, N= 137, Z = -1.073, Wilcoxon signed rank test; Animal I: p= 0.397, N = 118, Z = -0.847, Wilcoxon signed rank test).

Multi-unit activity in area V1

Firing rate and transient responses in area MT are dependent on the local input signals. The dominant contributor to MT input is area V1 (cf. Chapter I) and activity in this area might precede and predict transient response in MT. We were therefore interested in firing rate modulation in are V1 and recorded with up to 6 chronically implanted electrodes in area V1. Most of the recordings did not allow for good isolation of single spikes, thus multi- unit activity in V1 was estimated using the ESA signal (Drebitz et al. 2019). V1 units were selected based on the same criteria as above and the orientation preference of the V1 units were not allowed to differ by more than 45° of the orientation of the motion grating. In Figure 24, the activation traces throughout the trial are displayed. Both stimulus onset and motion onset evoked clear transients, while the response to the speed change was less visible. However, for the RTF I and II clear and short transients are visible and arrange according to the RTF succession. For the other 3

RTFs differences were less clear. The time and amplitude differences between groups I and V were biased towards larger and faster transients for fast trials for animal II (Figure 25, significance of a left shift in the time shift distribution, p=0.0141, N = 57, t-test; significance of an upshift of the amplitude shift distribution, p= 0.0016, N=57, Z = 2.9488, Wilcoxon signed rank test). For animal I amplitude shifts were less conclusive and were not significantly shifted (Figure 25, significance of left shift in the time shift distribution, p=0.0462, N = 19, t-test; significance of an upshift of the amplitude shift distribution, p= 0.9283, N=19, t-test).

Neural variability and reaction time

In Galashan et al. (2013), the authors investigated whether neurons in area MT fire more reliable across trials in the time interval previous to the stimulus-change, presumably enabling a faster expression of transients. In fact, a lower Fano Factor seemed to relate to faster RT, however the authors could also show that a low pre-change Fano Factor does not necessarily precede fast transients in the attend-out condition.

A reduction in the Fano Factor is commonly regarded as a reduction of the variability in the firing pattern of individual neurons. The reduction of firing pattern variability may enhance readability of a neural code but should diminish if averaged across many

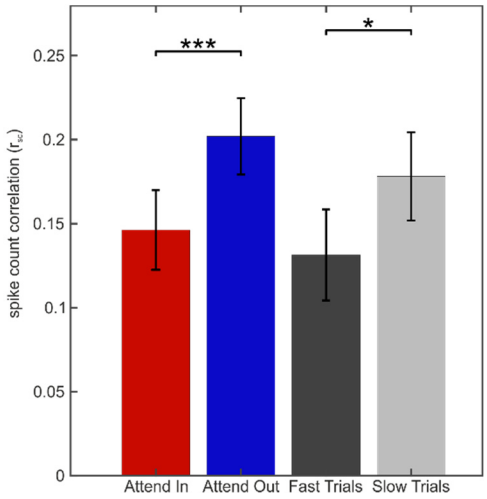

Figure 25 Noise correlation pooled across both animals. Spike counts from the pre- change period were obtained in 50 ms counting windows, z-transformed and correlated across trials via the Pearson correlation coefficient (r_{sc}). Two attentional conditions are shown for comparison. Fast trials are the 30% fastest trials of the Attend-in condition and slow trials the 30% slowest trials in the same condition. Asterisks indicate significance (p<=0.05;**p<=0.005;***p<=0.0005).*

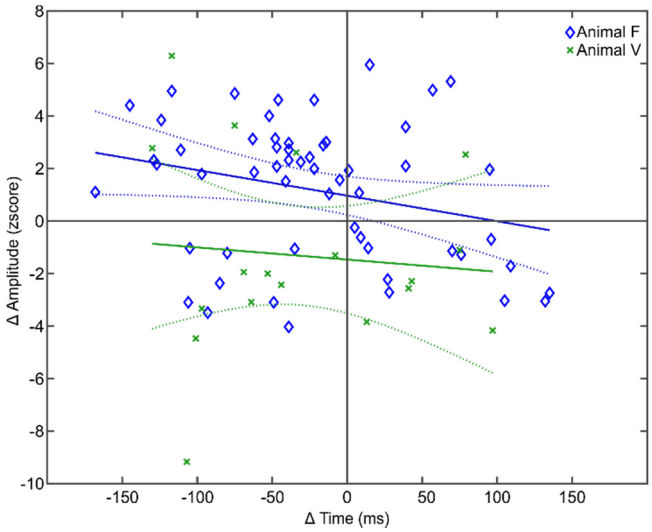

Figure 26 Amplitude and Time shifts of the ESA response in area V1. Quadrant I-II display larger amplitudes for the fast group and quadrant II-III display faster transients for the fast group. Conventions follow figure 3.

neurons. Common neural noise, i.e. neural activity which cannot be related to the external stimulation *and* which is correlated between many neurons, however, remains stable across a whole population and may thus be detrimental in terms of readability (Zohary et al. 1994; Shadlen et al. 1996; Shadlen and Newsome 1998; Averbeck et al. 2006; Mitchell et al. 2009). The reduction of spiking correlation between pairs of neurons (spike count correlation / noise correlation) could be a driving factor in enabling neurons to respond with fast transients.

We measured spike count correlations between single- and multi-units recorded simultaneously at two different electrodes within area MT. Pairs of neurons fulfill the same criteria as for the previous firing rate analysis, while their direction preferences were required to lie within 90°. Noise correlations between 75 pairs of units were calculated across ~8 trials resulting in 3 RTFs. Thus, for this analysis the comparison between fast and slow trials is the comparison between the third of the available trials with fastest RTs and the third of trials with slowest RTs. Spike count correlations are significantly reduced during the pre-change period when fast RT ensue (Figure 26, fast vs. slow, $p = 0.0188$, $N= 75$, t-test). For comparison, I also show spike count correlations in the attend-out condition that increase significantly as well (att vs. natt, $p <= 0.0001$, $N= 75$, t-test).

Conclusion

The transient neuronal responses to the abrupt acceleration of the stimulus relate to the behavioral performance. MT transient responses occurred earlier and with larger amplitude for fast RT trials. This finding is accompanied by shorter latencies for fast RT trials in the afferent input area V1. That means larger amplitudes and earlier expression of the transient increase of firing rate in areas MT/V1 lead to a faster occurrence of the representation of the stimulus-change in the following and ultimately, as the case may be, the last brain area involved in the reaction of the animal. The results are in particular compliant with a study that identified latency accumulations across successive areas. Wang et al. (2014) conducted in-vivo whole-cell recordings in area V1 and in the LGN of both awake and anaesthetized rats. They found that in a desynchronized state, a brain state that is related to high vigilance of the animal, visually evoked increases in conductance were higher than in a synchronized state. In area V1 the increase of conductance elevated the membrane potential close to the firing threshold and resulted in shorter response latencies. However, the effect of conductance elevation could only partially explain the difference in response latency. The authors simultaneously recorded in LGN and found latency shifts of a magnitude smaller than in V1. Furthermore, across cortical layers in area V1 response latency shifted as well. These findings suggest that shifts in response latency accumulate across the succession of processing units. Our finding that response latency in both, V1 and MT, the receiving area, relates to reaction time supports this interpretation as the delay in the subsequent area may result from accumulations of latency shifts across both areas and involved cortical layers. A closer investigation of the exact time constants in areas MT and V1 at individual recordings may reveal important evidence for the accumulation of latency shifts across visual areas.

Noise correlations have been found to reduce with spatial attention. For example, Mitchell et al. (2009) investigated V4 spiking activity in an visual attention task. They calculated the FF, spike-spike-coherence and spike count correlations and found that under attention all these measures decreased. Furthermore, reductions of spike-spike coherence occurred in a frequency range below 20 Hz and were maximal at 5 Hz. Similarly, spike-count correlations saturated when spike count intervals increased above

100 ms and attentional modulations were maximal at around 100 ms. Thus, the timescales at which attentional modulation of rate fluctuations occurred could be narrowed to a low-frequency band. Additionally, Mitchell et al. (2009) estimated the impact of attention-dependent increases in firing rate and the impact of the reduction of correlated noise onto the signal-to-noise ratio (SNR) as a function of neuronal pool size. To explain this in more detail consider the following. Visual neurons when presented with repeated presentations of identical stimuli vary in their response from trial to trial (Shadlen and Newsome 1998). Response variations, or neural noise, thus impacts the reliability of the information encoded by these neurons (Zohary et al. 1994; Shadlen et al. 1996; Averbeck et al. 2006). If these trial-to-trial fluctuations are independent between neurons, reducing neural noise can be achieved by pooling across large populations of neurons effectively increasing the SNR. If however, noise is correlated between neurons, pooling does not diminish noise and thus introduces an upper asymptote to the increase of SNR as a function of neuronal pool size. While independent noise may originate from synaptic transmission variability (Calvin and Stevens 1967), correlated noise may arise from shared inputs that are not necessarily related to the sensory input and were observed to occur between neurons with a spatial distance of up to 10 mm in cortex (Smith and Kohn 2008). Mitchell et al. (2009) estimated the impact of the reductions of correlated noise on the SNR and compared it with the impact of firing rate increases. Increasing firing rate elevated SNR maximally by 10% while the reduction of correlated noise led to a 39% increase of SNR. Thus a naïve read-out strategy such as pooling over large neuronal populations is enhanced most efficiently by reducing correlated neural noise. As mentioned before, attention achieves just that and therefore variations in the efficacy of noise reduction may also lead to variations in RT. Our finding of reduced SCC by spatial attention and for fast RT trials support this interpretation. In chapter III we additionally show that gamma-band activity that is related to spiking activity is locked to an alpha oscillation that concurs with the timescale reported for SCCs. Although our finding in chapter III is not a reduction in coupling to these phases it is consistent with the idea that spikes are correlated and that this correlation arises from low-frequent excitability fluctuations in the cortex.

It would be highly interesting to investigate the relationship of low-frequent oscillation observed in the local field potential to spike timing and gamma spindles in order to illuminate the specific role of such a coordination of population signals.

Complementary Methods

In this section the additional or complementary methodology that was utilized for the analysis in the Complementary Results chapter is reported. Differences between methods between these two chapters are stated at the beginning of the Complementary Result chapter. Methods concerning data analysis that is specific to the investigation in Chapter III is reported in the respective Material and Method section.

Electrophysiology

The surgical probes were tungsten microelectrodes of different impedances (0.8–5 MΩ, 125-µm shank diameter; Frederic Haer, Bowdoin, ME). Impedances varied across recording session mainly because we tried to achieve a better resonance for LFP recording. For most of the recording session impedances were 2 MΩ, which proofed to robustly maintain sufficient impedances to be able to stabilize single unit activity across several penetrations. Electrodes were lowered to area MT through an adapted G-23 cannula (guide tube) reaching until ~ 7 (5) mm below the dura mater. Brain tissue was allowed to settle for approx. 30 minutes by holding the electrode in position as soon as the tip of the electrode reached area MT. V1 electrodes were semi – chronic in that they were only moved to correct the position relative to the recorded units or for initial positioning. The positioning of the electrodes was determined by manual inspection of the visually evoked spiking response and subsequent validation with an automated mapping procedure (cf. Chapter IV).

Brain signals were recorded relative to a reference electrode positioned on the anterior part of the skull, 10 fold pre-amplified, submitted to main amplifier (amplification factor of 300 and 1000) and digitized at 25 kHz within a range of $\pm$10 V (16 bit resolution). Spike times used in the main analysis were cut and sorted offline (cf. Spike cutting and sorting) and obtained from a band pass filtered signal (0.7 – 5 kHz), either filtered with an custom made hardware filter or an offline bidirectional equiripple finite impulse response filter (FIR). For the online analysis of direction tuning, spikes were detected using a manually set threshold.

Similarly, entire spiking activity (ESA) was obtained from the band pass filtered signal using a equiripple FIR filter in forward and reverse direction (pass band: 0.7-12.2 kHz, flanks: 0.2 kHz, 40 dB suppression on either side). Designated ESA signals were full wave rectified before low-pass filtering. Signals resulting in the local field potential (LFP) and the ESA signal were filtered with a low pass equiripple FIR filter (pass frequency: 300Hz; stop frequency 500 Hz, 80 dB suppression) and decimated to a sampling frequency of 1kHz.

Before offline filtering, each channel was cleaned from any line noise in the raw data. This was achieved by applying a running average Hum Bug filter (cf.

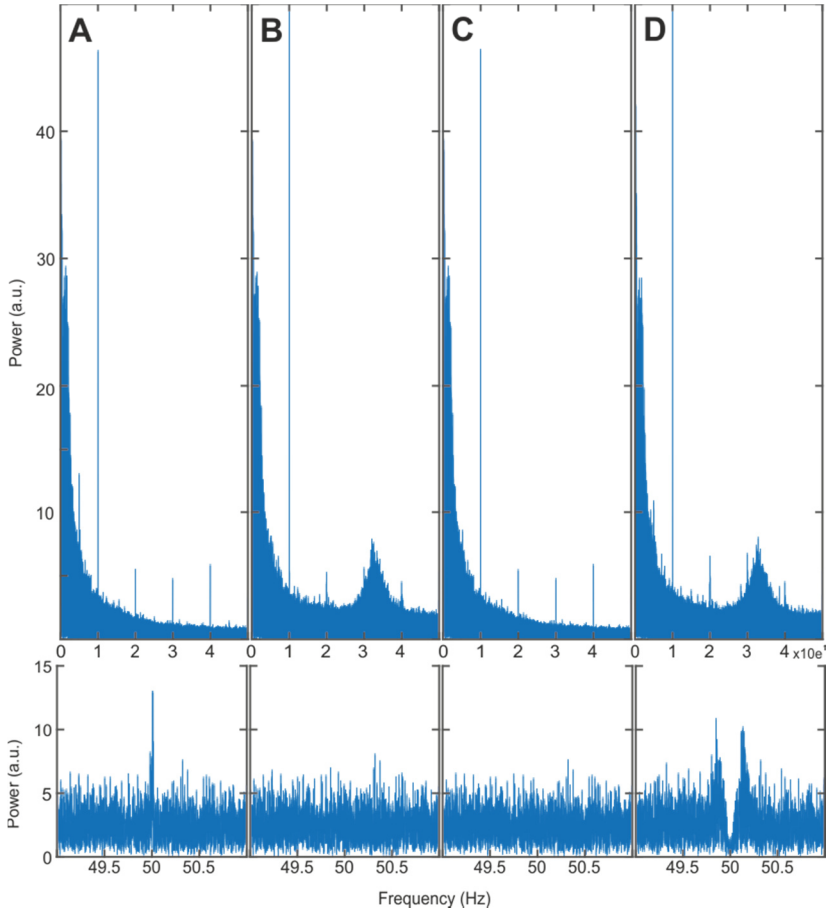

*Figure 27 Example of line noise removal via "Hum – Bug" implementation. In Panel **A** the power spectrum of the raw signal [F_V5_322_axxx_agsc_1] is displayed up to 500 Hz. A prominent 50 Hz peak and its harmonics is clearly visible in the spectrum. In Panel **B** the spectrum of a signal is shown after the application of the line noise removal tool for a raw signal sampled at 1 kHz. Panel **C** shows the same as in **B** but with a 25 kHz sampled input signal. Panel **D** shows the spectrum of the signal after removal of a phase locked 50 peak filter. In the lower Panels the respective blow up around the 50 Hz band is shown. The "Hum – Bug" implementation in Panel **B** and **C** effectively removes any line noise oscillation without altering the remaining spectra, as the peak filter removal (**D**) does. Artificial oscillatory power in high frequencies in Panel **B** and **D** might be related to an imprecision of the phase estimation of the line signal if sampled at 1 kHz.*

Hum- Bug line noise removal) if raw data was available with a sufficiently high sampling rate (25 kHz) or via the subtraction of a 50 Hz peak filter phase locked to a simultaneously recorded line signal.

Spike cutting and sorting

Spikes were detected by thresholding the designated band pass filtered signal by either four times the median of the absolute signal (Quiroga et al. 2004) or by three times the standard deviation of the signal. Spike wave forms were stored in 32 bins spanning 1.28 ms and were initially automatically clustered on the basis of the first 4 principal components (Glaser and Marks 1968; Abeles and Goldstein 1977), the minima/maxima and the extreme values of the slope. Spike cluster were obtained using the open source Klustakwik algorithm (Harris et al. 2000) and subsequently merged and labeled manually resulting in meaningful and well sorted spike units.

Hum- Bug line noise removal

Line noise was removed by obtaining a template of any constant and thus artificial oscillation locked to the 50 Hz line noise and subtracting that template from the raw data. This approach is inspired by commercially used online line noise eliminator called “Hum– Bug” filter. The template was constructed from data in a 180 s window that ran across entire length of the recording session in steps of one cycle of the recorded 50 Hz line signal. Averaging occurred across *N* snippets of 20 ms length dividing the 180 s running window while each snippet was phase aligned to the recorded line signal. The resulting template of the artificial oscillation was stored and subtracted from raw data as soon as the end of the data stream was reached. In Figure 27 E example raw data and the application of the line-noise tool is displayed.

Visual stimulation and task

Visual stimuli were presented using two 22 inch cathode ray tube (CRT) Monitors (1280 x 1024 px, 100 Hz refresh rate) placed 80 (83) cm in front of the animal. All visual stimuli

within the RF of the recorded neurons were drifting high contrast sine wave gratings (Gabors). Gabors had a spatial frequency of 2 cycles /°, had a mean luminance of 10 cd/m^2 and were enveloped with a Gaussian of 0.75° at half height. Motion was induced by shifting phases of the grating in a predetermined direction at a speed of 2.17 °/s. Speed changes were induced by an abrupt acceleration to 4.17 °/s of inherent motion and color changes by an abrupt change to an isoluminant pale yellow. All stimuli, the fixation dot and spatial cues were presented on a grey background, isoluminant to the stimuli (10 cd/m^2). The data in used in this thesis was recorded while animals performed two variants of a feature change detection task. Only one minor change to the experimental paradigm was introduced within the scope of recordings, namely the prolongation of the baseline period from 350 ms to 1050 ms. The two animals were trained to attend one of two presented Gabors, one presented in left visual hemifield and the other at the point reflected position in the opposite hemifield. Depending on the current task the animal had to react either to an abrupt 100% acceleration of the attended Gabor (target event speed task) or to an abrupt switch to a pale yellow (target event color task). Each trial began when the animal fixated and maintained fixation on a centrally presented rectangular fixation dot (0.14° side length) and suppressed a lever. The fixation dot indicated the task type by their color (red: detect speed change, yellow: detect color change). The baseline period of 1050 ms (350 ms, see above) preceded the appearance of a rectangular spatial cue indicating the position of the behaviorally relevant stimuli. The spatial cue was displayed for 700 ms followed by a 200 ms delay period after which the two static Gabors appeared and started moving intrinsically after another 200 ms. After a random number of time intervals of 220 ms within the next 5500 ms, distractor or target events could occur, with 660 ms as the earliest possible event. Depending on the task type a distractor event could consist of a speed or color change at the cued or non-cued grating. These changes had to be deliberately ignored. Monkeys were allowed to respond by relieving the lever within 150 to 750 ms after the change event. In order to avoid any neural responses due to eye movements after the target event, monkeys had to keep fixation for another 300 ms. Monkeys had to keep fixation within an eye window of 2° around the fixation point throughout the trial. In 60.2 % of the trials of the speed-change task, the speed change in the RF was the first change event to happen at any stimulus. In half of those trials this event was at target

position. The remaining trials consisted either of color changes preceding the speed change at RF position or speed changes in the opposite hemifield. For the color-change task 83.3% of the trials exhibited first a speed change at the RF before any other change. In half of those trials the speed change occurred at the cued stimuli. Remaining trials were color changes at target positions with no distractor event before the change. In order to achieve maximal certainty about the monkey's attentional focus, namely that it is directed towards the relevant feature-change and not any change, we presented the two tasks in successive blocks. Task order was alternated between recording sessions in order to avoid any session dependent effects.

Software

All data analysis was performed using custom-made analysis scripts in the MATLAB (The MathWorks, Natick, MA, R2011b and later releases) script language. I made use of two open source MATLAB toolboxes: the CircStat toolbox (Berens et al. 2009) for the circular statistics and the function "ft_preproc_bandpassfilter" of FieldTrip toolbox (Oostenveld et al. 2011) for the application of the Butterworth filter in Chapter III. Visual stimulation and the recording of electrophysiological signals was controlled and executed by a custom-made software provided by the research institute.

RF eccentricity

Eccentricities for MT receptive fields could vary between 4° - 15° from the central fixation point and RF sizes increased linearly with eccentricity. Positioning of recording electrodes in are V1 was chosen such that they overlap with the RFs in are MT and were subject to more detailed analysis which is reported in Chapter IV.

Direction and Orientation tuning

Before execution of the behavioral paradigm the size and location of the receptive field (RF) was mapped manually and the neuron's direction and orientation tuning was determined using Gabor gratings moving into 24 different directions, spanning 360° motion directions, while the monkey performed a dimming detection task at fixation.

For the online calculation of preferred motion directions the length of the resultant vector representing response strength and motion direction was used. If more than one electrode was recorded in area MT the motion direction of the stimulus was chosen such that both units were sufficiently driven. This could lead to differences in the direction of motion stimulation and preference, but were in most of the cases below 90° (97% of the cases). Preferred directions and orientations were assessed by computing the reproducibility of the preference across trials (Grabska-Barwińska et al. 2012). This approach quantifies $PO(k)$, the preferred orientation (or direction) for *N* repetitions by calculating the vector average of the responses to all motion directions once (e.g. within a single trial) and asses the dispersion across all normalized vectors from all repetitions (e.g. trials). The trial- wise normalized vector average is:

$$\langle z_{PO} \rangle = \frac{1}{n_K} \sum_k \frac{z_{PO(k)}}{|z_{PO(k)}|} = \frac{1}{n_K} \sum_k e^{2iPO(k)}.$$

The dispersion or reproducibility of vector average is defined by the length of $\langle z_{PO} \rangle$

$$r_{PO} = \frac{1}{n_K} \left| \sum_k e^{2iPO(k)} \right|.$$

r_{PO} is maximal ($r_{PO} = 1$) if all POs are identical, and approaches zero if POs are uniformly distributed. The significance of orientation or direction tuning is determined by comparing the probability distributions $P(r_{PO}(n_K))$ with the current value. The distributions of $r_{PO}(n_K)$ are computed using Monte Carlo simulations (Grabska-Barwińska et al. 2012).

Reaction time correction

The timing of reactions to the detection of a probe stimulus is very well documented to depend on stimulus onset asynchrony (SOA, Posner 1980) or preparation time (PT) , the time interval between the stimulus onset and target event. Typically, RTs are longest following the shortest PTs in the experimental paradigm (Niemi and Naatanen 1981; Monsell 2003). In the paradigm used in this thesis target-changes occurred pseudo-randomly (cf. Visual stimulation and task) with different time intervals between the onset of the two stimuli and the actual target-event. The reason why we need to eliminate any effect on RT due to PT in our analysis is twofold. First, it may impose a

relation between RT and cortical stimulus representation that is not homogenous between trials of different durations and secondly, it may obscure neural correlates of enhanced perceptual neural computation that is indicated by fast reaction times. Indeed we found that trials with short PT had on average longer reaction times than trials with longer presentation times before the behaviorally relevant event (Figure 28 B). Due to the structure of the experimental paradigm for trials that went into analysis, SOAs could be one out of 5 different durations. In Figure 28 B the mean RT of the 5 different preparation times are displayed. We found a prominent and significant difference in RT between the first and all other trial types (Figure 28 B, first vs. all other $p \leq 0.001$, *N*=

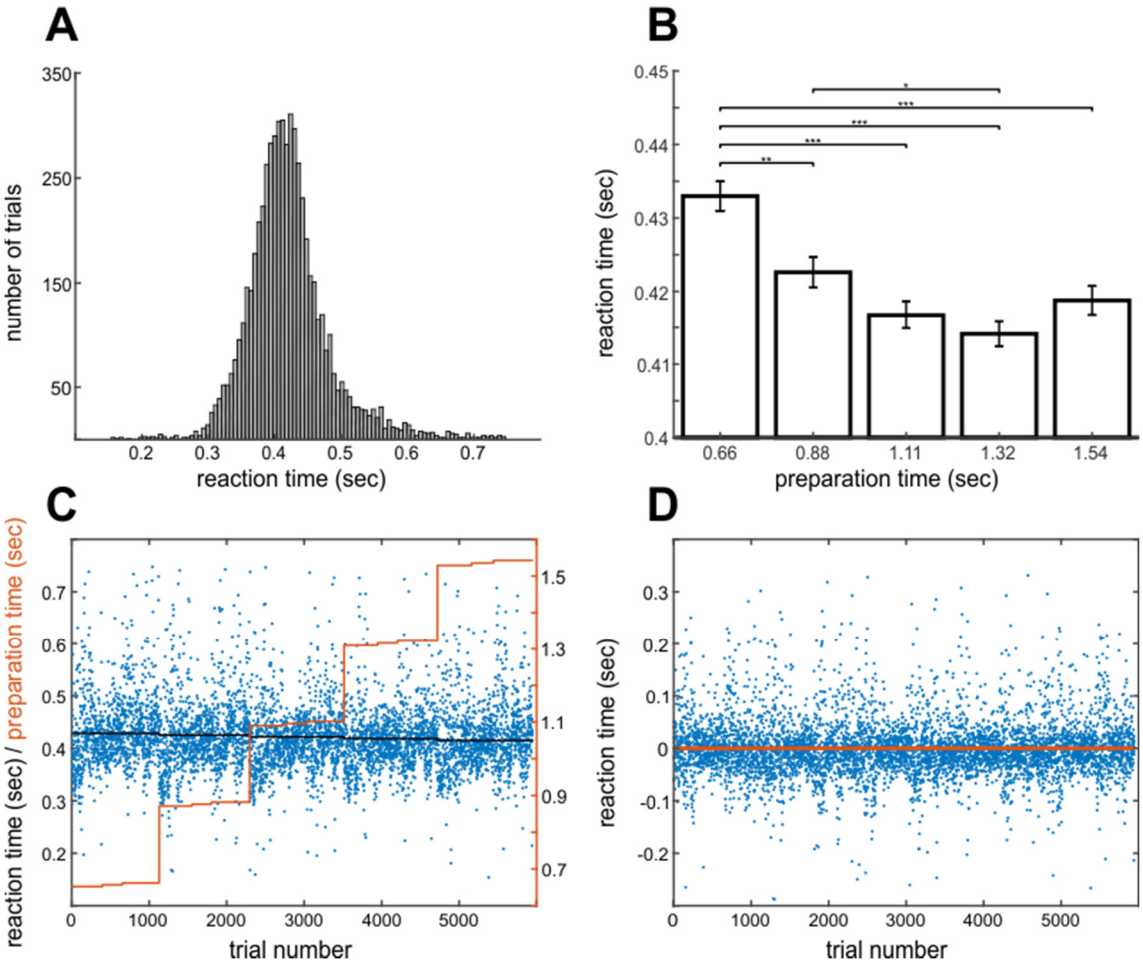

*Figure 28 Reaction times (RT) depends on the timing of target presentation. In Panel **A** the distribution of total amount of available RTs is displayed. RTs distribute well around its mean RT with a slightly skewed towards large reactions times. In **B** average RTs of groups of trials (all N = 1129) with different preparation times (PT) are shown. RTs of the first and second group are significantly larger than one or more other groups indicating an effect of PT on RT. In **C** RTs and corresponding PTs are displayed for every trial. The linear model (black line) on the responses RT and the predictors PT fits the data well and is used to obtain bias free estimates of the underlying RT (residuals, **D**).*

1129, one-way anova, Bonferroni corrected) and the second and the fourth trial type (second vs. fourth, $p \leq 0.018$, *N*= 1129 , one-way anova, Bonferroni corrected).

To validate the effect of PT on RTs in our dataset we pooled all available RTs and fitted a linear model to the data. A linear regression model of the form:

$$RT = \beta_0 1 + \beta_1 PT,$$

showed that the term PT had a significant effect on RT (F = 33,6, p $\leq$ 0.001, $r^2 = 0.00546$) with an RT reduction of $\beta_1 = -0{,}015$ sec per second PT (SD = 0.002 sec). In Figure 28 C RTs are sorted according to the timing of the target event. RTs decrease as a function of preparation time as modeled by the linear fit (black curve). In order to correct for this bias in RT, the RT groups were constructed on the basis of the residuals (raw data minus the linear fit) estimated for each session respectively (Buschman et al. 2012). Residuals (Figure 28 D) by definition do not show PT bias ($\mathrm{F} = 0, \mathrm{p} = 1, r^2 = -0.000168$) and thus qualify as adequate marker of PT independent RT estimates.

The analysis of Spikes

SDF and ESA responses in the complementary section were treated identical in order to provide comparability between the two measures. Spike density functions (SDF) were calculated in 40 ms time windows shifted in 1 ms steps across the trial and SDFs and ESA responses were smoothed with a Gaussian with a standard deviation of $\sigma = 8\,ms$ and a length of 5 times σ. Both the SDFs and ESA responses were expressed as $zscores$ based on baseline activity.

Spike count correlation

Spike count correlations in the complementary result section were quantified by the Pearson correlation of spike counts between pairs of simultaneously measured neurons across multiple presentations of a single stimulus (spike count correlations, r_{SC}). Spike were counted in successive non-overlapping windows of 50 ms. We converted the raw spike counts into z scores before correlation to assure comparability between unit pairs and excluded data segments exceeding 3 SDs of the mean spikes counts.

Supplements

Supplementary table 2 P-value matrix for each comparison of Time and Amplitude shifts of the spiking data. Statistical differences were quantified by either a Student t-test or Wilcoxon signed rank test depending on the distributions parametrization. P- values are Bonferroni corrected.

	Animal I				
Group	II	III	IV	V	
I	0.001	0.0993	0.0001	<0.0001	Time
II		1	0.1152	0.0102	
III			0.057	0.0003	
IV				1	
V					
I	0.076	0.0105	<0.0001	<0.0001	Amplitude
II		1.289	0.0177	0.0002	
III			0.5932	0.0004	
IV				0.2478	
V					
	Animal II				
	II	III	IV	V	
I	0.41530	0.3528	0.0254	0.0353	Time
II		1	1	0.0503	
III			0.7367	0.2186	
IV				1	
V					
I	1	1	1	0.1726	Amplitude
II		1	1	0.4379	
III			1	0.6559	
IV				0.3958	
V					

References

Abeles M, **Goldstein MH**. Multispike train analysis. *Proc IEEE* 65: 762–773, 1977.

Adelson EH, **Movshon JA**. Phenomenal coherence of moving visual patterns. *Nature* 300: 523, 1982.

Akyurek EG, **Dinkelbach A**, **Schubo A**, **Muller HJ**. Electrophysiological correlates of detecting a visual target and detecting its absence: the role of feature dimensions. *Neuropsychologia* 48: 3365–3370, 2010.

Albright TD. Direction and orientation selectivity of neurons in visual area MT of the macaque. *J Neurophysiol* 52: 1106–1130, 1984.

Albright TD, **Desimone R**, **Gross CG**. Columnar organization of directionally selective cells in visual area MT of the macaque. *J Neurophysiol* 51: 16–31, 1984.

Anllo-Vento L, **Hillyard SA**. Selective attention to the color and direction of moving stimuli: electrophysiological correlates of hierarchical feature selection. *Percept Psychophys* 58: 191–206, 1996.

Aru JJ, **Aru JJ**, **Priesemann V**, **Wibral M**, **Lana L**, **Pipa G**, **Singer W**, **Vicente R**. Untangling cross-frequency coupling in neuroscience. *Curr Opin Neurobiol* 31: 51–61, 2015.

Van Atteveldt N, **Murray MM**, **Thut G**, **Schroeder CE**. Multisensory integration: Flexible use of general operations. *Neuron* 81: 1240–1253, 2014.

Averbeck BB, **Latham PE**, **Pouget A**. Neural correlations, population coding and computation. *Nat Rev Neurosci* 7: 358–66, 2006.

Axmacher N, **Henseler MM**, **Jensen O**, **Weinreich I**, **Elger CE**, **Fell J**. Cross-frequency coupling supports multi-item working memory in the human hippocampus. *Proc Natl Acad Sci U S A* 107: 3228–3233, 2010.

Bankman IN, **Johnson KO**, **Schneider W**. Optimal detection, classification, and superposition resolution in neural waveform recordings. *IEEE Trans Biomed Eng* 40: 836–841, 1993.

Battaglia D, **Witt A**, **Wolf F**, **Geisel T**. Dynamic effective connectivity of inter-areal brain circuits. *PLoS Comput Biol* 8: e1002438, 2012.

Bear MF, **Connors BW**, **Paradiso MA**. *Neuroscience*. Lippincott Williams & Wilkins, 2007.

Belluscio MA, **Mizuseki K**, **Schmidt R**, **Kempter R**, **Buzsáki G**. Cross-frequency phase-phase coupling between theta and gamma oscillations in the hippocampus. *J Neurosci* 32: 423–435, 2012.

Berens P, **Baclawski K**, **Berens P**, **Baclawski K**. CircStat: A MATLAB Toolbox for Circular Statistics. *J Stat Softw* 30: 1–3, 2009.

Berkes F, **Davidson–Hunt IJ**. Communities and social enterprises in the age of globalization. *J Enterprising Communities People Places Glob Econ* 1: 209–221, 2007.

Bichot NP, **Rossi AF**, **Desimone R**. Parallel and serial neural mechanisms for visual search in macaque area V4. *Science* 308: 529–34, 2005.

Biran R, **Martin DC**, **Tresco PA**. Neuronal cell loss accompanies the brain tissue response to chronically implanted silicon microelectrode arrays. *Exp Neurol* 195: 115–126, 2005.

Bisley JW. The neural basis of visual attention. *J Physiol* 589: 49–57, 2011.

Blaser E, **Pylyshyn ZW**, **Holcombe AO**. Tracking an object through feature space. *Nature* 408: 196, 2000.

Bonnefond M, **Jensen O**. Alpha oscillations serve to protect working memory maintenance against anticipated distracters. *Curr Biol* 22: 1969–1974, 2012.

Bonnefond M, **Kastner S**, **Jensen O**. Communication between Brain Areas Based on Nested Oscillations. *Eneuro* 4: ENEURO.0153-16.2017, 2017.

Born RT, **Bradley DC**. Structure and function of visual area MT. *Annu Rev Neurosci* 28: 157–89, 2005.

Bosman CA, **Schoffelen J-M**, **Brunet N**, **Oostenveld R**, **Bastos AM**, **Womelsdorf T**, **Rubehn B**, **Stieglitz T**, **De Weerd P**, **Fries P**. Attentional stimulus selection through selective synchronization between monkey visual areas. *Neuron* 75: 875–88, 2012.

Bosman CA, **Womelsdorf T**, **Desimone R**, **Fries P**. A Microsaccadic Rhythm Modulates

Gamma-Band Synchronization and Behavior. *J Neurosci* 29: 9471–9480, 2009.

Braitenberg V, **Schüz A**. *Anatomy of the cortex: Statistics and geometry*. Berlin: Springer-Verlag., 1991.

Brendel W, **Romo R**, **Machens CK**. Demixed principal component analysis. In: *Advances in neural information processing systems*. 2011, p. 2654–2662.

Britten KH, **Newsome WT**, **Shadlen MN**, **Celebrini S**, **Movshon JA**. A relationship between behavioral choice and the visual responses of neurons in macaque MT. *Vis Neurosci* 13: 87–100, 1996.

Broadbent DE. A mechanical model for human attention and immediate memory. *Psychol Rev* 64: 205–215, 1957.

Brodmann K. Vergleichende Lokalisationslehre der Großhirnrinde: in ihren Prinzipien dargestellt auf Grund des Zellenbaues. .

Brosch M, **Bauer R**, **Eckhorn R**. Stimulus-dependent modulations of correlated high-frequency oscillations in cat visual cortex. *Cereb Cortex* 7: 70–76, 1997.

Buschman TJ, **Denovellis EL**, **Diogo C**, **Bullock D**, **Miller EK**. Synchronous Oscillatory Neural Ensembles for Rules in the Prefrontal Cortex. *Neuron* 76: 838–846, 2012.

Buzsáki G. Large-scale recording of neuronal ensembles. *Nat Neurosci* 7: 446, 2004.

Calvin WH, **Stevens CF**. Synaptic Noise as a Source of Variability in the Interval between Action Potentials. *Science* 155: 842 LP-844, 1967.

Canolty RT, **Edwards E**, **Dalal SS**, **Soltani M**, **Nagarajan SS**, **Kirsch HE**, **Berger MS**, **Barbare NM**, **Knight RT**. High gamma power is phase-locked to theta oscillations in human neocortex. *Science* 313: 1626–1628, 2006.

Canolty RT, **Knight RT**. The functional role of cross-frequency coupling. *Trends Cogn Sci* 14: 506–515, 2010.

Cant JS, **Large M-E**, **McCall L**, **Goodale MA**. Independent processing of form, colour, and texture in object perception. *Perception* 37: 57–78, 2008.

Capilla A, **Schoffelen JM**, **Paterson G**, **Thut G**, **Gross J**. Dissociated α-band modulations

in the dorsal and ventral visual pathways in visuospatial attention and perception. *Cereb Cortex* 24: 550–561, 2014.

Carrasco M. Visual attention: the past 25 years. *Vision Res* 51: 1484–1525, 2011.

Chawla D, **Rees G**, **Friston KJ**. The physiological basis of attentional modulation in extrastriate visual areas. *Nat Neurosci* 2: 671–676, 1999.

Chelazzi L, **Duncan J**, **Miller EK**, **Desimone R**. Responses of neurons in inferior temporal cortex during memory-guided visual search. *J Neurophysiol* 80: 2918–2940, 1998.

Chen X, **Hoffmann K-P**, **Albright TD**, **Thiele A**. Effect of feature-selective attention on neuronal responses in macaque area MT. *J Neurophysiol* 107: 1530–1543, 2012.

Chen Y, **Martinez-Conde S**, **Macknik SL**, **Bereshpolova Y**, **Swadlow HA**, **Alonso J-M**. Task difficulty modulates the activity of specific neuronal populations in primary visual cortex. *Nat Neurosci* 11: 974–982, 2008.

Cohen MR, **Kohn A**. Measuring and interpreting neuronal correlations. *Nat Neurosci* 14: 811–819, 2011.

Cohen MR, **Maunsell JHR**. Attention improves performance primarily by reducing interneuronal correlations. *Nat Neurosci* 12: 1594–600, 2009.

Cohen MR, **Newsome WT**. Context-dependent changes in functional circuitry in visual area MT. *Neuron* 60: 162–173, 2008.

Cohen MX, **Axmacher N**, **Lenartz D**, **Elger CE**, **Sturm V**, **Schlaepfer TE**. Good vibrations: cross-frequency coupling in the human nucleus accumbens during reward processing. *J Cogn Neurosci* 21: 875–889, 2009.

Colgin LL, **Denninger T**, **Fyhn M**, **Hafting T**, **Bonnevie T**, **Jensen O**, **Moser M-B**, **Moser EI**. Frequency of gamma oscillations routes flow of information in the hippocampus. *Nature* 462: 353, 2009.

Coon WG, **Gunduz A**, **Brunner P**, **Ritaccio AL**, **Pesaran B**, **Schalk G**. Oscillatory phase modulates the timing of neuronal activations and resulting behavior. *Neuroimage* 133: 294–301, 2016.

Corbetta M, **Miezin FM**, **Dobmeyer S**, **Shulman GL**, **Petersen SE**. Selective and divided

attention during visual discriminations of shape, color, and speed: functional anatomy by positron emission tomography. *J Neurosci* 11: 2383–2402, 1991.

Corbetta M, **Shulman GL**. Control of goal-directed and stimulus-driven attention in the brain. *Nat Rev Neurosci* 3: 201–215, 2002.

Corchs S, **Deco G**. Feature-based attention in human visual cortex: simulation of fMRI data. *Neuroimage* 21: 36–45, 2004.

Courtin J, **Chaudun F**, **Rozeske RR**, **Karalis N**, **Gonzalez-Campo C**, **Wurtz H**, **Abdi A**, **Baufreton J**, **Bienvenu TCM**, **Herry C**. Prefrontal parvalbumin interneurons shape neuronal activity to drive fear expression. *Nature* 505: 92–96, 2014.

Croner LJ, **Albright TD**. Segmentation by color influences responses of motion-sensitive neurons in the cortical middle temporal visual area. *J Neurosci* 19: 3935–3951, 1999.

Czuba TB, **Huk AC**, **Cormack LK**, **Kohn A**. Area MT encodes three-dimensional motion. *J Neurosci* 34: 15522–15533, 2014.

David S V, **Hayden BY**, **Mazer JA**, **Gallant JL**. Attention to Stimulus Features Shifts Spectral Tuning of V4 Neurons during Natural Vision. *Neuron* 59: 509–521, 2008.

DeAngelis GC, **Newsome WT**. Organization of disparity-selective neurons in macaque area MT. *J Neurosci* 19: 1398–1415, 1999.

deCharms RC, **Blake DT**, **Merzenich MM**. A multielectrode implant device for the cerebral cortex. *J Neurosci Methods* 93: 27–35, 1999.

Desimone R, **Duncan J**. NEURAL MECHANISMS OF SELECTIVE VISUAL. *Annu Rev Neurosci* : 193–222, 1995.

Desimone R, **Ungerleider LG**. Multiple visual areas in the caudal superior temporal sulcus of the macaque. *J Comp Neurol* 248: 164–189, 1986.

Dias R, **Robbins TW**, **Roberts AC**. Dissociation in prefrontal cortex of affective and attentional shifts. *Nature* 380: 69–72, 1996.

DiCiccio TJ, **Efron B**. Bootstrap confidence intervals. *Stat Sci* 11: 189–228, 1996.

Dougherty K, **Cox MA**, **Ninomiya T**, **Maier A**, **Leopold DA**. Ongoing Alpha Activity in V1

Regulates Visually Driven Spiking Responses. *Cereb Cortex* 27: 1113–1124, 2015.

Drebitz E, **Haag M**, **Grothe I**, **Mandon S**, **Kreiter AK**. Attention Configures Synchronization Within Local Neuronal Networks for Processing of the Behaviorally Relevant Stimulus. *Front Neural Circuits* 12: 71, 2018.

Drebitz E, **Schledde B**, **Wegener D**, **Kreiter AK**. Optimizing the Yield of Multi-Unit Activity by Including the Entire Spiking Activity. *Front Neurosci* 13: 83, 2019.

Driver J, **Frith C**. Shifting baselines in attention research. *Nat Rev Neurosci* 1: 147–148, 2000.

Dubner R, **Zeki SM**. Response properties and receptive fields of cells in an anatomically defined region of the superior temporal sulcus in the monkey. *Brain Res* 35: 528–532, 1971.

Duncan J. Selective attention and the organization of visual information. *J. Exp. Psychol. Gen.* 113American Psychological Association: 501–517, 1984.

Eckhorn R. Stimulus-Specific Synchronizations in the Visual Cortex: Linking of Local Features Into Global Figures? In: *Neuronal Cooperativity*, edited by Krüger J. Springer, p. 184–224.

Eckhorn R. Principles of global visual processing of local features can be investigated with parallel single-cell and group-recordings from the visual cortex. In: *Information Processing in the Cortex*, edited by Aertsen A, Braitenberg V. Berlin, Heidelberg: Springer, 1992, p. 385–420.

Eckhorn R, **Obermueller A**. Single neurons are differently involved in stimulus-specific oscillations in cat visual cortex. *Exp Brain Res* 95: 177–182, 1993.

Efron B, **Tibshirani RJ**. *An introduction to the bootstrap*. CRC press, 1994.

Ernst ZR, **Boynton GM**, **Jazayeri M**. The spread of attention across features of a surface. *J Neurophysiol* 110: 2426–2439, 2013.

Esghaei M, **Daliri MR**, **Treue S**. Attention Decreases Phase-Amplitude Coupling, Enhancing Stimulus Discriminability in Cortical Area MT. *Front Neural Circuits* 9, 2015.

Fanini A, **Nobre AC**, **Chelazzi L**. Selecting and ignoring the component features of a visual

object: A negative priming paradigm. *Vis cogn* 14: 584–618, 2006.

Fannon S, **Saron C**, **Mangun G**. Baseline shifts do not predict attentional modulation of target processing during feature-based visual attention. *Front Hum Neurosci* 2: 7, 2008.

Felleman DJ, **Van Essen DC**. Distributed hierarchical processing in the primate cerebral cortex. *Cereb Cortex* 1: 1–47, 1991.

Fennema CL, **Thompson WB**. Velocity determination in scenes containing several moving objects. *Comput Graph Image Process* 9: 301–315, 1979.

Fiorani M, **Azzi JCB**, **Soares JGM**, **Gattass R**. Automatic mapping of visual cortex receptive fields: a fast and precise algorithm. *J Neurosci Methods* 221: 112–126, 2014.

Found A, **Müller HJ**. Searching for unknown feature targets on more than one dimension: Investigating a "dimension-weighting" account. *Percept Psychophys* 58: 88–101, 1996.

Freeman E, **Macaluso E**, **Rees G**, **Driver J**. fMRI correlates of object-based attentional facilitation vs. suppression of irrelevant stimuli, dependent on global grouping and endogenous cueing. *Front Integr Neurosci* 8: 12, 2014.

Friedman-Hill S, **Maldonado PE**, **Gray CM**. Dynamics of striate cortical activity in the alert macaque: I. Incidence and stimulus-dependence of gamma-band neuronal oscillations. *Cereb Cortex* 10: 1105–1116, 2000.

Fries P. A mechanism for cognitive dynamics: neuronal communication through neuronal coherence. *Trends Cogn Sci* 9: 474–480, 2005.

Fries P. Rhythms for Cognition: Communication through Coherence. *Neuron* 88: 220–235, 2015.

Fries P, **Neuenschwander S**, **Engel a K**, **Goebel R**, **Singer W**. Rapid feature selective neuronal synchronization through correlated latency shifting. *Nat Neurosci* 4: 194–200, 2001.

Fries P, **Roelfsema PR**, **Engel AK**, **Konig P**, **Singer W**. Synchronization of oscillatory responses in visual cortex correlates with perception in interocular rivalry. *Proc Natl Acad Sci U S A* 94: 12699–12704, 1997.

Galashan FO, **Rempel HC**, **Meyer A**, **Gruber-Dujardin E**, **Kreiter AK**, **Wegener D**. A new type of recording chamber with an easy-to-exchange microdrive array for chronic recordings in macaque monkeys. *J Neurophysiol* 105: 3092–3105, 2011.

Galashan FO, **Saßen HC**, **Kreiter AK**, **Wegener D**. Monkey area MT latencies to speed changes depend on attention and correlate with behavioral reaction times. *Neuron* 78: 740–750, 2013.

Geesaman BJ, **Born RT**, **Andersen RA**, **Tootell RB**. Maps of complex motion selectivity in the superior temporal cortex of the alert macaque monkey: a double-label 2-deoxyglucose study. *Cereb Cortex* 7: 749–757, 1997.

Gilbert CD, **Wiesel TN**. Functional organization of the visual cortex. *Prog Brain Res* 58: 209–218, 1983.

Girard P, **Salin PA**, **Bullier J**. Response selectivity of neurons in area MT of the macaque monkey during reversible inactivation of area V1. *J Neurophysiol* 67: 1437–1446, 1992.

Glaser EM, **Marks WB**. On-line separation of interleaved neuronal pulse sequences. *Data Acquis Process Biol Med* 5: 137–156, 1968.

Gledhill D, **Grimsen C**, **Fahle M**, **Wegener D**. Human feature-based attention consists of two distinct spatiotemporal processes. *J Vis* 15: 1–17, 2015.

Gold C, **Henze DA**, **Koch C**, **Buzsáki G**. On the Origin of the Extracellular Action Potential Waveform: A Modeling Study. *J Neurophysiol* 95: 3113–3128, 2006.

Grabska-Barwińska A, **Ng BSW**, **Jancke D**. Orientation selective or not? - Measuring significance of tuning to a circular parameter. *J Neurosci Methods* 203: 1–9, 2012.

Gramann K, **Toellner T**, **Krummenacher J**, **Eimer M**, **Muller HJ**. Brain electrical correlates of dimensional weighting: an ERP study. *Psychophysiol* 44: 277–292, 2007.

Gramann K, **Tollner T**, **Muller HJ**. Dimension-based attention modulates early visual processing. *Psychophysiol* 47: 968–978, 2010.

Gray CM, **Engel AK**, **Konig P**, **Singer W**. Synchronization of oscillatory neuronal responses in cat striate cortex: temporal properties. *Vis Neurosci* 8: 337–347, 1992.

Gray CM, **Maldonado PE**, **Wilson M**, **McNaughton B**. Tetrodes markedly improve the

reliability and yield of multiple single-unit isolation from multi-unit recordings in cat striate cortex. *J Neurosci Methods* 63: 43–54, 1995.

Griffith RW, **Humphrey DR**. Long-term gliosis around chronically implanted platinum electrodes in the Rhesus macaque motor cortex. *Neurosci Lett* 406: 81–86, 2006.

Grinvald A, **Lieke E**, **Frostig RD**, **Gilbert CD**, **Wiesel TN**. Functional architecture of cortex revealed by optical imaging of intrinsic signals. *Nature* 324: 361–364, 1986.

Grothe I, **Neitzel SD**, **Mandon S**, **Kreiter AK**. Switching neuronal inputs by differential modulations of gamma-band phase-coherence. *J Neurosci* 32: 16172–80, 2012.

Grzywacz NM, **Yuille AL**. A model for the estimate of local image velocity by cells in the visual cortex. *Proc R Soc London Ser B, Biol Sci* 239: 129–161, 1990.

Gur M, **Kagan I**, **Snodderly DM**. Orientation and Direction Selectivity of Neurons in V1 of Alert Monkeys: Functional Relationships and Laminar Distributions. *Cereb Cortex* 15: 1207–1221, 2005.

Harris KD, **Henze DA**, **Csicsvari J**, **Hirase H**, **Buzsáki G**. Accuracy of Tetrode Spike Separation as Determined by Simultaneous Intracellular and Extracellular Measurements. *J Neurophysiol* 84, 2000.

Heeger DJ. Model for the extraction of image flow. *J Opt Soc Am A* 4: 1455–1471, 1987.

van der Heijden AHC. *Selective attention in vision*. Routledge, 2003.

Henrie JA, **Shapley R**. LFP power spectra in V1 cortex: the graded effect of stimulus contrast. *J Neurophysiol* 94: 479–490, 2005.

Herrington TM, **Assad JA**. Neural activity in the middle temporal area and lateral intraparietal area during endogenously cued shifts of attention. *J Neurosci* 29: 14160–14176, 2009.

Herrmann K, **Montaser-Kouhsari L**, **Carrasco M**, **Heeger DJ**. When size matters: attention affects performance by contrast or response gain. *Nat Neurosci* 13: 1554–1559, 2010.

Holm S. A Simple Sequentially Rejective Multiple Test Procedure. *Source Scand J Stat Scand J Stat* 6: 65–70, 1979.

Horwitz GD. What studies of macaque monkeys have told us about human color vision. *Neurosci* 296: 110–115, 2015.

Hubel DH. Eye, Brain, and Vision. Henry Holt and Company.

Hubel DH, **Wiesel TN**. Receptive fields, binocular interaction and functional architecture in the cat's visual cortex. *J Physiol* 160: 106–154, 1962.

Hubel DH, **Wiesel TN**. Receptive Fields and Functional Architecture of monkey striate cortex. *J Physiol* 195: 215–243, 1968.

Hubel DH, **Wiesel TN**. Uniformity of monkey striate cortex: A parallel relationship between field size, scatter, and magnification factor. *J Comp Neurol* 158: 295–305, 1974.

Hubel DH, **Wiesel TN**. Functional architecture of macaque monkey visual cortex. *Proc Royla London Biol Soc B* 198: 1, 1977.

Huk AC, **Heeger DJ**. Task-related modulation of visual cortex. *J Neurophysiol* 83: 3525–3536, 2000.

Hulata E, **Segev R**, **Ben-Jacob E**. A method for spike sorting and detection based on wavelet packets and Shannon's mutual information. *J Neurosci Methods* 117: 1–12, 2002.

Hyafil A, **Giraud AL**, **Fontolan L**, **Gutkin B**. Neural Cross-Frequency Coupling: Connecting Architectures, Mechanisms, and Functions. *Trends Neurosci* 38: 725–740, 2015.

Itti L, **Koch C**, **Way W**, **Angeles L**. COMPUTATIONAL MODELLING OF VISUAL ATTENTION. *Neurosci* 2: 194–203, 2001.

Jack AI, **Shulman GL**, **Snyder AZ**, **McAvoy M**, **Corbetta M**. Separate modulations of human V1 associated with spatial attention and task structure. *Neuron* 51: 135–147, 2006.

Jensen O, **Bonnefond M**, **Marshall TR**, **Tiesinga P**. Oscillatory mechanisms of feedforward and feedback visual processing. *Trends Neurosci* 38: 192–194, 2015.

Jensen O, **Bonnefond M**, **VanRullen R**. An oscillatory mechanism for prioritizing salient unattended stimuli. *Trends Cogn Sci* 16: 200–205, 2012.

Jensen O, **Mazaheri A**. Shaping Functional Architecture by Oscillatory Alpha Activity: Gating by Inhibition. *Front Hum Neurosci* 4: 1–8, 2010.

Kastner S, **Pinsk MA**, **Weerd P De**, **Desimone R**, **Ungerleider LG**. Increased Activity in Human Visual Cortex during Directed Attention in the Absence of Visual Stimulation. 22: 751–761, 1999.

Katzner S, **Busse L**, **Treue S**. Attention to the Color of a Moving Stimulus Modulates Motion-Signal Processing in Macaque Area MT: Evidence for a Unified Attentional System. *Front Syst Neurosci* 3: 12, 2009.

Khayat PS, **Martinez-Trujillo JC**. Effects of attention and distractor contrast on the responses of middle temporal area neurons to transient motion direction changes. *Eur J Neurosci* 41: 1603–1613, 2015.

Khayat PS, **Niebergall R**, **Martinez-Trujillo JC**. Frequency-dependent attentional modulation of local field potential signals in macaque area MT. *J Neurosci* 30: 7037–48, 2010.

Kobak D, **Brendel W**, **Constantinidis C**, **Feierstein CE**, **Kepecs A**, **Mainen ZF**, **Qi X-LL**, **Romo R**, **Uchida N**, **Machens CK**. Demixed principal component analysis of neural population data. *Elife* 5: e10989, 2016.

Koch C, **Ullman S**. Shifts in selective visual attention: towards the underlying neural circuitry. *Hum Neurobiol* 4: 219–227, 1985.

Koch C, **Wang HT**, **Mathur B**. Computing motion in the primate's visual system. *J Exp Biol* 146: 115–139, 1989.

Kravitz DJ, **Saleem KS**, **Baker CI**, **Ungerleider LG**, **Mishkin M**. The ventral visual pathway: an expanded neural framework for the processing of object quality. *Trends Cogn Sci* 17: 26–49, 2013.

Kreiter AK. Functional implications of temporal structure in primate cortical information processing. *Zoology (Jena)* 104: 241–255, 2001.

Kreiter AK. How do we model attention-dependent signal routing? *Neural Netw* 19: 1443–1444, 2006.

Lacour SP, **Courtine G**, **Guck J**. Materials and technologies for soft implantable neuroprostheses. *Nat Rev Mater* 1: 16063, 2016.

Lagae L, **Raiguel S**, **Orban GA**. Speed and direction selectivity of macaque middle temporal neurons. *J Neurophysiol* 69: 19–39, 1993.

Landau AN, **Fries P**. Attention samples stimuli rhythmically. *Curr Biol* 22: 1000–4, 2012.

Landau AN, **Schreyer HM**, **Van Pelt S**, **Fries P**. Distributed Attention Is Implemented through Theta-Rhythmic Gamma Modulation. *Curr Biol* 25: 2332–2337, 2015.

Lauwereyns J, **Sakagami M**, **Tsutsui K**, **Kobayashi S**, **Koizumi M**, **Hikosaka O**. Responses to task-irrelevant visual features by primate prefrontal neurons. *J Neurophysiol* 86: 2001–2010, 2001.

Lebedev MA, **Nicolelis MAL**. Brainmachine interfaces: past, present and future. *Trends Neurosci* 29: 536–546, 2006.

Lee J, **Maunsell JHR**. Attentional modulation of MT neurons with single or multiple stimuli in their receptive fields. *J Neurosci* 30: 3058–66, 2010.

Lee J, **Williford T**, **Maunsell JHR**. Spatial attention and the latency of neuronal responses in macaque area V4. *J Neurosci* 27: 9632–7, 2007.

Legatt AD, **Arezzo J**, **Vaughan HG**. Averaged multiple unit activity as an estimate of phasic changes in local neuronal activity: effects of volume-conducted potentials. *J Neurosci Methods* 2: 203–217, 1980.

Lemon R. Methods for Neuronal Recording in Conscious Animals. Chichester, UK: Wiley & Sons, 1984.

Lewis CM, **Bosman CA**, **Fries P**. Recording of brain activity across spatial scales. *Curr Opin Neurobiol* 32: 68–77, 2015.

Liu J, **Newsome WT**. Functional organization of speed tuned neurons in visual area MT. *J Neurophysiol* 89: 246–256, 2003.

Liu J, **Newsome WT**. Local Field Potential in Cortical Area MT: Stimulus Tuning and Behavioral Correlations. *J Neurosci* 26: 7779–7790, 2006.

Liu T, **Larsson J**, **Carrasco M**. Feature-based attention modulates orientation-selective responses in human visual cortex. *Neuron* 55: 313–323, 2007.

Luck SJ, **Chelazzi L**, **Hillyard S a**, **Desimone R**. Neural mechanisms of spatial selective attention in areas V1, V2, and V4 of macaque visual cortex. *J Neurophysiol* 77: 24–42, 1997.

Maldonado PE, **Friedman-Hill S**, **Gray CM**. Dynamics of striate cortical activity in the alert macaque: II. Fast time scale synchronization. *Cereb Cortex* 10: 1117–1131, 2000.

Marcar VL, **Zihl J**, **Cowey A**. Comparing the visual deficits of a motion blind patient with the visual deficits of monkeys with area MT removed. *Neuropsychologia* 35: 1459–1465, 1997.

Martinez-Trujillo JC, **Treue S**. Attentional Modulation Strength in Cortical Area MT. *Neuron* 35: 365–370, 2002.

Martinez-Trujillo JC, **Treue S**. Feature-based attention increases the selectivity of population responses in primate visual cortex. *Curr Biol* 14: 744–751, 2004.

Masse NY, **Cook EP**. The Effect of Middle Temporal Spike Phase on Sensory Encoding and Correlates with Behavior during a Motion-Detection Task. *J Neurosci* 28: 1343 LP-1355, 2008.

Maunsell JH, **van Essen DC**. The connections of the middle temporal visual area (MT) and their relationship to a cortical hierarchy in the macaque monkey. *J Neurosci* 3: 2563–2586, 1983.

Maunsell JH, **Van Essen DC**. Functional properties of neurons in middle temporal visual area of the macaque monkey. I. Selectivity for stimulus direction, speed, and orientation. *J Neurophysiol* 49: 1127–1147, 1983.

Maunsell JHR, **Newsome WT**, **York N**, **Maunsell JHR**, **Newsome WT**, **York N**, **Maunsell JHR**, **Newsome WT**. Visual Processing in Monkey Extrastriate Cortex. *Annu Rev Neurosci* 10: 363–401, 1987.

Maunsell JHR, **Treue S**. Feature-based attention in visual cortex. *Trends Neurosci* 29: 317–22, 2006.

McAdams CJ, **Maunsell JH**. Effects of attention on orientation-tuning functions of single neurons in macaque cortical area V4. *J Neurosci* 19: 431–441, 1999.

McAdams CJ, **Maunsell JH**. Attention to both space and feature modulates neuronal responses in macaque area V4. *J Neurophysiol* 83: 1751–1755, 2000.

McMains SA, **Fehd HM**, **Emmanouil T-A**, **Kastner S**. Mechanisms of Feature- and Space-Based Attention: Response Modulation and Baseline Increases. *J Neurophysiol* 98: 2110–2121, 2007.

Mendoza G, **Peyrache A**, **Gámez J**, **Prado L**, **Buzsáki G**, **Merchant H**. Recording extracellular neural activity in the behaving monkey using a semichronic and high-density electrode system. *J Neurophysiol* 116: 563–574, 2016.

Mikami A, **Newsome WT**, **Wurtz RH**. Motion selectivity in macaque visual cortex. II. Spatiotemporal range of directional interactions in MT and V1. *J Neurophysiol* 55: 1328–1339, 1986.

Miller EK, **Cohen JD**. An Integrative Theory of Prefrontal Cortex Function. *Annu Rev Neurosci* 24: 167–202, 2001.

Mishkin M, **Ungerleider LG**, **Macko KA**. Object vision and spatial vision: two cortical pathways. *Trends Neurosci* 6: 414–417, 1983.

Mitchell JF, **Sundberg KA**, **Reynolds JH**. Spatial attention decorrelates intrinsic activity fluctuations in macaque area V4. *Neuron* 63: 879–88, 2009.

Monsell S. Task switching. *Trends Cogn Sci* 7: 134–140, 2003.

Moran J, **Desimone R**. Selective attention gates visual processing in the extrastriate cortex. *Science* 229: 782–784, 1985.

Motter BC. Neural correlates of feature selective memory and pop-out in extrastriate area V4. *J Neurosci* 14: 2190–2199, 1994.

Movshon J, **Adelson EH**, **Gizzi MS**, **Newsome WT**. The analysis of moving visual patterns. In: *Pattern Recognition Mechanisms*, edited by Chagas C, Gattass R, Gross C. Rome:Vatican: PONTIFICIAE ACADEMIAE SCIENTIARVM, 1985, p. 117–151.

Movshon JA, **Newsome WT**. Visual response properties of striate cortical neurons

projecting to area MT in macaque monkeys. *J Neurosci* 16: 7733–7741, 1996.

Müller HJ, **Heller D**, **Ziegler J**. Visual search for singleton feature targets within and across feature dimensions. *Percept Psychophys* 57: 1–17, 1995.

Murre JMJ, **Sturdy DPF**. The connectivity of the brain: multi-level quantitative analysis. *Biol Cybern* 73: 529–545, 1995.

Nenadic Z, **Burdick JW**. Spike detection using the continuous wavelet transform. *IEEE Trans Biomed Eng* 52: 74–87, 2005.

Neumann O. Chapter 10 Theories of attention. 1996.

Newsome WT, **Pare EB**. A selective impairment of motion perception following lesions of the middle temporal visual area (MT). *J Neurosci* 8: 2201–2211, 1988.

Ni J, **Wunderle T**, **Lewis CM**, **Desimone R**, **Diester I**, **Ni J**, **Wunderle T**, **Lewis CM**, **Desimone R**, **Diester I**, **Fries P**. Article Gamma-Rhythmic Gain Modulation. *Neuron* 92: 240–251, 2016.

Niebur E, **Koch C**. A model for the neuronal implementation of selective visual attention based on temporal correlation among neurons. *J Comput Neurosci* 1: 141–158, 1994.

Niemi P, **Naatanen R**. Foreperiod and Simple Reaction Time. *Psychol Bull* 89: 133–162, 1981.

Nobre AC, **Rao A**, **Chelazzi L**. Selective attention to specific features within objects: behavioral and electrophysiological evidence. *J Cogn Neurosci* 18: 539–561, 2006.

Nover H, **Anderson CH**, **DeAngelis GC**. A logarithmic, scale-invariant representation of speed in macaque middle temporal area accounts for speed discrimination performance. *J Neurosci* 25: 10049–10060, 2005.

Nowlan SJ, **Sejnowski TJ**. Filter Selection Model for Generating Visual Motion Signals. In: *Advances in Neural Information Processing Systems 5*, edited by Hanson SJ, Cowan JD, Giles CL. Morgan-Kaufmann, p. 369–376.

O'Craven KM, **Downing PE**, **Kanwisher N**. fMRI evidence for objects as the units of attentional selection. *Nature* 401: 584, 1999.

Obeid I, **Wolf PD**. Evaluation of spike-detection algorithms fora brain-machine interface application. *IEEE Trans Biomed Eng* 51: 905–911, 2004.

Onslow ACE, **Jones MW**, **Bogacz R**. A canonical circuit for generating phase-amplitude coupling. *PLoS One* 9, 2014.

Oostenveld R, **Fries P**, **Maris E**, **Schoffelen JM**. FieldTrip: Open source software for advanced analysis of MEG, EEG, and invasive electrophysiological data. *Comput Intell Neurosci* 2011: 1, 2011.

Orban GA, **Kennedy H**, **Bullier J**. Velocity sensitivity and direction selectivity of neurons in areas V1 and V2 of the monkey: influence of eccentricity. *J Neurophysiol* 56: 462–480, 1986.

Osipova D, **Hermes D**, **Jensen O**. Gamma power is phase-locked to posterior alpha activity. *PLoS One* 3: e3990, 2008.

Pack CC, **Born RT**. Temporal dynamics of a neural solution to the aperture problem in visual area MT of macaque brain. *Nature* 409: 1040–1042, 2001.

Parker AJ, **Newsome WT**. Sense and the single neuron: probing the physiology of perception. *Annu Rev Neurosci* 21: 227–277, 1998.

Pashler HE, **Sutherland S**. *The psychology of attention*. MIT press Cambridge, MA, 1998.

Polikov VS, **Tresco PA**, **Reichert WM**. Response of brain tissue to chronically implanted neural electrodes. *J Neurosci Methods* 148: 1–18, 2005.

Polk TA, **Drake RM**, **Jonides JJ**, **Smith MR**, **Smith EE**. Attention Enhances the Neural Processing of Relevant Features and Suppresses the Processing of Irrelevant Features in Humans: A Functional Magnetic Resonance Imaging Study of the Stroop Task. *J Neurosci* 28: 13786–13792, 2008.

Pollmann S, **Weidner R**, **Muller HJ**, **von Cramon DY**. A fronto-posterior network involved in visual dimension changes. *J Cogn Neurosci* 12: 480–494, 2000.

Pollmann S, **Weidner R**, **Muller HJ**, **Maertens M**, **von Cramon DY**. Selective and interactive neural correlates of visual dimension changes and response changes. *Neuroimage* 30: 254–265, 2006.

Posner MI. Orienting of attention. *Q J Exp Psychol* 32: 3–25, 1980.

Posner MI, **Snyder CRR**, **Davidson BJ**. Attention and the Detection of Signals. 109: 160–174, 1980.

Pouzat C, **Mazor O**, **Laurent G**. Using noise signature to optimize spike-sorting and to assess neuronal classification quality. *J Neurosci Methods* 122: 43–57, 2002.

Price NSC, **Born RT**. Timescales of sensory- and decision-related activity in the middle temporal and medial superior temporal areas. *J Neurosci* 30: 14036–14045, 2010.

Price NSC, **Born RT**. Adaptation to speed in macaque middle temporal and medial superior temporal areas. *J Neurosci* 33: 4359–4368, 2013.

Quiroga RQ, **Nadasdy Z**, **Ben-Shaul Y**. Unsupervised spike detection and sorting with wavelets and superparamagnetic clustering. *Neural Comput* 16: 1661–1687, 2004.

Raiguel S, **Van Hulle MM**, **Xiao DK**, **Marcar VL**, **Orban GA**. Shape and spatial distribution of receptive fields and antagonistic motion surrounds in the middle temporal area (V5) of the macaque. *Eur J Neurosci* 7: 2064–2082, 1995.

Rall W. Electrophysiology of a Dendritic Neuron Model. *Biophys J* 2: 145–167, 1962.

Reynolds JH, **Heeger DJ**. The Normalization Model of Attention. *Neuron* 61: 168–185, 2009.

Reynolds JH, **Pasternak T**, **Desimone R**. Attention increases sensitivity of V4 neurons. *Neuron* 26: 703–14, 2000.

Richert M, **Albright TD**, **Krekelberg B**. The complex structure of receptive fields in the middle temporal area. *Front Syst Neurosci* 7: 2, 2013.

Richter CG, **Thompson WH**, **Bosman CA**, **Fries P**. A jackknife approach to quantifying single-trial correlation between covariance-based metrics undefined on a single-trial basis. *Neuroimage* 114: 57–70, 2015.

Ringach DL, **Shapley RM**, **Hawken MJ**. Orientation selectivity in macaque V1: diversity and laminar dependence. *J Neurosci* 22: 5639–5651, 2002.

Rodman HR, **Gross CG**, **Albright TD**. Afferent basis of visual response properties in area

MT of the macaque. I. Effects of striate cortex removal. *J Neurosci* 9: 2033–2050, 1989.

Rodman HR, **Gross CG**, **Albright TD**. Afferent basis of visual response properties in area MT of the macaque. II. Effects of superior colliculus removal. *J Neurosci* 10: 1154–1164, 1990.

Rodríguez V, **Valdés-Sosa M**, **Freiwald W**. Dividing attention between form and motion during transparent surface perception. *Cogn Brain Res* 13: 187–193, 2002.

Saenz M, **Buracas GT**, **Boynton GM**. Global effects of feature-based attention in human visual cortex. *Nat Neurosci* 5: 631–632, 2002.

Salatino JW, **Ludwig KA**, **Kozai TDY**, **Purcell EK**. Glial responses to implanted electrodes in the brain. *Nat Biomed Eng* 1: 862–877, 2017.

Sceniak MP, **Hawken MJ**, **Shapley R**. Visual Spatial Characterization of Macaque V1 Neurons. *J Neurophysiol* 85: 1873–1887, 2001.

Schledde B, **Galashan FO**, **Przybyla M**, **Kreiter AK**, **Wegener D**. Task-specific, dimension-based attentional shaping of motion processing in monkey area MT. *J Neurophysiol* 118: 1542–1555, 2017.

Schoenfeld MA, **Tempelmann C**, **Martinez A**, **Hopf J-M**, **Sattler C**, **Heinze H-J**, **Hillyard SA**. Dynamics of feature binding during object-selective attention. *Proc Natl Acad Sci U S A* 100: 11806–11811, 2003.

Schwartz AB. CORTICAL NEURAL PROSTHETICS. *Annu Rev Neurosci* 27: 487–507, 2004.

Self MW, **Peters JC**, **Possel JK**, **Reithler J**, **Goebel R**, **Ris P**, **Jeurissen D**, **Reddy L**, **Claus S**, **Baayen JC**, **Roelfsema PR**. The Effects of Context and Attention on Spiking Activity in Human Early Visual Cortex. *PLoS Biol* 14: e1002420, 2016.

Serences JT, **Ester EF**, **Vogel EK**, **Awh E**. Stimulus-Specific Delay Activity in Human Primary Visual Cortex. *Psychol Sci* 20: 207–214, 2009.

Shadlen MN, **Britten KH**, **Newsome WT**, **Movshon JA**. A computational analysis of the relationship between neuronal and behavioral responses to visual motion. *J Neurosci* 16: 1486–1510, 1996.

Shadlen MN, **Newsome WT**. The variable discharge of cortical neurons: implications for

connectivity, computation, and information coding. *J Neurosci* 18: 3870–3896, 1998.

Shapley R, **Hawken M**, **Ringach DL**. Dynamics of Orientation Selectivity in the Primary Visual Cortex and the Importance of Cortical Inhibition. *Neuron* 38: 689–699, 2003.

Shipp S, **Zeki S**. The Organization of Connections between Areas V5 and V1 in Macaque Monkey Visual Cortex. *Eur J Neurosci* 1: 333–354, 1989.

Shulman GL, **Ollinger JM**, **Akbudak E**, **Conturo TE**, **Snyder AZ**, **Petersen SE**, **Corbetta M**. Areas involved in encoding and applying directional expectations to moving objects. *J Neurosci* 19: 9480–9496, 1999.

Simoncelli EP, **Heeger DJ**. A model of neuronal responses in visual area MT. *Vision Res* 38: 743–61, 1998.

Singer W. Neuronal synchrony: a versatile code for the definition of relations? *Neuron* 24: 49-65,111-125, 1999.

Smith M a, **Kohn A**. Spatial and temporal scales of neuronal correlation in primary visual cortex. *J Neurosci* 28: 12591–12603, 2008.

Snowden RJ, **Treue S**, **Erickson RG**, **Andersen RA**. The response of area MT and V1 neurons to transparent motion. *J Neurosci* 11: 2768–2785, 1991.

Snyder AC, **Foxe JJ**. Anticipatory Attentional Suppression of Visual Features Indexed by Oscillatory Alpha-Band Power Increases:A High-Density Electrical Mapping Study. *J Neurosci* 30: 4024–4032, 2010.

Steinmetz PN, **Roy A**, **Fitzgerald PJ**, **Hsiao SS**, **Johnson KO**, **Niebur E**. Attention modulates synchronized neuronal firing in primate somatosensory cortex. *Nature* 404: 187–190, 2000.

Stepniewska I, **Qi HX**, **Kaas JH**. Do superior colliculus projection zones in the inferior pulvinar project to MT in primates? *Eur J Neurosci* 11: 469–480, 1999.

Stormer VS, **Alvarez GAA**, **Störmer VSS**, **Alvarez GAA**. Feature-based attention elicits surround suppression in feature space. *Curr Biol* 24: 1985–1988, 2014.

Sundberg K a, **Mitchell JF**, **Gawne TJ**, **Reynolds JH**. Attention influences single unit and local field potential response latencies in visual cortical area V4. *J Neurosci* 32: 16040–

50, 2012.

Supèr H, **Roelfsema PR**. Chronic multiunit recordings in behaving animals: advantages and limitations. *Prog Brain Res* 147: 263–282, 2005.

Szczepanski SM, **Crone NE**, **Kuperman RA**, **Auguste KI**, **Parvizi J**, **Knight RT**. Dynamic Changes in Phase-Amplitude Coupling Facilitate Spatial Attention Control in Fronto-Parietal Cortex. *PLoS Biol* 12: e1001936, 2014.

Tallon-Baudry C, **Bertrand O**, **Delpuech C**, **Permier J**. Oscillatory gamma-band (30-70 Hz) activity induced by a visual search task in humans. *J Neurosci* 17: 722–734, 1997.

Taya S, **Adams WJ**, **Graf EW**, **Lavie N**. The fate of task-irrelevant visual motion: Perceptual load versus feature-based attention. *J Vis* 9: 12, 2009.

Taylor K, **Mandon S**, **Freiwald W a**, **Kreiter a K**. Coherent oscillatory activity in monkey area v4 predicts successful allocation of attention. *Cereb Cortex* 15: 1424–37, 2005.

Thiele A, **Dobkins KR**, **Albright TD**. The contribution of color to motion processing in Macaque middle temporal area. *J Neurosci* 19: 6571–6587, 1999.

Tochitsky I, **Polosukhina A**, **Degtyar VEE**, **Gallerani N**, **Smith CMM**, **Friedman A**, **Van Gelder RN**, **Trauner D**, **Kaufer D**, **Kramer RHH**, **Van Gelder RN**, **Trauner D**, **Kaufer D**, **Kramer RHH**. Restoring Visual Function to Blind Mice with a Photoswitch that Exploits Electrophysiological Remodeling of Retinal Ganglion Cells. *Neuron* 81: 800–813, 2014.

Tollner T, **Gramann K**, **Muller HJ**, **Kiss M**, **Eimer M**. Electrophysiological markers of visual dimension changes and response changes. *J Exp Psychol Hum Percept Perform* 34: 531–542, 2008.

Töllner T, **Zehetleitner M**, **Gramann K**, **Müller HJ**. Top-down weighting of visual dimensions: Behavioral and electrophysiological evidence. *Vision Res* 50: 1372–1381, 2010.

Tootell RB, **Dale AM**, **Sereno MI**, **Malach R**. New images from human visual cortex. *Trends Neurosci* 19: 481–489, 1996.

Torrence C, **Compo GP**. A Practical Guide to Wavelet Analysis. *Bull Am Meteorol Soc* 79: 61–78, 1998.

Torriente I, **Valdes-Sosa M**, **Ramirez D**, **Bobes MA**. Visual evoked potentials related to motion-onset are modulated by attention. *Vision Res* 39: 4122–4139, 1999.

Tort ABL, **Komorowski R**, **Eichenbaum H**, **Kopell N**. Measuring Phase-Amplitude Coupling Between Neuronal Oscillations of Different Frequencies. *J Neurophysiol* 104: 1195–1210, 2010.

Traschütz A, **Kreiter AK**, **Wegener D**. Transient activity in monkey area MT represents speed changes and is correlated with human behavioral performance. *J Neurophysiol* 113: 890–903, 2015.

Traschütz A, **Zinke W**, **Wegener D**. Speed change detection in foveal and peripheral vision. *Vision Res* 72: 1–13, 2012.

Treisman A, **Gormican S**. Feature analysis in early vision: Evidence from search asymmetries. *Psychol Rev* 95: 15–48, 1988.

Treisman A, **Sato S**. Conjunction search revisited. *J Exp Psychol Hum Percept Perform* 16: 459–478, 1990.

Treue S. Visual attention: The where, what, how and why of saliency. *Curr Opin Neurobiol* 13: 428–432, 2003.

Treue S, **Martínez Trujillo JC**. Feature-based attention influences motion processing gain in macaque visual cortex. *Nature* 399: 575–9, 1999.

Treue S, **Maunsell JH**. Effects of attention on the processing of motion in macaque middle temporal and medial superior temporal visual cortical areas. *J Neurosci* 19: 7591–7602, 1999.

Treue S, **Maunsell JHR**. Attentional modulation of visual motion processing in cortical areas MT and MST. *Nature* 382: 539, 1996.

Turner JN, **Shain W**, **Szarowski DH**, **Andersen M**, **Martins S**, **Isaacson M**, **Craighead H**. Cerebral Astrocyte Response to Micromachined Silicon Implants. *Exp Neurol* 156: 33–49, 1999.

Ungerleider LG, **Mishkin M**. Two cortical visual systems. *Anal. Vis. Behav.* : 549–586, 1982.

Voloh B, **Valiante TA**, **Everling S**, **Womelsdorf T**. Theta–gamma coordination between anterior cingulate and prefrontal cortex indexes correct attention shifts. *Proc Natl Acad Sci U S A* 112: 8457–8462, 2015.

Voytek B, **Canolty RT**, **Shestyuk A**, **Crone NE**, **Parvizi J**, **Knight RT**. Shifts in gamma phase–amplitude coupling frequency from theta to alpha over posterior cortex during visual tasks. *Front Hum Neurosci* 4: 1–9, 2010.

Wagatsuma N, **Potjans TC**, **Diesmann M**, **Sakai K**, **Fukai T**. Spatial and Feature-Based Attention in a Layered Cortical Microcircuit Model. *PLoS One* 8: e80788, 2013.

Wang X -d., **Chen C**, **Zhang D**, **Yao H**. Cumulative latency advance underlies fast visual processing in desynchronized brain state. *Proc Natl Acad Sci U S A* 111: 515–520, 2014.

Wannig A, **Rodríguez V**, **Freiwald WA**. Attention to Surfaces Modulates Motion Processing in Extrastriate Area MT. *Neuron* 54: 639–651, 2007.

Watrous AJ, **Deuker L**, **Fell J**, **Axmacher N**. Phase-amplitude coupling supports phase coding in human ECoG. *Elife* 4: 1–15, 2015.

Wegener D, **Ehn F**, **Aurich MK**, **Galashan FO**, **Kreiter AK**. Feature-based attention and the suppression of non-relevant object features. *Vision Res* 48: 2696–2707, 2008.

Wegener D, **Freiwald WA**, **Kreiter AK**. The Influence of Sustained Selective Attention on Stimulus Selectivity in Macaque Visual Area MT. *J Neurosci* 24: 6106 LP-6114, 2004.

Wegener D, **Galashan FO**, **Aurich MK**, **Kreiter AK**. Attentional spreading to task-irrelevant object features: experimental support and a 3-step model of attention for object-based selection and feature-based processing modulation. *Front Hum Neurosci* 8: 414, 2014.

Weidner R, **Pollmann S**, **Muller HJ**, **von Cramon DY**. Top-down controlled visual dimension weighting: an event-related fMRI study. *Cereb Cortex* 12: 318–328, 2002.

Williford T, **Maunsell JHR**. Effects of spatial attention on contrast response functions in macaque area V4. *J Neurophysiol* 96: 40–54, 2006.

Wolfe JM. Guided Search 2 . 0 A revised model of visual search. *Psychnomic Bull Rev* 1: 202–238, 1994.

Womelsdorf T, **Anton-Erxleben K**, **Pieper F**, **Treue S**. Dynamic shifts of visual receptive fields in cortical area MT by spatial attention. *Nat Neurosci* 9: 1156, 2006a.

Womelsdorf T, **Anton-Erxleben K**, **Treue S**. Receptive field shift and shrinkage in macaque middle temporal area through attentional gain modulation. *J Neurosci* 28: 8934–44, 2008.

Womelsdorf T, **Fries P**, **Mitra PP**, **Desimone R**. Gamma-band synchronization in visual cortex predicts speed of change detection. *Nature* 439: 733–6, 2006b.

Xu Y. The Neural Fate of Task-Irrelevant Features in Object-Based Processing. *J Neurosci* 30: 14020–14028, 2010.

Yabuta NH, **Sawatari A**, **Callaway EM**. Two Functional Channels from Primary Visual Cortex to Dorsal Visual Cortical Areas. *Science* 292: 297–300, 2001.

Yang X, **Shamma SA**. A totally automated system for the detection and classification of neural spikes. *IEEE Trans Biomed Eng* 35: 806–816, 1988.

Yuille AL, **Grzywacz NM**. A computational theory for the perception of coherent visual motion. *Nature* 333: 71–74, 1988.

Zhang X, **Kendrick KM**, **Zhou H**, **Zhan Y**, **Feng J**. A computational study on altered theta-gamma coupling during learning and phase coding. *PLoS One* 7, 2012.

Zihl J, **von Cramon D**, **Mai N**. Selective disturbance of movement vision after bilateral brain damage. *Brain* 106: 313–340, 1983.

Zohary E, **Shadlen MN**, **Newsome WT**. Correlated neuronal discharge rate and its implications for psychophysical performance. *Nature* 370: 140–143, 1994.

List of Figures

conditions that were subtracted from each other. E: Distribution of TCIs (top) and SCIs (bottom). Open bars, all units; gray bars, significantly modulated units. Black arrows, median AIs of all units; Gray arrows, median AIs of significantly modulated units. F: Cumulative distribution of response latencies during test epoch 3. Inlet: median latencies; error bars, 95% CI.

Figure 4 Variability of responses depending on attentional condition. A and B: Fano Factor of spike counts for integration windows between 5 ms and 125 ms width (A), and color-coded P-values for Friedman tests (top rows) investigating the factors task and spatial condition, and Wilcoxon tests (bottom rows) comparing single conditions (B). Color coding ranges between P-values of 10^{-4} and 10^{-1}. Larger and smaller values are colored black and white, respectively. C: Spike-count correlation of 38 pairs of simultaneously recorded neurons for different integration windows. D: Statistical outcome for different integration window widths. Conventions as in B.

Figure 5 Influence of motion and speed preference on task-dependent response modulation. A: Sketch of two direction-tuning curves with small and larger deviation between preferred direction φ_{pref} (black vertical lines) and stimulus direction φ_{stim} (red line). B: Distribution of neurons depending on the absolute deviation $\varphi_{pref} - \varphi_{stim}$. C: Sketch of two log-Gaussian shaped speed-tuning curves. Straight black curve, speed-dependent responses of a neuron for which the base speed of the stimulus (straight vertical red line) is close to preferred and target speed (dashed vertical red line) is preferred; Dashed black curve, speed-dependent responses of a neuron preferring higher speeds; red arrows, vectors indicating the FR increase for a jump from base to target speed, as expected from each neuron's speed tuning. Note that the to-be-expected FR change of the sub-optimally driven neuron is about twice the size of the well-driven neuron. D: Distribution of transients with different amplitude, as expressed by the ratio between the post-change response and the pre-change response (test epochs 3 and 2 in Figure 3). E: Distribution of ranksum values after sorting all neurons according to the deviation between preferred speed and stimulus speed, and to their transient's amplitude, split by median (dashed black line). Blue bars indicate the 50% of neurons with the highest ranksum, indexing units with least-matching tuning properties regarding the actual stimulus properties. F: Combination of Δ_ϕ and T_A values for all units. Blue dots indicate the neurons with highest ranksum. G, H: Population responses of neurons with highest ranksum (units with least-matching tuning) (G) and lowest ranksum (remaining units) (H).

Figure 6 Amount of explained variance as a function of stimulus and task parameters. A, B: Percentage of explained variance for 50% of units with least-matching tuning (A) as compared to the remaining 50% of units (B), estimated by dPCA. Colors in pie plots correspond to variance explained independent of condition (grey), by spatial condition (blue), task condition (red), and interaction between spatial condition and task (purple). C, D: Reconstructed spike trains showing explained variance essentially independent of experimental condition, due to visual stimulation. E, F: Reconstructed spike trains showing explained variance due to spatial condition, G, H: task condition, and I, J: interaction of spatial condition and task. Black lines indicate periods of significant classification.

Figure 7 Normalized spontaneous activity depending on direction and speed-tuning preferences. Errors bars, 95% CI; *: P < 0.05, **: P < 0.01, ***: P < 0.001; n.s.: not significant.

Figure 8 Time shifts and amplitude shifts quantify the difference between a test transient (solid line) and a reference transient (dashed line). Each of the four quadrants display one possible relationship between a test and a reference transient.

Figure 9 Experimental paradigm. Monkeys were trained on a feature change detection paradigm. Trials were initiated by depressing a lever while fixating on a central fixation point. Following an initial delay period of 1050 ms a spatial cue was presented for 700 ms indicating the position of the target event. Static Gabor gratings appeared 250 ms after cue offset and started moving intrinsically after another 200 ms. After motion onset a series of distractor or targets event could occur. Target events in this task were 100 % acceleration of the motion speed and distractor events were either color changes at the cued or un-cued position or speed changes at the un-cued position. Monkeys could respond to the target event in a time interval from 150 ms to 750 ms after the speed change. Trials ended either after another 300 ms delay after the correct responses, late responses or responses to a distractor event. Target speed changes could occur in a random time interval after the motion onset between 660 – 5500 ms. We only analyzed trials during which the target speed change was the first event to occur at any position, thus recorded neurons underwent identical visual stimulation across trials and conditions.

Figure 10 Reaction time distributions and firing rate analysis. A Reaction time distributions of the two animals (top panel: anima I; bottom panel: animal II). Cumulative reaction time distributions, mean and 95 % confidence intervals are shown. Reaction times (RT) above 0.5 sec were excluded from analysis. B Time course of the baseline corrected spike density functions (SDF) are shown locked to the Stimulus onset (left) and relative to the target speed change (right). Colors indicate the RTF according to the distributions in A. C Average mean firing rates of the 3 RTFs in the post-motion interval. Error bars indicate S.E.M., n.s. mean no significant difference. D Same as in C but data is taken from the pre-change interval. E Display of latency and amplitude modulations. Triangles represent unit-wise modulations between RTF I and RTF III and squares represent unit-wise modulations between RTF I and RTF II. The center of the purple and green crosses represent the mean latency/amplitude modulation (purple for RTF I vs. RTF III; green RTF I vs. RTF II), the extent of the crosses represent S.E.M.

Figure 11 Example trials of animal 1 (A) and animal 2 (B). The x_filt traces display the phase supplying raw signal that was filtered in a designated alpha frequency band. Traces of the y_filt signal display the gamma band filtered raw signal at 35 Hz. Phase and amplitude traces are displayed in between the two filtered raw signals. Phases were obtained by extracting the angle of the analytical signal (Hilbert transform) and amplitude were given by the absolute value of the analytical signal. Vertical dashed lines designate the time of the gamma amplitude peaks. For fast RT trials these peaks fell into different phases of the alpha oscillation for both animals. The individual directional unit vectors at the time of gamma amplitude peaks are displayed on the right side.

Figure 12 Comodulogram of animal I (left) and animal II (right). Cross frequency correlations were estimated via the modulation index (see Material and Methods)). Low frequencies were scanned from 4 to 20 Hz in 1 Hz steps with a variable band width of ±1/3 of the center frequency that was limited to a filter bandwidth of ±3.5 Hz. High frequencies were scanned from 25 to 100 Hz in 5 Hz steps using the same choice band width rule (see Methods). Regions of interest (ROIs) are located within the black rectangles.

Figure 13 Gamma amplitude as a function of alpha phase and preferred phases of PAC. Population probability density functions of gamma amplitude as a function of the alpha phase. Alpha phases were binned in 18 non-overlapping bins and mean gamma amplitude was calculated for each bin. For each recorded pair gamma amplitude within each bin was normalized to the total amplitude across bins, resulting in a probability density (PDF) like function across phase bins. PDFs were calculated for each RTF within each session. Mean PDF across the population of neuronal pairs are shifted between RT for animal I (A) and animal II (B). Error bars represent S.E.M. C & D display the average angular direction and 95 % CI (shaded area) of the population PDFs. For comparison the full cycle of the alpha phase is shown as the black solid line.

Figure 14 Variance of the location of gamma peaks relative to Stimulus Onset vs. alpha phase. On the ordinate the circular standard deviations of alpha phases at the time of gamma peak within the first full cycle of the alpha phase are plotted. The temporal delay from stimulus onset to the gamma peak are plotted along the abscissa. Crosses represent the mean of both animals. Variation for both animals is larger for the stimulus delay times in comparison to the phase variations.

Figure 15 Visualization of the Jackknife correlation statistic. In all panels the histogram shows the distribution of correlation coefficients resulting from the correlations between the randomly shuffled Jackknife resamples of RT and the non-shuffled Jackknife resamples of either mean preferred phase (top) or mean firing rate (bottom). The histograms resemble chance-level distribution of the Jackknife correlations. Red vertical lines are centered on the Jackknife correlation coefficient that was actually observed in the data (non-shuffled data). A Trial-wise correlation between RT and mean preferred phases of the population of recording pairs for animal I, B the same for animal II. C Trial-wise correlation of RT and mean firing rates for animal I, D the same for animal II.

Figure 16 Exemplary trace of a single-trial illustrating analysis of MUA and ESA. (A) For MUA, a threshold (dashed line, cf. equation 1) based on the method introduced by Quian Quiroga et al. (2012) was applied to the high-passed signal (grey trace). All events surpassing the threshold were then used for calculating the SDF (blue line). (B) For ESA, analysis is based on the full-wave rectified signal, i.e. the absolute values of the high-passed signal (grey trace), and then low-pass filtered (red line), using the same filter settings as for the SDF. This computation is independent of setting a threshold. Ordinate scaling is identical in both plots, SDF and ESA traces are both upscaled by a factor of 5 for visual purposes. Note that due to line thickness and time span, gaps

between adjacent spike events are hardly visible. The inset in (B) shows a time period of 100 ms to illustrate the time course of the rectified signal in more detail.

Figure 17 Comparison of RF detection rate between LFP, ESA, and MUA. (A) Standard approach for thresholding MUA. (B) Optimized, iterative approach for thresholding MUA to maximize MUA-based detection rate. For each signal type, boxplots are based on detection rates of individual animals. Detection rates refer to the absolute number of RFs detected relative to the number of recording sites with a significant visual activation for at least one of the signals, merged over all animals. Boxes indicates the 25^{th} and 75^{th} percentile, dashed lines indicate the medians, and whiskers indicate the full range of data. Asterisks indicate statistical difference for $\alpha < 0.5\%$ (*) and $\alpha < 0.05\%$ (**), respectively.

Figure 18 RF detection rates in dependence of signal-to-noise ratio (SNR). (A) High-pass filtered neuronal activity with very poor SNR (rank 4 out of 653). The upper panel depicts a single trial in response to a motion direction that reliably modulated the LFP. The dashed line indicates the threshold as calculated over all trials, using the method of Quian Quiroga et al. (2004) with a median multiplication factor of a = 2. Events surpassing the threshold are used to calculate spike density functions. The lower panel shows the same high-passed signal after full-wave rectification. Subsequent low-pass filtering provides the ESA-signal (thick line), revealing a small amplitude modulation during the course of the trial. (B) Cumulative distribution of the number of RFs detected using either MUA or ESA, sorted by SNR. Dashed lines distinguish equally large fractions of recording sites with low, medium, and high SNR, as used for statistical analysis. Arrows indicate the SNR ranks of the five example sites shown in (E, F). (C) Detection rates for low, medium, and high SNR sites, based on the respective detection rates of data from the individual animals, separately for ESA and MUA. Disks and lines indicate mean ± S.D, respectively. (D) Same as in (A), for a recording site with high SNR (rank 632). (E, F) Visual response maps based on thresholded MUA (E) and ESA (F) for the five recording sites indicated in (B). SNR rank increases from left to right. Vertical and horizontal white bars in the lower left corners indicate 1° of visual space. White outlined areas depict significant visual responses (receptive fields). For the two left-most maps in (E) no significant visual response was found with any of the thresholds tested during the iterative procedure. Actual maps were calculated based on a median multiplication factor of a = 2 for setting the threshold. Remaining maps (middle to right) were calculated after thresholding with a = 3.

Figure 19 . Comparison of stimulus selectivity between ESA and MUA. (A) RF area of recording sites with significant visually evoked response modulation for both ESA and MUA (N = 385). Boxplot conventions as in Figure 17. (B) RF area as a function of SNR for same units as in (A). Error bars indicate S.D. (C, D) Distribution of orientation indexes for ESA (C) and MUA (D). Dotted lines indicate median OI. Polar plot insets show exemplary orientation selective responses at median OI value for either signal type. (E) Direct comparison of orientation selectivity of units with significant orientation-selective responses for both MUA and ESA (N = 275). Box plot

with different preparation times (PT) are shown. RTs of the first and second group are significantly larger than one or more other groups indicating an effect of PT on RT. In C RTs and corresponding PTs are displayed for every trial. The linear model (black line) on the responses RT and the predictors PT fits the data well and is used to obtain bias free estimates of the underlying RT (residuals, D).

Appendix

Acknowledgements

I want to thank first and foremost my supervisor Dr. Detlef Wegener, who has endured and shared with me all of the effort, concerns and pitfalls that accompanied this work. It is also mainly on his part that this project was initially approved and funded and I want to thank him for that. In retrospection I think we set quite some ambitious goals for the project and, despite some drawbacks, we were able to yield valuable and important insights into the functioning of cortical processing.

I would like to thank also Prof. Dr. Andreas Kreiter who stood by us the entire time and was always willing to help out, discuss and sharpen our scientific method. I remember crouching below the lab tables with him to install or check our newly established recording system and remember that I very much appreciated the engagement he put into my project. Not only in this situation but in many, throughout the years.

I would like to thank Eric Drebitz, my colleague and friend that I worked close with during the entire time in the lab but also before, during our Master studies. We grew very much together and often experienced many aspects of the work in lab, institute and conferences together and it was quite reassuring to have someone in such close exchange about it. I think that also many of the thoughts that went into each of our projects were born, merged and forged in our close scientific exchange in our office but also quite often in the bar. Thank you Eric!

I would also like to thank all other staff and friends that worked in the lab and made any scientific work possible in the first place. Thanks to Kathrin and Rama for the great work with the animals. Thanks Peter, Alex, Katja, Sabine and Dieter for the animal care but also technical and organizational assistance and the friendly environment that you have created in the lab. Thanks, also and in particular to Deniz whom I have recorded many sessions with and also build up parts of our recording chamber.

Thank you all.

Article contributions

The individual manuscripts that are part of this thesis were conducted in cooperation with a number of Researchers. In the following I will name the contributions to each work that I have made.

For the article that has been published in “The Journal of Neurophysiology”, I have trained the animals, conducted the electrophysiological recordings and most of the data analysis. The co-authors were involved in training, recording and the development of the experimental paradigm. The manuscript was written by Detlef Wegener and myself.

For the manuscript in preparation that is presented in chapter III all recordings were performed by me and Deniz Parmuk. Data analysis, the conception and writing of the manuscript was done by myself.

For the manuscript that has been published in the journal “Frontiers of Neuroscience”, I have contributed by supplying a substantial amount of electrophysiological data and was involved in the revision of manuscript draft.

Declaration on the contribution of the candidate to a multi-author article/manuscript which is included as a chapter in the submitted doctoral thesis

Chapter II: Task-specific, dimension-based attentional shaping of motion processing in monkey area M

Contribution of the candidate in % of the total work load (up to 100% for each of the following categories):

Experimental concept and design:	ca. 0 %
Experimental work and/or acquisition of (experimental) data:	ca. 75%
Data analysis and interpretation:	ca. 75%
Preparation of Figures and Tables:	ca. 50%
Drafting of the manuscript:	ca. 50%

Chapter III: Phase shifts of cross frequency coupling predicts reaction time

Contribution of the candidate in % of the total work load (up to 100% for each of the following categories):

Experimental concept and design:	ca. 50 %
Experimental work and/or acquisition of (experimental) data:	ca. 80%
Data analysis and interpretation:	ca. 90%
Preparation of Figures and Tables:	ca. 100%
Drafting of the manuscript:	ca. 100%

Chapter IV: Optimizing the Yield of Multi-Unit Activity by Including the Entire Spiking Activity

Contribution of the candidate in % of the total work load (up to 100% for each of the following categories):

Experimental concept and design:	ca. 0%
Experimental work and/or acquisition of (experimental) data:	ca. 25%
Data analysis and interpretation:	ca. 15%
Preparation of Figures and Tables:	ca. 0%
Drafting of the manuscript:	ca. 0%

Date:

Signatures:

Eigenständigkeitserklärung

Hiermit erkläre ich, dass ich die Doktorarbeit mit dem Titel:

Attention-dependent processing of motion in middle temporal area and striate cortex and its relation to behavioral detection speed

selbstständig verfasst und geschrieben habe und außer den angegebenen Quellen keine weiteren Hilfsmittel verwendet habe.

Ebenfalls erkläre ich hiermit, dass es sich bei den von mir abgegebenen Arbeiten um drei identische Exemplare handelt.

_____

(Unterschrift)